Magnetic Resonance Imaging in the Assessment of Anti Prion Mediated Neurotoxicity *In Vivo*

Dissertation

zur

Erlangung der naturwissenschaftlichen Doktorwürde

(Dr. sc. nat.)

vorgelegt der

Mathematisch-naturwissenschaftlichen Fakultät

der

Universität Zürich

Von

Regina Rose Désirée Reimann

von

Basel BS und Winterthur ZH

Promotionskomitee

Prof. Dr. Adriano Aguzzi (Vorsitz)

Prof. Dr. Markus Rudin

Dr. Irene Knüsel

Zürich, 2015

Table of Contents

SUMMARY

The normal cellular prion protein (PrP^c) plays a dual role in transmissible spongiform encephalopathies (TSE), which is a group of lethal disease affecting humans and a variety of animal species. First PrP^C is hypothesized to be the source of the causative agent “the prion” in TSE, as the pathologic missfolded scrapie isoform of the prion protein (PrP^{SC}) catalyses its own conversion from the prion protein. Second, there is substantial evidence that PrP^C is the receptor mediating neurotoxicity and disease progression in TSE. In support of this theory, some antiprion antibodies have been found to induce neurotoxicity, an important discovery that may provide a new model system to investigate the pathologic interaction between PrP^{SC} and PrP^C.

In the first part of the thesis I investigated antiprion mediated toxicity *in vivo*. Towards this goal, I established two read outs based on magnetic resonance imaging (MRI) volumetry allowing the measurment of antiprion induced neurotoxicity in intact mice over time. In the beginning I worked with Manganese Enhanced MRI (MEMRI) to visualize cerebellar lesion induction. As this was less well suited to the measurement of the neurotoxic induction in the hippocampus, I additionally established a diffusion weighted imaging (DWI) scan protocol. Diffusion restriction can be found within an hour after the injection of high concentration of monovalent fragments of the neurotoxic antiprion antibody POM1. As previously found in cerebellar organotypic slice cultures (COCS) antiprion mediated neurotoxicity was found to be target and eptiopic specific. Neuronal expression of PrP^C is sufficient for lesion induction and lesion induction is independent from cross-linking.

Further I investigated important signalling pathways downstream of PrP^C. Reactive oxygen species (ROS) are a known mediator of neurodegenerative disease and I could demonstrate that they are important in the pathologic cascade of antiprion mediated neurotoxicitiy *in vivo*. As a major source of ROS, I identified NADPH oxidase 2 (NOX2). As in bona fide prion infection, I could detect fodrin cleavage as a marker for calpain activation in homogenates from antiprion injected brain tissue. These findings are indicative that similar pathways are

activated in both pathological conditions. Further, my data shows that the NCX3 antiporter is a possible source of pathologic Ca^{2+} currents in the antiprion antibody model.

In the second part of this thesis, I focused on the risk characterization of neurotoxic antiprion antibodies. Despite reports about the neurotoxic side effects of antiprion antibodies, passive immunotherapy with these ligands is still a therapeutic strategy under investigation in the treatment of TSE. Using my established MRI based quantification system and basic histological methods, I assessed the neurotoxic potential of the antiprion antibody ICSM18, which is under evaluation as a therapeutic agent for TSE in humans. Unless further investigations can confirm a safe therapeutic window for the use of these antibodies and others, my findings suggest that utmost caution is indicated.

Here I show that Magnetic Resonance Imaging is a valuable tool in the assessment of anti prion mediated neurotoxicity *in vivo*. This technique can be used for the risk characterization of antiption antibodies. In addition, our work *in vivo* and in cerebellar slice cultures provides new evidence that neurotoxic antiprion antibodies model the pathologic interaction of PrP^{SC} with PrP^{C}. Thus, the established tool can be used in further studies to investigate prion-mediated neurotoxicity, in a much shorter time frame and within biosafety level one.

ZUSAMMENFASSUNG

Das normale zelluläre Prionprotein (PrP^Z) spielt eine duale Rolle in transmissiblen spongiformen Enzephalopathien (TSE), eine Gruppe von lethalen Erkrankungen, welche Menschen und diverse Tierspezies betrifft. Erstens besteht die Hypothese das PrP^Z die Quelle des kausativen Agens "dem Prion" in TSE ist, da die pathologische misgefaltete "scrapie" Isofrom des Prionproteins (PrP^{SC}) seine eigene Konversion vom Prionprotein katalysiert. Zweitens, gibt es eine fundierte Evidenz, dass PrP^Z der Rezeptor ist, welcher die Neurotoxizität weiterleitet und zur Krankheitsprogression in TSE beiträgt. Unterstützend für diese Theorie ist der Befund, dass Antikörper gegen das Prionprotein neurotoxisch sind; dies stellt eine wichtige Entdeckung dar, da es ein neues Modelsystem ermöglicht, um pathologische Interaktionen zwischen PrP^{SC} and PrP^Z zu untersuchen.

Im ersten Teil meiner Thesis habe ich die Neurotoxizität vermittelt durch anti Prion Antikörper *in vivo* erforscht. Um dieses Ziel zu erreichen habe ich zwei Messsysteme basierend auf Volumetrie mittels des Einsatzes von Magnet Resonanz Tomographie (MRT) etabliert, welches das Messen von anti Prion induzierter Toxizität über die Zeit in lebenden Mäusen erlaubt. Um Läsionen im Kleinhirn darzustellen habe ich am Anfang mit Mangan unterstütztem MRT gearbeitet. Da sich herausgestellt hat, dass diese Technik weniger geeignet für die Messung von anti Prion Antikörper induzierter Neurotoxizität im Hippokampus ist, etablierte ich zusätzlich ein Bildgebungs Protokoll mittels der Verwendung einer Diffusions gewichteten Sequenz. Eine Diffusionsrestriktion kann innerhalb von einer Stunde nach Injektion von konzentrierten monovalenten Fragmenten des neurotoxischen anti Prion Antikörpers POM1 gefunden werden. Wie bereits in zerebellären organotypischen Schnittkulturen gezeigt, ist die anti Prion vermittelt Neurotoxizität Antigen und Epitop spezifisch. Für eine Induktion einer Läsion ist die neuronale Expression von PrP^Z ausreichend und eine Vernetzung von PrP^Z unnötig.

Weiter habe ich Signalwege welche dem PrP^Z nachgeordnet sind untersucht. Reaktive Sauerstoffverbindungen sind ein bekannter Mediator neurodegenerativer Erkrankungen und

ich konnte demonstrieren, dass jene wichtig sind in der pathologischen Kaskade der anti Prion Antikörper induzierten Toxizität *in vivo*. Als eine Hauptquelle der reaktiven Sauerstoffverbindungen habe ich die NADPH Oxidase 2 identifiziert. Wie bei einer echten Prioneninfektion konnte ich zudem ein typisches Verdau Muster des Fodrin Proteins als Marker für eine Calpain Aktivierung im Homogenat von anti Prion Antikörper injeziertem Gehirngewebe finden. Diese Befunde sind hinweisend dafür, dass in beiden pathologischen Bedingungen ähnliche Signalwege aktiviert werden. Zusätzlich zeigen meine Daten, dass der NCX3 Antiporter eine mögliche Quelle für pathologische Ca^{2+} Ströme im anti Prion Antikörper Modell ist.

Im zweiten Teil meiner Thesis habe ich mich auf die Risikocharakterisierung von anti Prion Antikörper fokusiert. Trotz den Berichten bezüglich der neurotoxischen Nebenwirkungen dieser Antikörper, ist die passive Immunotherapie immer noch eine häufig getestete Behandlungsstrategie in TSE. Mittels des MRI basierten Quantifikationssystems und Histologie habe ich das neurotoxische Potential des anti Prion Antikörpers ICSM18 untersucht, welcher in Evaluation als ein Therapeutikum in TSE beim Menschen steht. Meine Befunde mahnen zur Vorsicht in Bezug auf den therapeutischen Gebrauch dieses und anderer Antikörper.

Hier zeige ich, dass MRT ein wertvolles Werkzeug für die Bewertung von anti Prion Antikörper vermittelte Neurotoxizität *in vivo* darstellt. Diese Techik kann für die Risikobewertung von anti Prion Antikörper verwendet werden. Zweitens liefern unsere Arbeiten *in vivo* und in zerebellären organotypischen Schnitt Kulturen eine Evidenz, dass neurotoxische anti Prion Antikörper pathologische Interaktionen von PrP^{SC} mit PrP^{C} imitieren. Das hier etablierte *in vivo* Model kann deshalb auch für weitere Studien zur Untersuchung der Prion vermittelte Neurotoxizität verwendet werden. Dies bietet den Vorteil, dass jene in einer viel kürzeren Zeitperiode und unter einem Biosicherheitlevel eins untersucht werden können.

ABBREVIATIONS

129	SV129 wild type inbred mouse strain
Aβ	amyloid β protein
AcHyt	acetylated hydroxytyrosol
AP	anterior-posterior
ATP	adenosine triphosphate
BL6	black 6 wild type inbred mouse strain
BL6.129	mouse on a mixed black 6 and 129 background
BL10	black 10 wild type inbred mouse strain
BMD	benchmark dose
BSE	bovine spongiform encephalopathy
CA1	hypocampal cornus ammonis region one
CA3	hippocampal cornus ammonis region three
CaM	calcium/calmodulin-dependent
CaN	calcineurin
CaKC	Ca^{2+} -activated K^{+} channels
CC1	charged cluster one
CC2	charged cluster two
CGC	cerebellar granular cells
CJD	Creutzfeldt-Jakob disease
fCJD	familial Creutzfeldt-Jakob disease
sCJD	sporadic Creutzfeldt-Jakob disease
vCJD	variant Creutzfeldt-Jakob disease
cl	contra lateral
CNS	central nervous system
COCS	cerebellar organotypic cultured slices
D13	antiprion antibody binding epitope 95 to 105
D18	antiprion antibody binding epitope 133 to 157
DG	dentate gyrus
DV	dorsal ventral
DWI	diffusion weighted imaging
DAPI	4,6-diamidino-2-phenylindole
DNA	deoxyribonucleic acid
DPI	diphenyleneiodonium chloride
E64d	cell-penetrating calpain inhibitor
ER	endoplasmic reticulum

F(ab)$_1$	monovalent fragment antigen binding
F(ab)$_2$	divalent fragment antigen binding
FDA	U.S. food and drug administration
FFI	familial fatal insomnia
FID	free induction decay
FLAIR	fluid-attenuated inversion recovery
FT	flexible tail of PrP^C (redisures 23-125)
GCL	granular cell layer
GD	globular domain of PrP_C (residues 124-230)
GPI	glycosylphosphatidylinositol
GSS	Gerstmann-Sträussler-Scheinker disease
GluR	glutamate receptors
HC	hydrophobic core of PrP_C (residues 112-133)
H&E	hematoxylin and eosin
HRP	horseradish peroxidase
ic	intracerebral
ICSM	set of 27 anti-PrP monoclonal antibodies
IgG	Immunoglobulin G
il	ipsilateral
ip	intraperitoneal
IP3	inositol trisphosphate
i.v.	intravenous
LOAL	lowest observed adverse effect level
MEMRI	manganes enhanced magnetic resonance imaging
MIT	mitochondrium
ML	middle line
MLa	molecular layer
MRI	magnetic resonance imaging
NAc	N-Acetyl Cysteine
NADPH	nicotinamide adenine dinucleotide phosphate
NCX	Na^+/Ca^{2+} exchanger
NCX3	NCX isoform three
NCX3$^{o/o}$	NCX3 deficient mice
NEX	number of exitation
NeuN	Neural nuclei protein
NMDA	N-methyl-D-aspartate
NMR	nuclear magnetic resonance

NOAL	no-observed adverse effect level
NOS	nitric oxide synthase
NOX	NADPH oxidase
NOX2	NADPH oxidase 2
NEX	number of excitation
NSE	neuron specific enolase
OR	octapeptide repeats of PrP^{c} (residues 50-90)
ORF	open reading frame
P	antiprion antibody binding epitope 95-105
PBS	phosphate-buffered saline
PCL	purkinje cell layer
PCR	polymerase chain reaction
PDB	protein data bank
pi	post injection
p.i.i.	post intracerebal injection
PMCA	plasma membrane Ca2+ -ATPase
POMs	set of 19 anti-PrP monoclonal antibodies
Prnp	murine PrP^{C} gene locus
PRNP	human PrP^{C} gene
***Prnp*$^{o/o}$**	prnp knock-out mouse Zürich-I
***Prnp*$^{-/-}$**	prnp knock-out mouse Edinburgh
PrP	prion protein
$PrP_{\Delta 32-93}$	truncated PrP version (lacking residues 32-93)
$PrP_{\Delta 32-121}$	truncated PrP version (lacking residues 32-121)
$PrP_{\Delta 32-134}$	truncated PrP version (lacking residues 32-134)
$PrP_{\Delta 94-110}$	truncated PrP version (lacking residues 94-110, CC2)
$PrP_{\Delta 94-134}$	truncated PrP version (lacking residues 94-134)
$PrP_{\Delta 105-125}$	truncated PrP version (lacking residues 105-125)
PrP^{C}	cellular prion protein
^{Ctm}PrP	PrP isoform with the carboxyl terminus in the ER lumen
^{Ntm}PrP	PrP isoform with the amino terminus in the ER lumen
PrP^{SC}	scrapie-associated prion protein
PrP^{Res}	protease resistant isoform of the prion protein
rmPrP	recombinant mouse PrP
$rmPrP_{23-230}$	recombinant mouse PrP from amino acids 23 to 230
$rmPrP_{90-230}$	recombinant mouse PrP from amino acids 90 to 230
RF	radio frequence

RMIT	royal Melbourne institute of technology
RML	Rocky Mountain Labaratory strain mouse-adapted scrapie prions
ROI	region of interest
ROS	radical oxygen species
RyR	ryanodine receptor
ScFv	single chain variable fragment
SD	standard deviation
SDS-PAGE	sodium dodecyl sulfate polyacrylamide gel electrophoresis
SH3	Src homology domain 3
SNR	signal to noise ratio
SOC	store-operated Ca^{2+} channels
SV	synaptic vesicles
tga20	mice overexpressing PrP^{c}
T1	time of recovery of the longitudinal magnetization in a MRI experiment
T2	time of the decay of the transversal magnetization in a MRI experiment
TdT	Terminal deoxynucleotidyl transferase
TE	time of echo
TSE	transmissible spongiform encephalopathies
TR	time of repetition
TUNEL	transferase mediated deoxyuridine triphosphate nick end labelling
VGCC	voltage gated N-type calcium channels
VPSPr	variable protease sensitive prionopathy
WHO	world health organisation
wt	wild type mouse

DECLARATION

Publications

Parts of my thesis are reproduced from the publication in *Nature,* 05. Sept 2013, issue 501, pages 102-6;

The toxicity of antiprion antibodies is mediated by the flexible tail of the prion protein

Tiziana Sonati*, Regina R. Reimann*, Jeppe Falsig*, Pravas Kumar Baral, Tracy O'Connor, Simone Hornemann, Sine Yaganoglu, Bei Li, Uli S. Herrmann, Barbara Wieland, Mridula Swayampakula, Muhammad Hafizur Rahman, Dipankar Das, Nat Kav, Roland Riek, Pawel P. Liberski, Michael N. G. James, and Adriano Aguzzi.

* Equal contribution

Manuscript in preparation

Parts of my thesis are adapted or reproduced from the following manuscripts in preparation:

Risk characterization of toxic antiprion antibodies

Regina R. Reimann*, Tiziana Sonati*, Simone Hornemann, Uli S. Hermann, Michael Arand, Simon Hawek and Adriano Aguzzi.

* Equal contribution

NCX3 as a potential source of Ca^{2+} influx in antiprion mediated neurotoxicity

Regina R. Reimann*, Sakata Daiji*, Tiziana Sonati, Susi Senatore, Jeppe Falsig, Uli S. Hermann , and Adriano Aguzzi1.

* Equal contribution

INTRODUCTION

From the disease to the dual pathogenic role of the cellular prion protein

Transmissible spongiform encephalopathies and the protein only hypothesis

Transmissible spongiform encepahlopathies (TSE) diseases are untreatable, fatal neurodegenerative diseases with an unsolved pathological mechanism (Aguzzi and Calella, 2009). The first clinical manifestation of a TSE is known since 1738 (Figure 1A) in sheep and named scarpie (Aguzzi and Calella, 2009). Creutzfeldt (1920) and Jakob (1921) described the disease first in humans and gave the eponym for the disease in humans (Aguzzi et al., 2008). The majority (85%) of TSE cases in humans are the sporadic, and inherited (10-20%), associated with autosomal dominant *PRNP* gene alterations, forms of Creutzfeld-Jakob Disease (CJD) (Aguzzi and Calella, 2009).

Per definition, TSE are **transmissible**, which was first recognized for scrapie in 1946, when the contamination of a vaccine led to the infection of 1'500 sheeps (Aguzzi and Calella, 2009; Gordon, 1946). In man the infectious nature was initially recognized by Gajdusek, who discovered that the practice of ritual cannibalism led to the disease known as Kuru in 150 villages in New Guinea (Gajdusek and Zigas, 1957). The description of the new variant of CJD (Chazot et al., 1996; Will et al., 1996) generated global interest in the infectious nature of TSE. Subsequently, a global food panic (Aguzzi and Calella, 2009) was triggered by the announcement that the most likely aetiology of this form was the consumption of meat from cattle infected by the epidemic spread of Bovine Spongiform Encephalopathy (BSE) (Anderson et al., 1996).

The definitive diagnosis in TSE is to date based on neuropathological examination (WHO, 1998). The classical hallmark of the disease (Figure 1B) is **spongiform change**, neuronal loss and gliosis (Budka, 2003). On routine staining with hematoxylin & eosin (H&E), compact Kuru-type plaques are seen in some cases of TSE (Budka, 2003). These exhibit a

characteristic apple-green birefringence when stained with Congo red and observed under polarized light, a characteristic feature of amyloid proteins (Aguzzi and O'Connor, 2010).

The clinical presentation of the **encephalopathie** differs between and within entities. Based on World Health Organisation (WHO) criteria, patients are scored as probable or possible cases (WHO, 1998). Sporadic CJD (sCJD) cases typically present with rapidly progressive dementia and at least two of the following four clinical features: myoclonus, visual or cerebellar disturbances, pyramidal or extrapyramidal dysfunction, and akinetic mutism (WHO, 1998).

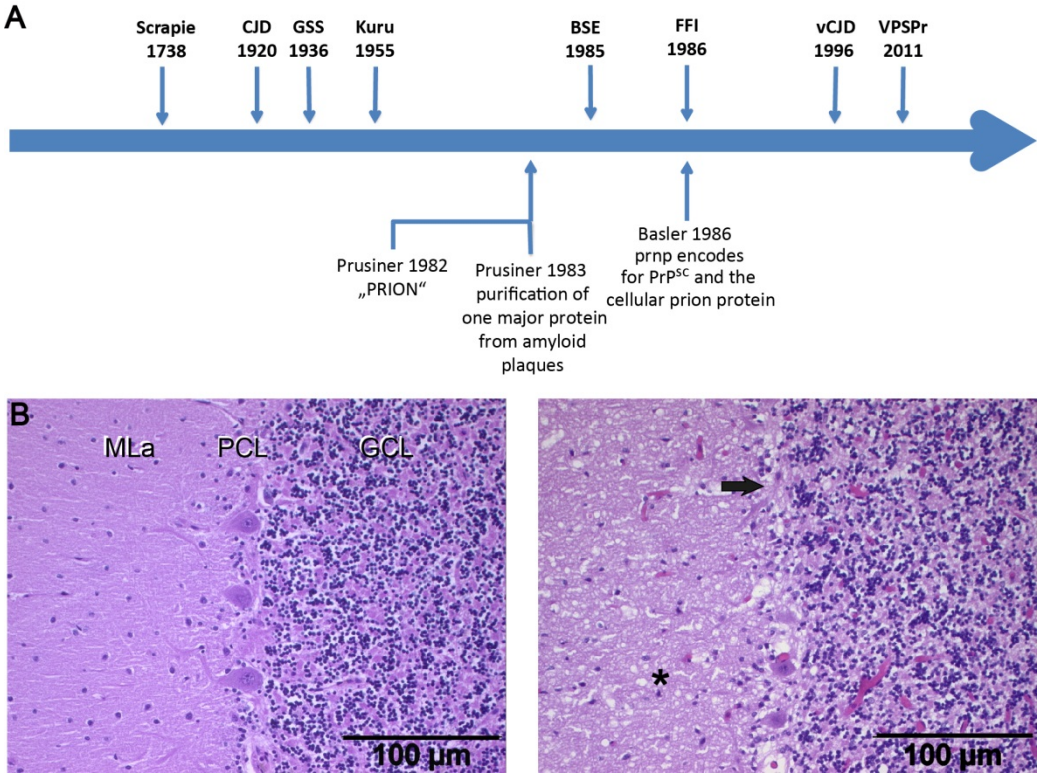

Figure 1: A pathologic protein isoform encoded by *PRNP* induces transmissible spongiform encephalopathy (TSE) in humans and animals

(A) The time bar illustrates the years of the first description of TSE in humans and animals (upper) and important discoveries leading to the identification of the infective agent (lower). CJD: Creutzfeld Jakob Disease, GSS: Gerstmann-Sträussler-Scheinker disease, FFI: Fatal Familial Insomnia, BSE: Bovine Spongiform Encephalopathie, vCJD: new variant CJD, VPSPr: variable Protease Sensitive Prionopathy. **(B)** Hematoxylin & Eosin (H&E)-stained micrograph of a cerebellar section from a patient who died from sCJD (left), depicts the classical neuropathological hallmarks of TSE: spongiform change (star), nerve cell (neuronal) loss and reactive gliosis (arrow). These changes are not found upon histological examination of unaffected patients (left). Molecular layer: ML; Purkinje cell layer: PCL; Granular cell layer: GCL. (Source of micrograph: National Reference Center for Prion Diseases, Switzerland)

The nature of the infectious agent was a scientific mystery for decades (Figure 1A). The „scrapie agent“possessed unusual properties such as resistance to high temperature (Stamp et al., 1959), fixation with formalin (Pattison, 1965) and ultra-violet irradiation (Alper et al., 1967). From these experiments, it was concluded that the agent replicates without nucleic acid (Alper et al., 1967). In 1967, Griffith proposed three possible mechanisms of how a protein could be the self-replicating agent in TSE (Griffith, 1967). The **protein only hypothesis** (Prusiner, 1991; Weissmann, 1991) was associated with the introduction of the term **prion** by Prusiner**,** denoting a small proteinacious infectious particle, which is today the common term for the infective agent in TSE (Prusiner, 1982). Only a few months later, his group presented data about a purified preparation of prions, which was found to consist of a single major protein (Bolton et al., 1982; Prusiner et al., 1983). Additionally, Prusiner discovered that this protein aggregated into amyloid-like birefrigent rods or fibrils, and thus concluded that the plaques found in TSE likely consist of prions (Prusiner et al., 1983). The gene known as ***Prnp*** encodes this pathologic protein and the normal cellular prion protein (Basler et al., 1986). **PrP^{C}** refers to the normal cellular isoform of the prion protein, which is protease sensitive and soluble in nondenaturing detergents, whereas the scarpie isoform of the prion protein **PrP^{SC}** is the disease-specific protein, which is insoluble in detergents (Aguzzi and Calella, 2009). Typically, this pathologic isoform has a protease-resistant core of a 33 to 35 kDa, designated as PrP^{Res} and used to detect prions in research or diagnostic tests. On immunohistochemical analysis of tissue from TSE infected animals and humans, aggregates of PrP^{Res} are found in a synaptic, patchy/perivacuolar, or plaque like pattern (Budka, 2003). Possible posttranslational modifications convert PrP^{C} in PrP^{SC} (Basler et al., 1986). There is evidence that certain “co-factors” like lipids or RNA increase the infectivity of PrP^{SC} (Deleault et al., 2007; Supattapone, 2010; Wang et al., 2010).

With the hallmark of the misfolding and aggregation of proteins into fibrils, TSE belong to a family of degenerative diseases, termed as **proteinopathies** or proteopathies. The best recognized member of this group is Alzheimer disease, associated with the pathologic accumulation of amyloid β (Aβ) and tau protein. Interestingly, there is a growing body of

knowledge that proteinopathies share additional features than just the aggregation of misfolded proteins (Aguzzi and Rajendran, 2009; Eisenberg and Jucker, 2012; Jucker and Walker, 2011).

The cellular prion protein

The *PRNP* gene was assigned to the human chromosome 20 and *Prnp* to the corresponding mouse chromosome 2 (Sparkes et al., 1986). The open reading frame (ORF) is contained within a single exon and codes for PrP^{C}, ubiquitously expressed, particularly in the nervous system by neurons and glial cells (Aguzzi and Calella, 2009). PrP^{C} is a glycosylphosphatidylinositol (GPI) anchored cell surface protein (Stahl et al., 1987) consisting of 209 Amino Acids (Aguzzi and Calella, 2009). Structurally, the protein (Figure 2) can be segmented into a N-terminal flexible tail (FT, amino acids 23-125) and a C-terminal globular domain (GD, amino acids 124-230) (Riek et al., 1997). Both segments can be further subdivided into structural or functional domains. The FT consists of two charged-clusters (CC1 and CC2), five octapeptide repeats (OR) and the hydrophobic core (HC) (Aguzzi et al., 2008). The structurally better defined GD is composed of two beta sheets (3% of the structure) and three alpha helices (Hornemann et al., 1997; Riek et al., 1997). In contrast, PrP^{SC} has been found to have a much higher beta sheet content of 43% (Pan et al., 1993).

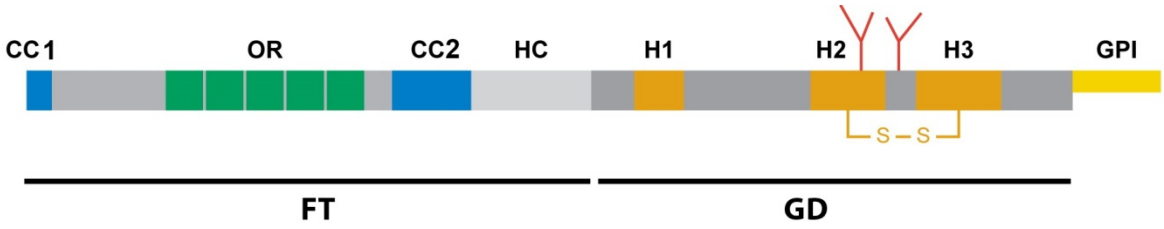

Figure 2: Structural and functional domains of the cellular prion protein (PrP^{C})
The two major structural components of PrP^{C} are the unstructured flexible tail (FT) and the C-terminal globular domain (GD). At the C-terminal, the protein is linked with a glycosylphosphatidylinositol (GPI) anchor with the cell membrane. CC1: charged amino acid cluster 1; OR: octa repeat, CC2: charged amino acid cluster 2; H1-H3: three α-helices (red boxes); S-S: disulfide bond; red forks: potential sides of N-linked glycosylation. **Modified from (Aguzzi et al., 2008)**.

Interestingly, no severe phenotype has been found in PrP^C deficient mice (*Prnp*$^{o/o}$) (Büeler et al., 1992). This observation was unexpected as the high conservation of central domains of PrP^C between species, was indicative for an essential function of the protein (Aguzzi et al., 2008). Later PrP^C expression was shown to be essential for myelin maintenance (Bremer et al., 2010) and to influence many cellular processes, including neuronal survival, neurite outgrowth and synapse formation (Aguzzi et al., 2008). However, the function of PrP^C is controversial, as some findings are based on genetic confounders (Nuvolone et al., 2013).

The pathologic agent is recruited from PrP^C

The central role of PrP^C in prion pathogenesis is illustrated by the striking phenotype of *Prnp*$^{o/o}$ mice with their resistance to prion infection (Büeler et al., 1992). Today the theory that prions are self-replicating proteins, which catalyse their own conversion from PrP^C, is widely accepted (Aguzzi and Calella, 2009). Thereby, not the monomeric form but oligomeric species of approximately 20 molecules show the most effective infectivity (Silveira et al., 2005). This finding speaks in favour of the seeded nucleation theory, one of the hypotheses explaining the recruitment of prions from normal PrP^C (Jarrett and Lansbury, 1993). This model makes the assumption that PrP^C and the pathological beta sheet rich isoform are in a thermodynamic equilibrium and shifted in the non-diseased state towards PrP^C. Highly ordered seeds of monomeric PrP^{SC} incorporate other monomers, aggregate or fragment into new seeds and thereby propagate (Aguzzi and Calella, 2009).

Evidence that PrP^C acts as a neurotoxic mediator in TSE

Neuronal cell loss is one of the three central neuropathological hallmarks of TSE. There is a growing body of evidence that the translated product of the *Prnp* gene is not only the main content of prions, but also that its normal isoform PrP^C anchored to the membrane is the receptor mediating neurotoxicity. Brain tissue devoid of PrP^C is not damaged by accumulating PrP^{SC}, even in close proximitry to the tissue graft with established prion infection (Brandner et al., 1996). Additionally, depletion of endogenous PrP^C expression

during prion infection resulted in preserved neuronal cell loss and spongiosis (Mallucci et al., 2003). Remarkably, prion infection in mice expressing only an anchorless Prion Protein fails to induce any clinical manifestations despite the deposition of PrP^{Res} (Chesebro et al., 2005). Different models of how PrP^{C} could act within the neurotoxic cascade have been promulgated: (1) PrP^{SC} could lead to a clustering and/or conformational change of PrP^{C} (Figure 3) on the cell surface and (2) PrP^{C} could mediate lysosomal uptake and/or clustering. This could lead to aggregation of misfolded protein within the endoplasmatic reticulum (ER), which triggers the Unfolded Protein Response (Halliday and Mallucci, 2014).

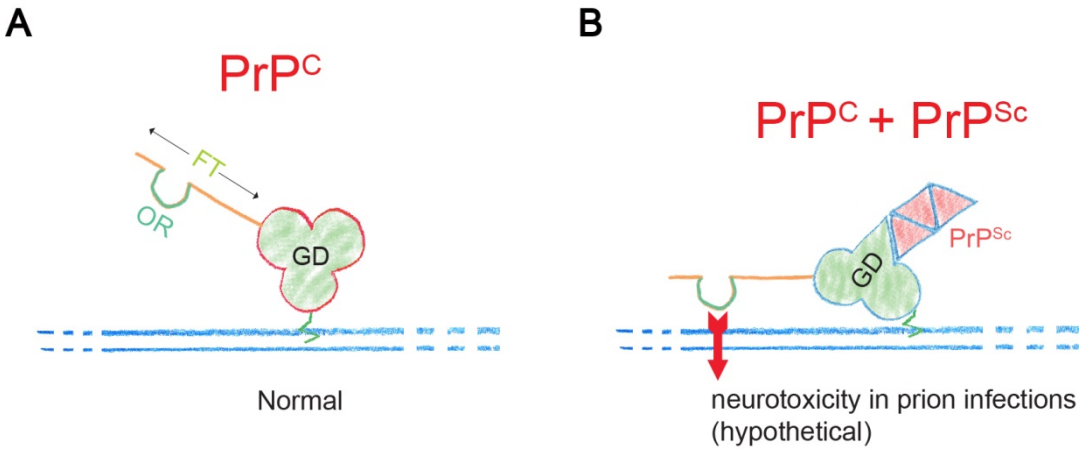

Figure 3: Bonafide PrP^{SC} infection hypothetically induces neurotoxicity through interaction with PrP^{C}

(A) Illustration of the normal PrP^{C}. Depicted is the Flexible Tail (FT), the Octapeptide Repeat (OR) and the Globular domain (GD). **(B)** Interaction of monomeric or oligomeric PrP^{SC} with PrP^{C} triggers neurotoxicity**.** Neurotoxicity is possibly induced through a conformation alteration (illustrated by a change in the conformation) of the FT.

In a broader hypothesis, PrP^{C} is believed to be a receptor for amyloids in general. This concept mainly developed from the identification of PrP^{C} (epitope 95-105) as an Aβ-oligomer receptor mediating synaptic dysfunction (Lauren et al., 2009). Although the interaction of Aβ-oligomer with PrP^{C} was later confirmed (Balducci et al., 2010), the blockage of Aβ-oligomer triggered synaptic plasticity impairment upon *Prnp* ablation is considered controversial (Aguzzi and Calella, 2009; Kessels et al., 2010).

Spontaneous neurodegeneration has been observed in mice expressing mutated CC2 ablated PrP in combination with a partial deletion of the HC: the mutants $PrP_{\Delta 32\text{-}121}$, $PrP_{\Delta 32\text{-}134}$,

$PrP_{\Delta 105\text{-}125}$ and $PrP_{\Delta 94\text{-}134}$ (Baumann et al., 2007; Li et al., 2007; Shmerling et al., 1998). A similar phenotype is seen in mice ectopically overexpressing Doppel in the absence of normal PrP^C (Mo et al., 2001; Moore et al., 1999; Rossi et al., 2001; Sakaguchi et al., 1996). Importantly, the co-expression of normal PrP^C in combination with the deletion mutants or Doppel is protective against these pathological effects (Anderson et al., 2004; Atarashi et al., 2003; Nishida et al., 1999; Shmerling et al., 1998), which argues for a neuroprotective activity of the full-length prion protein (Beland and Roucou, 2012).

Cellular signalling through PrP^C

PrP^C as a GPI anchored receptor could possibly influence intracellular signalling transduction pathways by two mechanisms: either by interaction with a transmembrane adapter or a cell-surface complex or by ligand induced PrP^C mislocalization into a transmembrane or cytosolic form (Aguzzi et al., 2008).

To identify the PrP^C interaction partners, a huge effort has been made, and several membrane proteins (receptors, enzymes, Caveolin-1, Na-K-ATPase, and a potassium channel), cytoplasmic proteins (components of the cytoskeleton, heat-shock proteins, and adaptor proteins involved in signalling), and even the nuclear protein CBP70 were identified (Aguzzi et al., 2008). However, many of these studies, which were based on yeast-two hybrid, co-immunoprecipitations, and cross-linking experiments, are limited due to technical issues (Aguzzi and Calella, 2009). To overcome some of these concerns, additional transgenic mice expressing a functionally tagged PrP^C were used and several proteins associated with axomyelinic maintenance were identified (Rutishauser et al., 2009).

Within the ER, PrP^C can adopt at least two transmembrane topologies, ^{Ctm}PrP and ^{Ntm}PrP, which have their carboxyl or amino terminus in the ER lumen, respectively (Aguzzi and Calella, 2009). Neurodegenerative changes have been reported for mice expressing the ^{Ctm}PrP transmembrane form (Hegde et al., 1998) and for the accumulation of the prion protein in the cytosol (Ma et al., 2002), which support the role of aberrant PrP^C topology in the neurotoxic cascade.

Antiprion antibodies

The first antiserum against prion protein was produced in 1984 (Bendheim et al., 1984); however, the generation of high affinity antiprion antibodies was complicated by host tolerance to endogenous PrP^{C}, which is nonpermissive to generate high-affinity antiprion cell-clones (Polymenidou et al., 2004). The first successful monoclonal antibody 3F4, was derived from a mouse immunized with hamster PrP^{res}, which binds to human and hamster but not to mice PrP (Kascsak et al., 1987). The breakthrough in generating larger panels of antibodies against different epitopes was achieved by immunization of *Prnp*$^{o/o}$ mice (Williamson et al., 1996). Specifically, a set of 19-specific antibodies, including the antiprion antibody D13 (epitope 95-105; Figure 4A), was produced with antibody-phage technology or liposome preparation (Williamson et al., 1998).

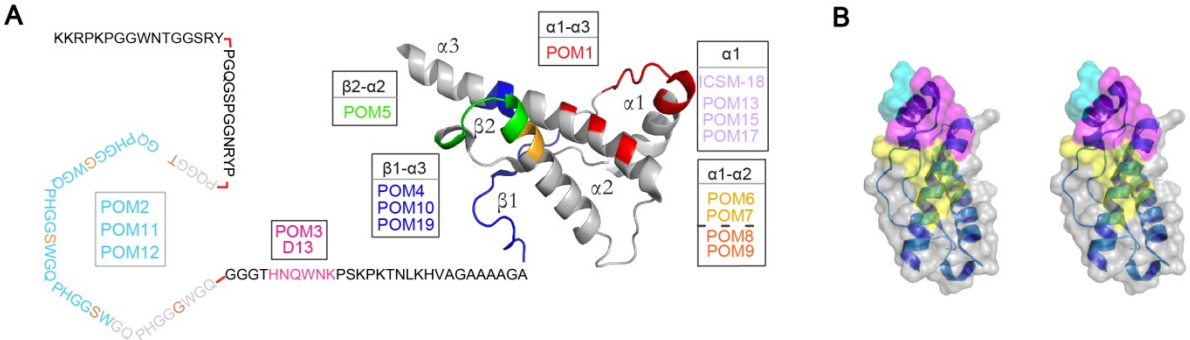

Figure 4: Illustration of epitopes of antiprion antibody binding sites

(A) Antibody binding sites on PrP (epitope 23-230). POM2, 11 and 12 bind epitopes of the OR (bright blue). Epitopes of CC2 are recognized by POM3 and D13 (pink) POM6-9, 13, 15 and 17 and ICSM-18 bind helix α1 and compete with POM1 (Polymenidou et al., 2004). POM6 and POM7 (light orange) show additional binding sites at helix α2 (dark orange), whereas POM5 recognizes a unique epitope at the β2-α2 transition (green). The GD image was generated using the RSCB Protein Data Bank (PDB) structure 2L1H. **(B)** Surface stereoview of human PrP(121-230). Yellow and cyan: POM1 and ICSM18 interfaces, respectively (PDB accession codes: 4DGI and 2W9E). Magenta: overlap between the POM1 and ICSM18 interfaces. Blue ribbon: polypeptide backbone. Interfaces are delineated by residues with ≤5 Å distance in the complexes comprising human PrP (epitope 121-230) and the respective F(ab) fragments. Structural images were prepared with the program PyMOL (www.pymol.org)

Based on the immunization of *Prnp*$^{o/o}$ with recombinant human PrP (residues 91-231), folded

either into α or β conformation, ICSM antibodies have been generated primarily to study differences in expression of PrP^C (Beringue et al., 2003). These sets mostly exclude epitope specificity with the FT. Accordingly POM monoclonals (Figure 4A) were generated by immunization of *Prnp*$^{o/o}$ with full length recombinant murine PrP ($rmPrP_{23-230}$) (Polymenidou et al., 2008). Crystallographic studies and nuclear magnetic resonance spectroscopy showed that 10 amino acids overlap in the binding epitope of POM1 with ICSM18 (Figure 4B).

Antiprion mediated neurotoxicity

Antiprion antibodies have been used to demonstrate signal transduction through PrP^C (Mouillet-Richard et al., 2000) by the use of the neuronal differentiation model 1C11. In 2004 Solforosi et al. induced neuronal apoptosis upon intrahippocampal and intracerebellar injection of antiprion antibodies *in vivo*. While two of their antibodies D13 and P, both recognizing epitopes within the 95 to 105 region of the prion protein, showed a pathologic effect, D18, binding within 133 to 157, was not toxic at the same dose. The toxic induction was a specific effect upon PrP^C binding, since it could be blocked upon incubation with $rmPrP_{90-230}$ and it was not seen upon injection into *Prnp*$^{o/o}$ mice. The neuronal damage was primarily characterized as pyknotic nuclei by conventional histology. Transferase mediated deoxyuridine triphosphate nick end labelling (TUNEL) revealed apoptotic neuronal cell death. Immunohistochemistry excluded complement activation and FC mediated toxicity. However, the injection of monovalent fragment antigen ($F(ab)_1$) of D13 and P did not cause anti-prion mediated toxicity. From this observation it was concluded that the toxicity is cross-link mediated. This neurotoxic effect was introduced as a possibile model for the negative prion interaction with PrP^C and as a justification to avoid the use of these antibodies for therapeutic intervention (Solforosi et al., 2004). The toxic effect of anti-prion antibodies was later confirmed (Lefebvre-Roque et al., 2007) by a model designed to treat prion-infected mice after the chronic administration of antiprion antibodies. However, subsequently there was a report that questioned the neurotoxic effect of D13 (Klöhn et al., 2012).

Magnetic resonance imaging in TSE

MRI as a non invasive tool in research and diagnosis

Magnetic resonance imaging (MRI) is an extraordinary technique that facilitates non-invasive *in vivo* imaging for diagnostic and research purposes. Due to the high contrast soft tissue structures on MRI, it is possible to examine anatomical structures and biochemical processes inside the body (Meier D. et al., 2012). The technique is based on the discovery in 1946 by Bloch and Purcell (Bloch et al., 1946a, b; Purcell E. M. et al., 1945) "that certain nuclei absorb energy in the electromagnetic spectrum when placed in a magnetic field, which is re-emitted when the nuclei return to their original energy state" (Geva, 2006), resulting in the birth of the field of Nuclear Magnetic Resonance (NMR). "With NMR the structures of molecules can be identified to facilitate the analysis of solutions and to follow chemical reactions in physics and chemistry" (Meier D. et al., 2012). In 1974, Lauterbur and Mansfield advanced the development of the technique (Lauterbur, 1973) with the spatial localization of the NMR signal, which provided the foundation of the MRI technique (Geva, 2006). Finally, the use of Fourier transformation, introduced by Ernst 1975, allowed rapid image reconstruction from NMR signals (Geva, 2006) and created the basis for the implementation of MRI as a routine clinical method.

Meier and Schild explain that MRI is mainly based on the magnetic properties of hydrogen (^{1}H) nuclei. ^{1}H possesses an inherent angular momentum or spin like other atomic nuclei with an odd number of protons or neutrons. As ^{1}H is a positively charged particle, this spin causes a magnetic moment. If a tissue or a body containing large number of ^{1}H is placed into a static magnetic field, net magnetization results parallel to this external field. This **longitudinal magnetization** (Figure 5A) is the sum of individual ^{1}H magnetic moments. Energy can then be transferred to this system by irradiation with a Radio Frequency (RF) Pulse in resonance to the ^{1}H nuclei. Some of the magnetic moments consequently assume a new position in the external magnetic field, what leads to a flip of the sum magnetic moment. Illustrated in a 3D coordinate system as a flip of the longitudinal magnetization vector into the xy-plane (Figure 5A), this new **transversal magnetization** induces an electromagnetic signal into an antenna

recorded in an MRI experiment known as the free induction decay (FID). After the RF pulse is switched off, the sum of the magnetic moments are again aligned with the external static magnetic field. In other words, longitudinal magnetization recovers and the transversal magnetization decays. The time it takes for longitudinal relaxation is known as the longitudinal or spin-lattice relaxation time **T1** and the signal decay is described with the transverse or spin-spin relaxation time **T2*** .In an MRI experiment, the RF pulse is applied several times. The time between two pulses is called the time of repetition (**TR**). Different tissues have a characteristic T1, thus after a short TR their longitudinal magnetization differs (Figure 5B). It is impossible to measure the FID directly when the RF pulse is switched on. Thus, an echo of the signal has to be generated at the time of echo (**TE**). This echo is induced in a **spin-echo-sequence** by applying a second 180° RF pulse (Figure 5C) and in a **gradient-echo-sequence** by inverting magnetic field gradients. By applying multiple echo pulses the signal decays slower than T2* with the time **T2** (Figure 5C) (Meier D. et al., 2012; Schild, 1990).

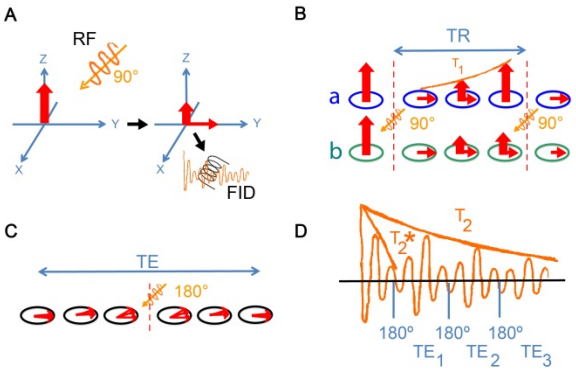

Figure 5: In MRI the transverse magnetization is measured

(A) Illustration of the net longitudinal magnetic moment (red vector), which stands parallel to the external magnetic field. A radio frequency (RF) pulse switches the net magnetic moment into the x-y plane resulting in a transverse magnetization (second red vector, right side). The transverse magnetization can induce a measurable signal in a transmitter coil, the Free Induction Decay (FID). **(B)** The time between two RF pulses is called time of repetition (TR). The recovery time of the longitudinal magnetization, known as T1 time, differs between tissues; illustrated here as tissue a (blue) and b (green). Depending on TR, a difference in the longitudinal and transverse magnetization between theses tissues result over time. **(C)** After the RF pulse is switched off, the protons diphase and the transverse magnetization disappear. A 180° signal can refocus the protons resulting in an echo signal. The time of echo (TE) refers to the time from the initial RF pulse until the echo appears. **(D)** Without echo pulses, the FID would decay with the time T2*. The 180° pulses are resulting in a prolongation of the signal with the time T2. Illustration in the style of *MRI made easy*, Prof. H. Schild (Schild, 1990).

Meier and Schild further explain, that in contrast to other imaging modalities, MRI allows the assessment of multi-dimensional information in a single scanning session. Basically, by altering TR or TE, either the proton density or the relaxation time T1 or T2 can be displayed, which are characteristic for different tissues (Figure 6A). A long TR and a short TE result in proton-weighted images (Figure 6B). In contrast, when a long TE is chosen, a strong T2 contrast results (Figure 6C). To record differences in signal intensity based on characteristic T1 times, sequences with a short TR and TE are used (Figure 6D) (Meier D. et al., 2012; Schild, 1990).

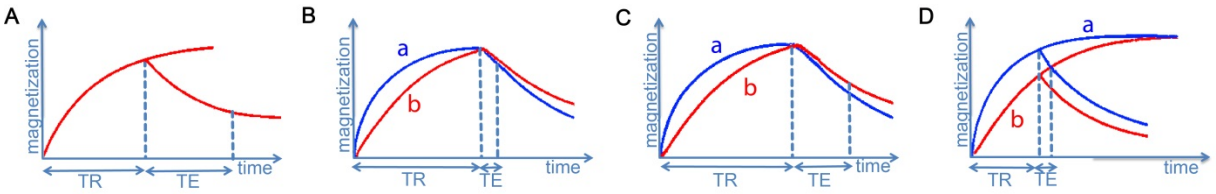

Figure 6: Image contrast depends on tissue characteristics and on the selection of TE and TR **(A)** Illustration of the longitudinal and the transversal magnetization in one graph. TR: Time of Repetition, TE: Time of Echo. **(B)** Tissue a (blue line) has a short T1 time, resulting in a fast recovery of the longitudinal magnetization and a short T2 time, resulting in fast decay of the transverse magnetization. In contrast, tissue b (red line) has a long T1 and T2 time. For an image determined by the proton density, the tissue a long TR and a short TE is selected. **(C)** A T2 weighted image has a long TR and a short TE. **(D)** If TR and TE are chosen short a T1 weighted image results. Illustration in the style of *MRI made easy*, Prof. H. Schild (Schild, 1990).

Important qualitative parameters of a MRI sequence are the signal to noise ratio (SNR), spatial resolution, the contrast to noise ratio and scanning time (Weishaupt et al., 2009). All these parameters are interconnected and influenced by each other (Figure 7A). The resolution is determined by the signal from a volume represented by a pixel on the MRI image. This volume is called a voxel and is determined by the size of its edges (Figure 7B). The smaller the voxel size, the higher the spatial resolution. In contrast, the voxel size is directly proportional to the SNR (Figure 7C). Thus, a large voxel results in good a SNR, but reduced spatial resolution. This can be compensated with a longer scan time. For example, optimization can be achieved by increasing the number of excitation (NEX), known as signal

averaging. The contrast to noise depends on the difference in the signal between two tissues and is indirectly proportional to the noise (Figure 7D).

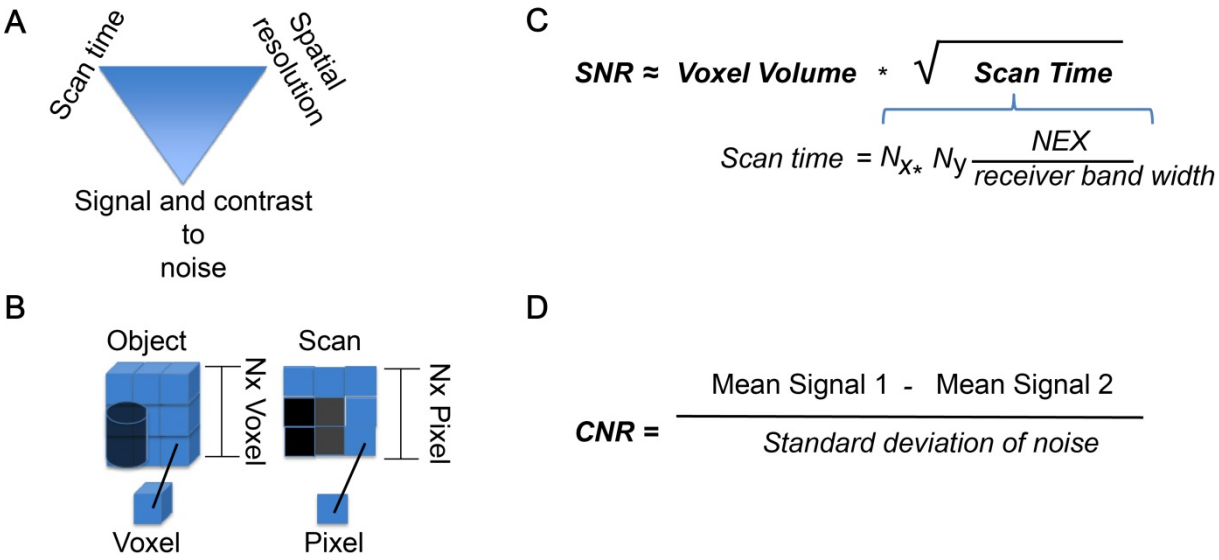

Figure 7: The signal to noise ratio is indirectly proportional to the spatial resolution
(A) Triangle illustrating the most important quality parameters in MRI: Scan time, spatial resolution, signal to noise and contrast to noise ratios. **(B)** A Pixel on a 2D MRI image represents the signal recorded from a 3D voxel measured in the object. The smaller the size of a voxel is chosen the higher the spatial resolution. **(C)** The signal to noise ratio is directly proportional to voxel volume and the square root of the scan time. The scan time depends on the number of voxels measured in the xy-plane, the number of excitations and the receiver bandwidth. **(D)** The contrast to noise ratio depends mainly on the difference in signal intensity between two tissues and is indirectly proportional to the standard deviation of noise.

DWI and FLAIR imaging as standard sequences in the diagnosis of CJD

In a multicentre study, Zerr et al. demonstrated the important role of MRI in the pre-mortem diagnosis of sCJD. Two sequences, fluid-attenuated inversion recovery (FLAIR) and diffusion-weight imaging (DWI) detected hyperintensities in basal ganglia and other cortical regions. DWI demonstrated a higher sensitivity over FLAIR and these signal abnormalities were rarely found in other proteinopathies like Alzheimer. Based on this MRI-CJD consortium the specified hyperintensities in FLAIR or DWI got included into the clinical pre-mortem diagnosis criteria for sCJD (Zerr et al., 2009). MRI has the additional potential to distinguish sCJD subtypes (Meissner et al., 2009) and DWI can detect changes as early as 3 weeks after the onset of symptoms (Shiga et al., 2004).

DWI measures the Brownian motion of molecules and thereby water diffusion properties across tissues (Meier D. et al., 2012). This sequence can detect stroke at an early phase, as diffusion becomes restricted very rapidly in ischemic brain tissue (Albers, 1998). The pathological correlate is known as cytotoxic edema, referring to the increase in intracellular water content due to an impaired function of the sodium pump (Albers, 1998). In contrast, the pathological substrate for the diffusion restriction in CJD remains unclear (Letourneau-Guillon et al., 2012). Mainly spongiform changes and altered molecular motion of water are proposed (Macfarlane et al., 2007). The initial hyperintensity disappears in the later stages of the disease (Matoba et al., 2001; Ukisu et al., 2005). Despite the frequent use of MRI in clinical diagnosis of CJD, the technique is infrequently applied to animal research in prion dissease, most likely due to biosafety issues.

Aims

After the detection of several TSE affecting animals and humans, decades of research have uncovered a dual pathological role of the prion protein. Neurodegeneration is a neuropathological hallmark of prion disease, but unlike the characteristic spongiform change, it is also found in other neurodegenerative diseases associated with amyloid formation of pathologically confirmed proteins (proteinopathies). The induction of acute neurotoxicity by antiprion antibodies represents a model to assess prion-mediated neurotoxicity. Biosafety issues do not affect this model system, which is an advantage for the application of a broader spectrum of techniques. In her PhD thesis, Tiziana Sonati substantially expanded our knowledge about antiprion mediated toxicity using cerebellar slice cultures (data will be summarized in subchapter: Results from modelling PrP^C mediated neurotoxicity *ex vivo*).

Aim 1: *In vivo* antiprion mediated toxicity has been mainly assessed by classical histology. The aim of **part I** of this thesis is to assess antiprion mediated neurotoxicity in living animals with MRI. I will first describe the **establishment** of the imaging protocol, then I will present central findings from the ex vivo system that were **verified** *in vivo* and lastly, I will present

data uncovering **NCX3** as a potential resource of rapid calcium influx upon administration of neurotoxic antiprion antibodies.

Aim 2: Antiprion antibodies represent one of the most promising therapeutic compounds in prion disease. However, reports about their neurotoxic potential underscore the need for caution. In recent years conflicting data have been reported about the neurotoxic potential of antiprion antibodies. The aim of the **part II** of this thesis is to evaluate the conflicting data and to address the question of the clinical relevance of the described toxicity.

PART I

Introduction

Results from modelling PrP^C mediated neurotoxicity *ex vivo*

Cerebellar organotypic slice cultures (COCS) have found to be a relevant tool in the investigation of various prion strains *ex vivo* (Falsig et al., 2008). During her PhD thesis, Dr. T. Sonati investigated antiprion mediated neurotoxicity using organotypic slice cultures in order to model pathologic PrP^{SC} interactions with PrP^C (Figure 8A). Based on this extensive research, antiprion mediated toxicity was found to be gene dosage dependent and the degree of toxicity modulated by the dose and duration of antibody treatment. The induced toxicity was found to be epitope specific, as FT ligands do not mediate these effects. In addition, neuronal PrP expression was sufficient for the induction of neurodegeneration. Several tests with antibody derivatives (monovalent $F(ab)_1$, divalent $F(ab)_2$ fragments and single chain variable fragment (ScFv) minibodies) demonstrated that it is unlikely that crosslinking of PrP is the cause of neurotoxic induction. Antibody mediated toxicity was shown to be caspase independent and ultrastructural analysis revealed non-necrotic but atypical apoptotic cell death.

Cerebellar slices from mice lacking a large part of the flexible tail including the OR, the $PrP_{\Delta 32\text{-}93}$ deletion mutant, were found to be resistant to the induction of antiprion mediated toxicity (Figure 8B).

In addition, antiprion antibodies binding to the FT were found to be non-toxic and protective upon the induction of antiprion mediated neurodegeneration. Accordingly, the conclusion was drawn that the FT is the effector domain of prion toxicity. In contrast cerebellar slice cultures from mice expressing a PrP construct, cultures depleted of CC2 were susceptible to the induction of PrP^C mediated neurotoxicity. Pharmacological inhibition studies uncovered the major contribution of reactive oxygen species (ROS) and calpains in the neurotoxic cascade downstream of PrP^C. A massive increase of intracellular Calcium ion (Ca^{2+}) was proposed,

but the source was not identifed.

Based on the observation that the synthetic PrP fragment 106-126 induces neurotoxicity in cultured cells, a similar model system had been proposed earlier (Forloni et al., 1993). However, these experiments were later challenged (Kunz et al., 1999) and the induction of neurotoxicity was not seen upon administration of these fragments into COCS (Sonati, 2013a).

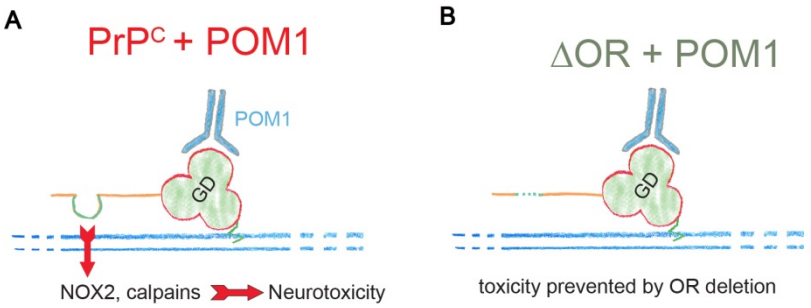

Figure 8: The FT hypothetically mediates the toxicity of antiprion antibodies **(A)** Ligands to the GD hypothetically model the neurotoxic induction found in bona fide prion induction. Antiprion antibodies binding the globular domain, like POM1, induce neurotoxicity mediated by the FT of PrP^C. Downstream of the cellular prion proteins, reactive oxygen species (ROS) and calpains mainly contribute to the cell damage. **(B)** Cerebellar slice cultures expressing an OR depleted form of PrP^C do not show antibody mediated neurotoxicity.

Oxidative stress is a mediator of prion disease

ROS, the radical or non-radical derivatives of oxygen play a role in molecular damage (Fatokun et al., 2008). ROS are spontaneously generated in the inner mitochondrial membrane, through the activity of the electron transport chain in the ER and enzymatically by nicotinamide adenine dinucleotide phosphate (NADPH) oxidases (NOX) or xanthine oxidases like the Ca^{2+} dependent nitric oxide synthase (NOS), which produce the free radical nitric oxide (Fatokun et al., 2008). Oxidative stress, which refers to excessive ROS levels, is an important mediator of neuronal degeneration in proteinopathies (Fatokun et al., 2008).

In TSE signs of oxidative stress have been demonstrated in the tissue of patients affected by CJD and in prion-inoculated mice (Choi et al., 1998; Guentchev et al., 2000; Ju et al., 1998). Additionally, oxidative stress has been described to be an early primary pathogenic effect in TSE (Brazier et al., 2006; Yun et al., 2006), providing evidence that oxidative stress, rather

than an unspecific phenomenon, is potentially a causative factor in the pathogenesis of prion disease.

Calpains are activated in TSE

Calpains are tightly regulated by Ca^{2+} cytoplasmatic cysteine protease, which can be divided into two species, Calpain-I (μ-calpain) and Calpain-II (m-calpain) (Suzuki, 2004). The above enzymes can be activated by either micromoles per litre or millimoles per litre, respectively (Suzuki, 2004). Calpains cleave only a restricted set of proteins, as N-methyl-D-aspartate (NMDA) receptor and α-spectrin (α-fodrin), participate in different signalling pathways (e.g. epithelial growth factor), in cellular transformation and tumorigenesis and mediate cell death (Croall and Ersfeld, 2007). In contrast to caspase 3, calpains are activated in various necrotic and apoptotic conditions (Wang, 2000).

Alzheimer brains show an increased level of activated calpains (Taniguchi et al., 2001). The involvement of calpains in TSE has been demonstrated in prion inoculated cerebellar slice cultures (Falsig et al., 2012).

Ca^{2+} homeostasis is altered in TSE

Calcium (Ca^{2+}) regulation systems are impaired in neurodegenerative disorders, leading to synaptic dysfunction, impaired plasticity and neuronal degeneration (Mattson, 2007). Ca^{2+} mediates neurotoxicity possibly by three different interactive cascades: first, through the activation of caspases; secondly, by the induction of oxidative stress; and thirdly, through the activation of pro-apoptotic enzymes (Mattson, 2007).

Calcium homeostasis has shown to be altered in TSE and is possibly regulated by the physiological aspects of PrP^{C} (Figure 9) (Sorgato and Bertoli, 2009). The demonstration of calpain activation in prion inoculated and in antiprion antibody treated cerebellar slice cultures indicates that increased calcium influx is an upstream event in TSE (Falsig et al., 2012). Additionally, there is evidence that oxidative stress renders neurons vulnerable to excitotoxicity, based on the overactivation of glutamate receptors (Mattson, 2007). Chronic

infection of neuronal cell lines with prions has been shown to reduce or eliminate bradykinin-activated increase in intracellular calcium concentration (Kristensson et al., 1993). Interestingly, it was found later that this process is linked to the reduction of the inositol triphosphate (IP3) second-messenger response (Wong et al., 1996). Increasing slowly over time, prion infection causes a dysfunction of voltage gated N-type calcium channels (VGCC) (Sandberg et al., 2004). The early release of calcium from the ER through the ryanodine receptor (RyR) and the IP3 receptor has been proposed as a mediator of neurotoxicity in prion disease (Ferreiro et al., 2008). Alteration of ER calcium homeostasis has also been found in prion infection models (Torres et al., 2010). Additionally, increased expression of the cytosolic calcium/calmodulin-dependent protein kinase two (CaM kinase II), important for long-term potentiation, has been found in prion infected mice (Jin et al., 1999).

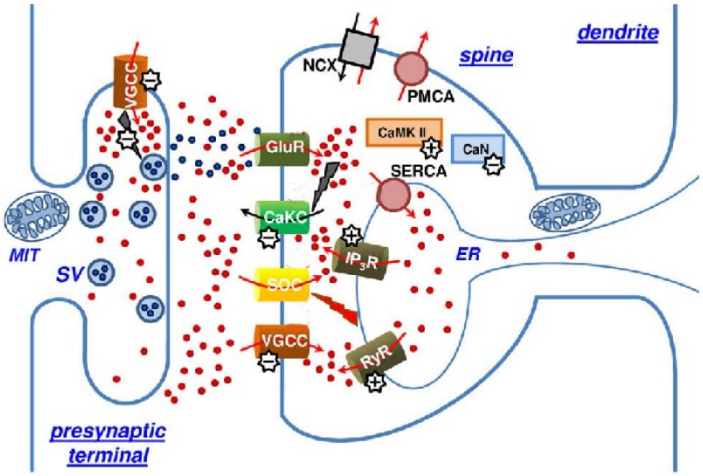

Figure 9: Alteration of calcium homeostasis upon prion infection

Illustration of prion down- (-) or up-regulated (+) Ca^{2+} dependent transporters or mechanisms. Affected transporters include Ca^{2+} channels responsive to inositol triphosphate (IP3), or ryanodine (RyR). Grey dashes point to activation events that normally take place when Ca^{2+} enters into the cell through voltage-gated Ca^{2+} channels (VGCC), or ionotropic glutamate receptors (GluR). This is the case of Ca^{2+} -activated K^{+} channels (CaKC) in postsynaptic membranes, and the fusion of synaptic vesicles (SV) in presynaptic terminals. The red dash indicates activation of store-operated Ca^{2+} channels (SOC) by depletion of ER Ca^{2+} stores. Also the expression of CaM kinase II, and of the phosphatase calcineurin (CaN), has been found to be affected in some models of prion disease. Conversely, to date, no association between alteration of calcium homeostasis and prion infection has been reported with respect to the Na^{+}/Ca^{2+} exchanger (NCX). Simillarly there is no effect either with plasma membrane Ca^{2+}-ATPase (PMCA) or mechanisms that control uptake and discharge from the Golgi network (not shown). Red and blue dots schematically represent Ca^{2+} ions and glutamate molecules, respectively. MIT: mitochondrion**.** Figure modified from Sorgato and Bertoli, 2009 with permission from Elsevier limited; Rightslink license number: 3485831120729, (Sorgato and Bertoli, 2009).

The bidirectional Na^+/Ca^{2+} exchanger (NCX), which exists in three different isoforms (NCX1, NCX2, NCX3) and is expressed in neurons and glial cells, plays an important role in intracellular free Ca^{2+} homeostasis, both in physiological and pathological conditions. Under physiological conditions, Ca extrusion via NCX is the dominant mechanism when a train of action potentials reaches the nerve terminal (forward mode). Under pathological conditions such as brain ischemia or A-β exposure (Pannaccione et al., 2012), the antiporter NCX3 has shown to be protective (Molinaro et al., 2008), by maintaining Ca homeostasis. However, an involvement of NCX transporters in prion disease has not been reported to date (Sorgato and Bertoli, 2009).

Manganese Enhanced Magnetic Resonance Imaging

Paramagnetic contrast agents generate magnetic moment 3-8 orders of magnitude stronger than the moment generated with the nuclei and accelerate T1 relaxation (Meier D. et al., 2012). For example, divalent ion manganese, which can enter excitable cells via a Ca^{2+} transport mechanism, is the basis for Manganese Enhanced Magnetic Resonance Imaging (MEMRI) (Silva and Bock, 2008). MEMRI has three major applications: (1) imaging of the neuroarchitecture based on the unique properties as an intracellular contrast agent, (2) mapping neuronal tracts in the living brain and (3) the demarcation of active brain regions (Silva and Bock, 2008). The technique has been used to measure a decline in axonal transport rates in an Alzheimer model (Smith et al., 2007). A manganese enhanced signal was reported in the cerebellum and hippocampus in the 1D4 mouse model, a cytosolic PrP expressing mouse line with corresponding neurodegenerative changes (Faas et al., 2010).

Outline

The concept of modelling the pathologic induction of neurotoxicity in TSE with antiprion antibodies is of interest due to several aspects. First, neurotoxicity is uncoupled from prion replication in this paradigm, allowing the investigation of this central hallmark of prion disease separate from prion replication. Secondly, this model solves a major biosafety issue in prion

research, which is a drawback of many other methods. Finally in the antiprion mediated model in contrast to prion inoculation, neurotoxicity is seen after days.

Here I have investigated whether antiprion mediated neurotoxicity can be used as a new bioassay *in vivo* to assess PrP mediated neurotoxicity. The aim was to develop a fast *in vivo* bioassay for prion disease, which circumvents biosafety issues. I have found MRI to represent a very useful technique to assess anti prion mediated neurotoxicity, since it allows precise quantification over time of lesion induction.

Based on this observation, I could demonstrate that antiprion mediated neurotoxicity is PrP^C expression level dependent and crosslinking independent *in vivo*. In fact, the latter was proposed as the mechanism of antiprion antibody toxicity in previous studies. Here I can provide an explanation for this discrepancy.

Oxidative stress is a crucial pathway that is activated upon antiprion antibody binding in COCS. I could verify this in my *in vivo* system and could additionally identify the NOX isoenzyme two as an important resource of ROS production.

Activation of Calpains points to an increase of Ca^{2+} in the cytoplasm. Here I provide evidence that NCX3 is the source of massive calcium influx upon antiprion antibody administration *in vivo*. Unexpectedly, NCX3 knockout mice had a shorter survival on prion infection than *wt* mice. This difference in the model system could point to important adaptive mechanisms in TSE upon chronic deregulation of calcium.

In our publication we identified the amino terminus as the executer of antiprion mediated neurotoxicity. The amino terminus consists of different functional units, which could be differentially involved in the induction of prion toxicity. We are now interested in how they regulate antiprion mediated neurotoxicity. In the last month of my doctoratal program I was working on the establishment of a new testing system that allowed the screening of different mutants. For this work I will provide an extended outlook at the end of Part I.

Results

Establishment of MEMRI

In order to visualize antiprion antibody toxicity *in vivo* in intact mice, I utilized the MEMRI parameters as a template that were established in a previous study (Faas et al., 2010) to optimize the scanning protocol. The imaging was performed on a Bruker PharmaScan® with a permanent magnetic field of 4.7 T (Figure 10A). To increase the signal to noise ratio, a ^{1}H mouse brain receive-only surface coil (Figure 10B) was used in combination with a transmission-only body coil. The position of the isoflurane-anesthetized mouse on the mouse-bed was optimized to reduce the distance between the receiver and the mouse head (Figure 10C and D). The mouse was warmed with a warming blanket during the scanning (Figure 10E).

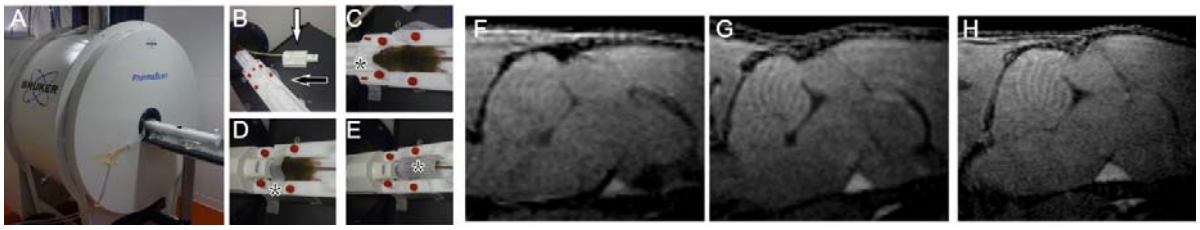

Figure 10: Establishment of scanning parameters.
(A) Image of the used Bruker PharmaScan® with a permanent magnetic field of 4.7 T. **(B)** To increase the signal to noise, a mouse surface coil was used to limit the spatial extend of the reception (white arrow). The black arrow points to the mouse bed. **(C)** Positioning of the anesthetized animal on the mouse bed. The star points to the cannula delivering isoflurane. **(D)** The surface coil was mounted on the mouse bed in a manner to allow maximal reception from the region of interest (here the cerebellum). **(E)** A warming blanket was used to prevent body temperature drop during scanning. **(F)** Representative sagittal image of a T1 weighted 3D-gradient echo sequence with a TE of 6 ms, TR of 50 ms using 10 averages at a voxel size of 120 µm x 120 µm x 120 µm. The mouse was ip injected with 37.7 mg/KG manganese 24 h prior to scanning. **(G)** The same scanning session and conditions were used as in F, with a decreased TE of 2.5 ms and TR of 15 ms to increase T1 contrast. **(H)** Maximally increased resolution at a voxel size of 78 µm x 100 µm x 156 µm. Images were generated within the same session as the images from G and F.

To enable exact volume measurements at a later timepoint, I used a 3D gradient echo sequence. Various TE, TR, average and voxel size were tested (Figure 10F and G) and the best results were finally achieved with a TE of 2.5 ms, TR of 15 ms, 10 averages at a voxel

size of 78 µm x 100 µm x 156 µm (Figure 10H).

Increasing anatomical contrast was found 24 h post intraperitoneal (ip) injection of rising single doses between 20–45 mg/KG of Manganese (Figure 11A). Discrimination of the cerebellar layers was found to be optimal with higher doses of the contrast agent. In order to reduce the toxic effects of manganese at high doses, I decided to utilize a fractionated injection protocol (Bock et al., 2008). A regime of six ip injections at 12-hour intervals was found to be optimal (Figure 11B).

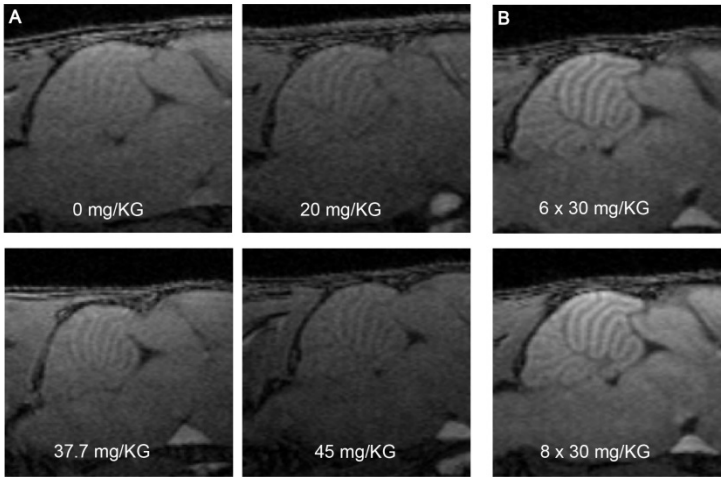

Figure 11: Fractionated manganese doses yield the highest anatomical contrast in the cerebellum.
(A) Representative images 24h post injection of increasing manganese single doses from 0 to 45 mg/KG ip injected into BL6 mice. **(B)** Representative images of mice injected with 6 fractions (12h interval) of 30 mg/KG manganese (upper panel). The same mouse was injected with two additional fractions of manganese (lower panel). Six fractions were found to be sufficient for appropriate contrast. Images were taken 24h after the last injection.

Volumetric quantification of MRI pictures

Stereotactic injection of antiprion antibodies *in vivo* induces a focal lesion (Solforosi et al., 2004). Therefore, volumetric quantification of this lesion seemed feasible. Towards this goal I produced eight volume phantoms out of polymer clay with different shapes and sizes (Figure 12A). In order to calculate the volume given the density, I weighted the phantoms. These were imaged with the established T1 weighted 3D gradient echo scan. From these images, I quantified the volume of the phantoms by either manual quantification using the ParaVision software (Version 5,Opl3, Bruker) or semi-automated segmentation by utilizing the Myrian® 3D diagnostic workstation. A regression analysis of the MRI based measurements was performed against the initial calculated volumes, which demonstrated a high accordance for both methods (Figure 12B and C). The volume difference estimated by the two models is

minimal (Figure 12D). Further analysis is based on the manual quantification using the ParaVision software.

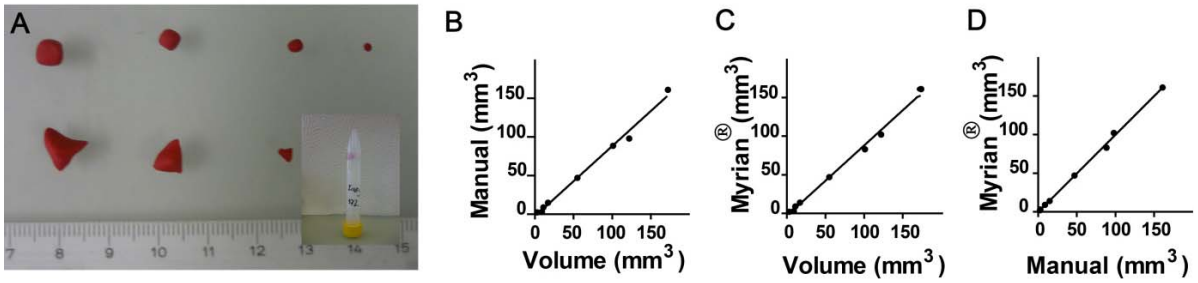

Figure 12: The established 3D gradient echo sequences can be used for an exact volumetric quantification.

(A) Volume Phantoms were generated with polymer clay. Upper row shows cube- shaped and the lower row angular-shaped objects of different sizes. **(B)** Prior to MRI measurement volume phantoms were hardened in the oven and embedded into low melting agarose. **(C)** Linear regression analysis of manual volume measurements (R^2: 0.992; slope: 0.909 ± 0.032). **(D)** Linear regression analysis of semi-automated quantification with Myrian® (R^2: 0.994; slope: 0.912 ± 0.029). **(E)** Linear regression analysis of Myrian® data versus semi-automated quantification (R^2: 0.998; slope: 1.001 ± 0.018).

Intra-cerebellar injection of antiprion antibody leads to rapid lesion induction

Intracerebral stereotactic injections were used to investigate antiprion mediated toxicity *in vivo* in a previous study (Klöhn et al., 2012; Solforosi et al., 2004; Song et al., 2008). These studies used histology as a qualitative read-out without quantitative analysis. After the successful establishment of the MEMRI protocol and volumetric quantification, we decided to use the system to visualize and quantify antiprion mediated lesion induction over time *in vivo*. PrP-overexpressing mice (*tga20*) (Fischer et al., 1996) were ip injected with fractions of manganese prior to antibody injection. I used a motorized stereotactic frame to inject 6 µg (dissolved in 2 µl, 20 µM) of the antiprion antibody POM1 or immunoglobulin G (IgG)-control into the fourth folium of the cerebellum (Figure 13A) of *tga20* mice. After recovery from anesthesia, an ataxic gait was seen in POM1 injected mice in contrast to IgG injection, where ataxia was not observed. These symptoms were strongest within the first hours after injection and disappeared within two days. Upon MEMRI examination, a large hypointense signal was found 24 and 72h post intracerebral injection (p.i.i.) on MRI examination (Figure 13B and E). Volume of signal alteration was greatest at 24h decreased somewhat thereafter (Figure

13E). In order to control for anatomical differences of cerebellar size between mice, the lesion volume was normalized against cerebellar volume (here and henceforth). As the previous investigation of antiprion toxicity *in vivo* is based upon histological analysis mice were euthanized after the last scan and the cerebellum was examined histologically with H&E stained paraffin step sections (100 µm steps). On comparison of the H&E sections 72h p.i.i. with the corresponding MRI image plane 24h p.i.i., I found good correlation in assessing the area of lesion induction (Figure 13B). On higher magnification, numerous granular cells with pyknotic nuclei were found within the lesion (Figure 13D). The morphological description is similar to previous reports (Solforosi et al., 2004).

To control for the possibility of vehicle contamination inducing toxicity, *Prnp*$^{o/o}$ was additionally injected with POM1. In contrast to *tga20* mice, evidence of lesion induction other than needle tract was not found in these mice (Figure 13C and E). As lesions were found to be maximal at 24h, I performed additional early time-point scans 4h p.i.i. A marginal hypointensity could be recorded at this time point in *tga20* mice (Figure 13D), indicative of rapid lesion induction.

The narrow lamina of hyperintense signal, hypothesized to correspond to the Purkinje cell layer, (Faas et al., 2010) is still present at 72h (Figure 11D). This observation is unexpected if the neurons were to undergo cell death; however, Purkinje cells in *tga20* mice lack transgene expression (Fischer et al., 1996) and therefore escape antibody mediated toxicity. Thus, the persistence of the hyperintense lamina confirms that the signal likely arises from Purkinje cells.

Antiprion antibody mediated toxicity have been found to be prion protein expression level dependent. Thus, I next injected POM1 intracerebral into *wt* mice (BL6 is not otherwise stated). A six fold smaller hypointense lesion could be detected 24h p.i.i (Figure 13D), illustrating the antigen expression level dependence of antiprion antibody induced toxicity *in vivo* (Figure 13E).

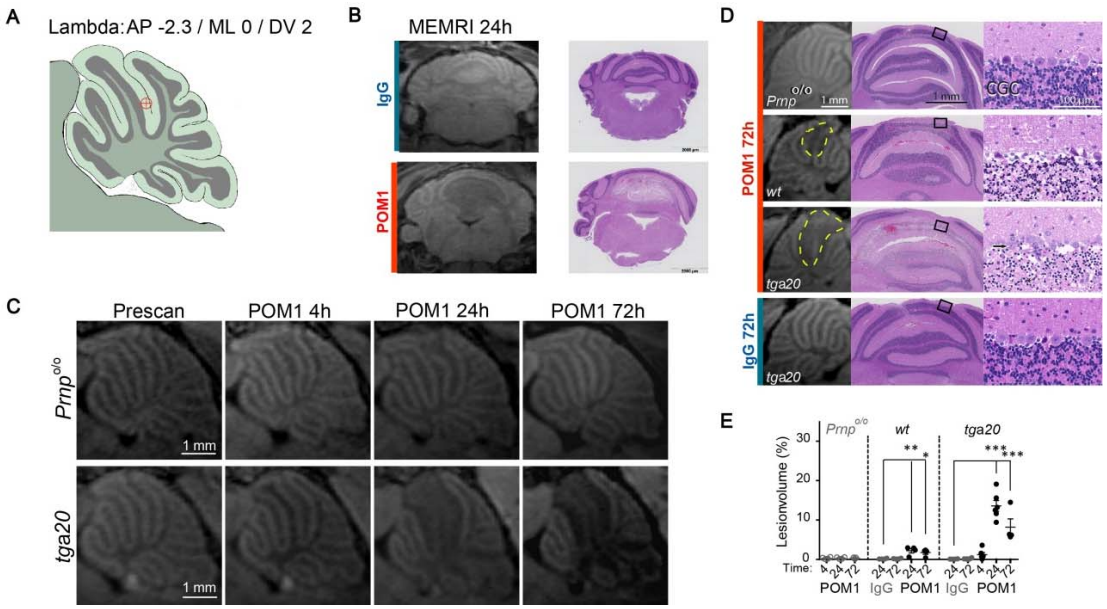

Figure 13: MEMRI volumetry is an efficient tool to quantify antiprion antibody mediated toxicity **(A)** Schematic representation of the murine cerebellum. The crosshair (red) denotes the site of the injection. **(B)** MEMRI scans showed a hypointense lesion in the POM1-treated (6 µg in 2 µl) mouse 24h post intracerebellar injection in contrast to IgG control injection (left panel). Structural tissue alterations are found on corresponding low-resolution coronal haematoxylin & eosin (H&E)-stained 72h p.i.i. micrographs. **(C)** Representative sagittal MRI scans before injection (prescan) and at 4h, 24h, and 72h after POM1 injection in *tga20* and Prnp$^{o/o}$ mice. In *tga20* mice, incipient edema was recognized as marginal hypointensity already at 4h. After 24h and 72h, hypointense lesions were fully developed and involved several folia. In contrast, POM1 injected Prnp$^{o/o}$ mice showed only a small focus of hypointensity along the needle tract. **(D)** Representative images of POM1-treated wild-type (WT) and *tga20* mice (left panels) 72h post intracerebellar injection. Yellow dashed lines delineate the lesions. Histology (middle and right panels) revealed CGC destruction (asterisks) and edema. Inset rectangles in the middle images indicate the regions magnified in the corresponding panels on the right. *Tga20* Purkinje cells (arrow), which do not express PrP^{C}, were largely preserved. **(E)** Lesion volumes at 4h, 24h and 72h post intracerebellar injection as percentages of total cerebellar volumes in wild type, tga20 and Prnp$^{o/o}$. Grey: control injections (6 µg, mean±s.d., n=4 except for Prnp$^{o/o}$ at 72h n=3, *tga*20 at 4h and 24h n=6,one-way ANOVA with Dunnett's post-hoc test).

To gain additional histological information, I euthanized some of the mice at earlier or later time point than 72h post injection. As already detected on the MEMRI images, early morphological alterations with chromatin condensation can be found as early as 5h (Figure 14A). Interestingly these early alterations have not been detected in the pervious study in *wt* mice, which may be an indication that prion protein expression levels have an influence on

the kinetics of lesion induction. At 24h mainly spongiosis and loosening of the tissue were seen, most likely indicative of edema formation (Figure 14B). The formation of true spongiform vacuoles was less well-defined. Mild macrophage infiltration as a minimal inflammatory reaction was noted (Figure 14B). A strong reactive astrocytic reaction was seen initial (Figure 14B) and later prominent Bergmann gliosis (Figure 14C).

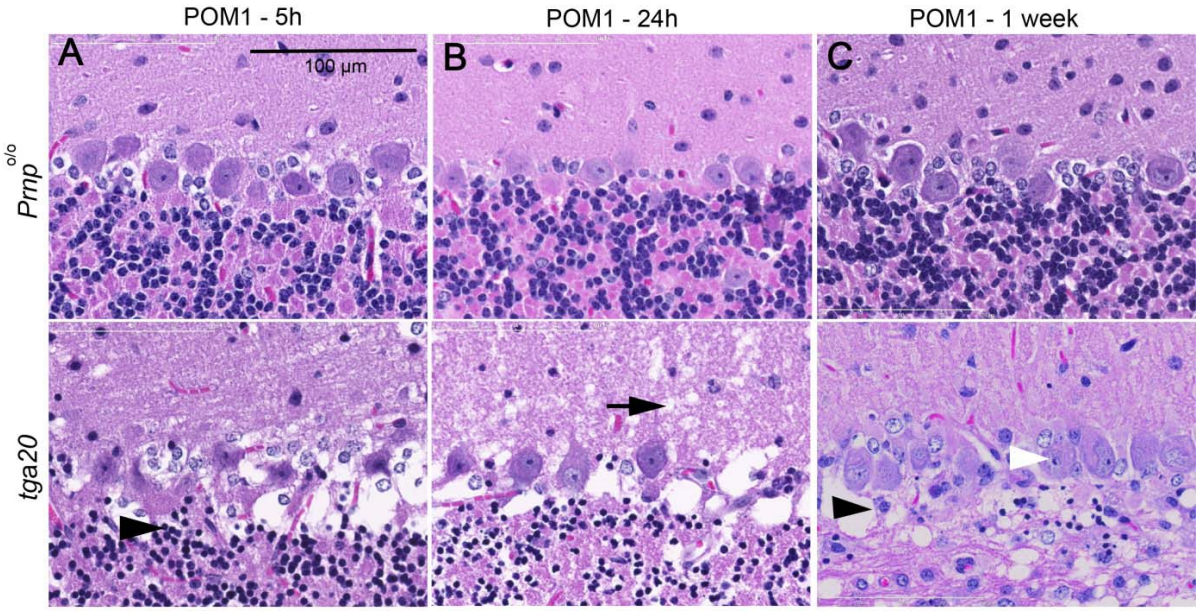

Figure 14: Representative haematoxylin-eosin sections from POM1-injected tga20 and *Prnp*$^{o/o}$ mouse cerebella.
(A) Chromatin condensation in cerebellar granular cells (black arrowhead) was seen as early as 5h post-injection. **(B)** Progression to edema and macrophage infiltration (black arrow) was seen after 24h. **(C)** One week post injection, prominent loss of granular cell neurons and brisk Bergmann glia proliferation (black arrow) were evident. The differential survival of Purkinje neurons (white arrowheads) is consistent with the lack of PrP^{C} expression in Purkinje neurons of *tga20* mice.

Difference in cerebellar volume is dependent on genetic background and not on prion protein expression

After normalizing the lesion size against cerebellar volume, I quantified the cerebellar volume of mice expressing PrP^{C} at different levels. For Zürich-I *Prnp*$^{o/o}$ (mixed genetic background BL6 and 129, BL6.129) I found a mean cerebellar volume of 66.2 mm^3, which was significantly larger than the mean cerebellar volumes of BL6.129-*tga20* (mean: 53.8 mm^3, Figure 15A). To assess if the mixed genetic background was confounding the results, I

quantified the cerebellar volume of *Prnp*$^{o/o}$ backcrossed for several generation with BL6 mice, which were found to be comparable to BL6.129-*tga20* mice. Additionally, cerebellar weights between coisogenic Edinburgh 129-*Prnp*$^{-/-}$ (Manson et al., 1994) and its 129-*Prnp*$^{+/-}$ and 129-*Prnp*$^{+/+}$ littermates did not differ (Figure 15B). The influence of 129 background on cerebellar volume is illustrated by the comparable cerebellar weights of BL6.129-*Prnp*$^{°/°}$ and 129-*Prnp*$^{-/-}$ in contrast to BL6.129-*tga20* (Figure 15B). The weight measurements of the cerebella correlate closely with the measured volumes based on the MEMRI dataset.

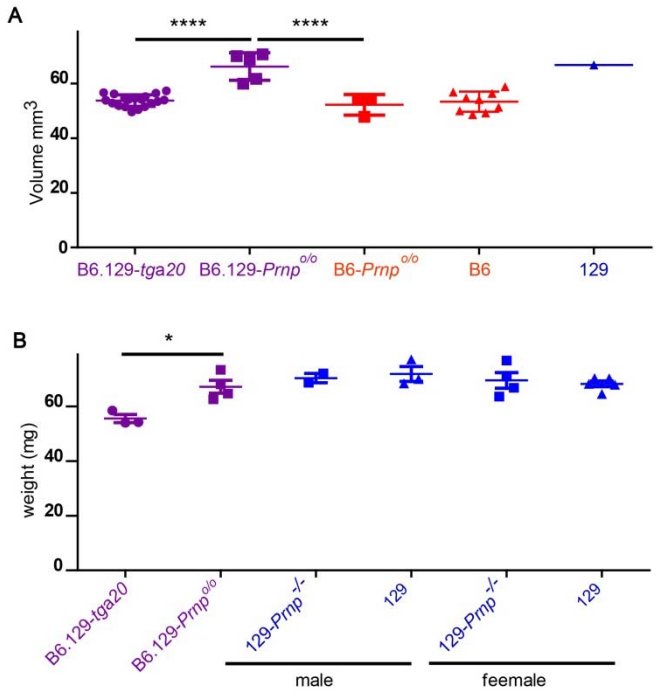

Figure 15: Genetic background confounds cerebellar volume between *tga20* and *Prnp*$^{o/o}$

(A) Volumetric measurement of cerebellum based on MEMRI enhanced scans of male *tga20* (n=19), *Prnp*$^{o/o}$ (n=4) mice on a mixed BL6.129 background (violet), of *Prnp*$^{o/o}$ backcrossed for several generation to BL6 (n=3) and of BL6 inbred mice (n=9) and one 129 mouse. Whereas there is a significant difference between BL6.129-*tga20* and BL6.129-prnp$^{o/o}$, there is no difference between BL6.129-*tga20* and BL6-*Prnp*$^{o/o}$. Cerebellar size in BL6.129-*Prnp*$^{o/o}$ mice on a mixed genetic background are potentially comparable to inbred 129 mice as indicated by a single measurement (One-way ANOVA with Tukey's post-hoc test). **(B)** Cerebellar weight of BL6.129-*tga20*, BL6.129-*Prnp*$^{o/o}$ males and of 129-*Prnp*$^{-/-}$ (Edbg) separated according to gender. Whereas a significant difference between BL6.129-*tga20* and BL6.129-*Prnp*$^{o/o}$ was found, there is no difference between cerebellar weights of 129-*Prnp*$^{-/-}$ in comparison to their 129-*Prnp*$^{+/+}$ littermates (One-way ANOVA with Tukey's post-hoc test).

Antiprion mediated neurotoxicity is crosslinking independent and neuronal PrP^{C} expression dependent *in vivo*

In contrast to the initial report (Solforosi et al., 2004), antibody mediated toxicity has been found to be independent of PrP crosslinking in cerebellar slice cultures (Sonati, 2013b). Therefore, I injected ScFv^{POM1} (2 µg in 2 µl, 40 µM) intracerebellar into BL6, *Prnp*$^{o/o}$ and

tga20 mice. As for whole antibody, an expression level dependent lesion induction was found (Figure 16). To demonstrate that vehicle components are not responsible for lesion induction, I additionally tested ScFv^{POM1} pre-incubated with its corresponding antigen (recombinant murine PrP, rmPrP), which was was found to be innocuous (Figure 16).

Since antiprion mediated neurotoxicity was found to be epitope specific in cerebellar slice cultures, I next administered the ScFv^{POM2} intracerebellar into *tga20* mice without a hypointesive lesion induction (Figure 16).

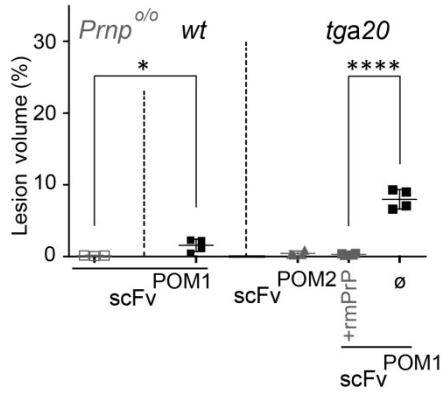

Figure 16: Antiprion mediated lesion induction *in vivo* is epitope specific and independent of PrP crosslinking
Lesions occurred in *tga20* (n=4) and wild-type (n=4) mice after injection of ScFv^{POM1} (2 µg) but not after ScFv^{POM2} (n=4), or ScFv^{POM1} (2 µg) preincubated with recombinant murine PrP (rmPrP, residues 23–230) (molar ratio 1:5, 24h, n=4). ScFv^{POM1}-treatment was innocuous to Prnp$^{o/o}$ (n=3) mice: ⦸ no recombinant prp added (mean±s.d., two-tailed Student's t-test).

PrP expression on neurons is required for antiprion mediated neurotoxicity, as demonstrated by the relative preservation of Purkinje cell in *tga20* mice. To investigate if PrP expression on neurons is sufficient for lesion induction *in vivo,* I utilized NSE-PrP mice, which express PrP under the neuron-specific enolase promoter (Radovanovic et al., 2005). Upon ScFv^{POM1} injection (3 µg in 2 µl), significant lesion induction was found in four mice in contrast to *Prnp*$^{o/o}$ mice (Figure 17). It should be emphasize that the size of lesions with a mean of 6.8% of the cerebellar volume is significantly larger than the mean of lesion induction in *wt* mice (at 3 µg, Figure 18) despite equal PrP expression (p=0.0003) (Sonati, 2013b). One explanation could be that other cellular elements such as glial cells absorb less neurotoxic antibody.

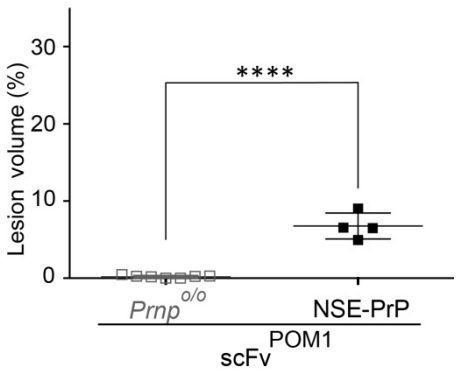

Figure 17: Neuronal prion protein expression is sufficient for lesion induction.
MEMRI volumetry (24h post intracerebellar injection) of neuron-specific enolase (NSE) NSE-PrP (NSE promoter driving specifically neuronal PrP expression) (n=4) and *Prnp*$^{o/o}$ (n=7) mice injected with ScFv^{POM1} (3 µg; mean±s.d., two-tailed Student's t-test).

CC2 depleted mice are hypersensitive to antiprion mediated neurotoxicity

Next I injected ScFv^{POM1} (3 µg in 2 µl, 60 µM) into the cerebella in mice that express a PrP form with a larger deletion in the FT including the OR, the PrP$_{\Delta 32–93}$ (Figure 18). As in COCS these mice were found to be resistant to antiprion mediated toxicity *in vivo*. In contrast 24 h post injection of ScFv^{POM1} large hyperintensive lesions were found in PrP$_{\Delta 94\text{-}110}$ (Figure 18). These mice are CC2-depleted and express the construct in similar amounts as wt mice (Sonati, 2013b). In addition to mild ataxia, these mice presented with repetitive movements of the forelimbs. MEMRI scans 48h post injection revealed a three-fold increase in lesion size.

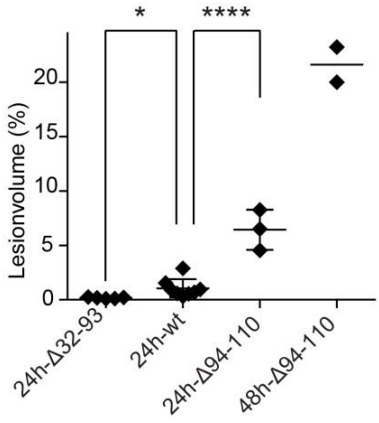

Figure 18: Depletion of larger segments of the FT prevents antiprion mediated neurotoxic induction in vivo
MEMRI volumetry 24h post intracerebellar injection of ScFv^{POM1} injected into PrP$_{\Delta 94–110}$ (L52, n=3), PrP$_{\Delta 32–93}$ (n=5) and wild type (n=8). An additional scan for the PrP(Δ94–110) mice got performed 48 h post injection, where a threefold increase in lesion size was found (mean±s.d.; two-tailed Student's t-test).

Monovalent fragment antigen mediates neurotoxicity

Initially no toxicity was observed upon injection of monovalent F(ab) fragments from toxic anti prion antibodies *in vivo* when the antibody was injected in the same dose as the whole antibody (Solforosi et al., 2004). Thus I injected $F(ab)_1$POM1 and $F(ab)_1$POM19 at a concentration of 60 µM (6 µg in 2 µl, 1:3 molar ratio in comparison to holoantibody injection) intracerebellarly into BL6 mice. Since whole antibody has two binding sides, a higher concentration was chosen. Upon MEMRI volumetric analysis, significant lesion induction was found only for $F(ab)_1$POM19 (Figure 19). $F(ab)_1$POM1 however, induced small hyperintense lesions (Figure 19). It is likely that $F(ab)_1$POM1would have induced significant toxicity at higher concentrations, indicative of a different kinetic of $F(ab)_1$ fragments in contrast to whole antibodies and single chains.

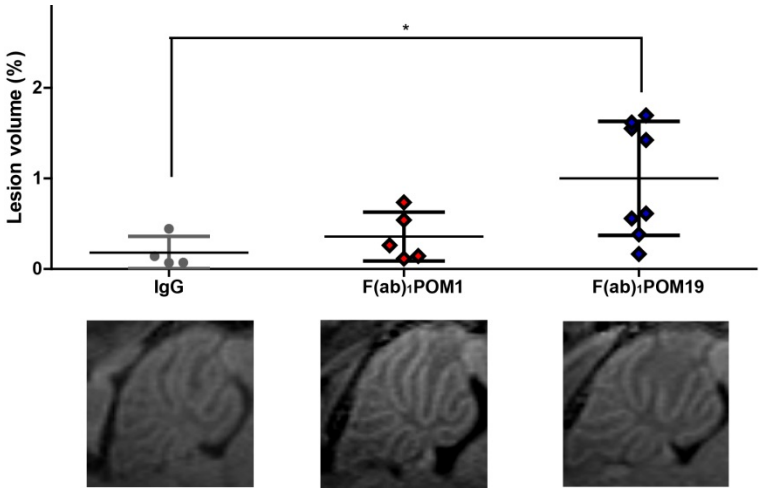

Figure 19: Significant lesion induction is found upon injection of $F(ab)_1$POM19, but not upon $F(ab)_1$POM1 injection

Intracerebellar injection of $F(ab)_1$POM1 led to the induction of small hypointense areas (star) in two out of five mice. Volumetric quantification against IgG injection revealed no significant difference. In contrast, $F(ab)_1$POM19 injection (n=8) led to significant lesion induction in contrast to IgG control (one-way ANOVA with Tukey's post-hoc test).

NADPH oxidase 2 is the major resource of reactive oxygen species

Ascorbate and N-Acetyl Cysteine (NAc) was neuroprotective against POM1 induced neurotoxicity in cerebellar slice cultures. I therefore administered the antioxidant acetylated hydroxytyrosol (AcHyt), which has been shown to cross the blood-brain barrier (Granados-Principal et al., 2010), in the drinking water to *tga20* mice. Seven days after the start of the treatment, I injected $ScFv^{POM1}$ into the cerebellum and found significant lesion induction in only one of six AcHyt treated *tga20* mice (Figure 20A and B).

The compound 1400W blocking the NOS 1 and 2 has been found to be non-protective in antibody mediated neurotoxicity *ex vivo* (Sonati, 2013b). In contrast, the NOX2 inhibitor diphenyleneiodonium chloride (DPI), suppressed a superoxide spike induced in antiprion treated slices, indicative that the superoxide source are NADPH oxidases (Sonati, 2013b). I therefore utilized the NOX2 deficient mice ($NOX2^{o/o}$) (Sorce et al., 2012) to study the involvement of this electron transporter upon neurotoxic antiprion antibody injection *in vivo*. Significantly smaller lesions developed in $NOX2^{o/o}$ mice upon POM1 injection than in wild type control (BL6J; Figure 20C).

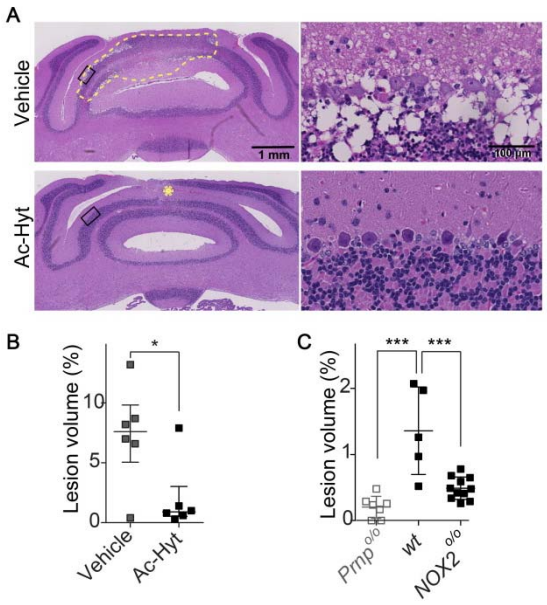

Figure 20: ROS are major mediators of antiprion mediated neurotoxicity *in vivo*

(A) Representative H&E histology of mice pretreated with acetylated hydroxyltyrosol and injected with $ScFv^{POM1}$. Haematoxylin-eosin stained sections of mouse cerebella. Whereas vehicle-treated mice developed large areas of cell death around the site of injection (yellow dashed line), only small lesions were visible in treated mice in the immediate vicinity of the needle tract (yellow asterisk). Rectangles indicate the position of high magnification pictures shown in the panels on the right. **(B)** *Tga20* mice 24h post intracerebellar injection of $ScFv^{POM1}$ (2 µg) and pre-treated with AcHyt (mean±s.d., n=56, one-tailed student t-test. P=0.013). **(C)** MEMRI volumetry at 24h post intracerebellar injection of $ScFv^{POM1}$ (3 mg) injected into $Prnp^{o/o}$ (n=7), wild-type (n=5) and NOX2-deficient (n=11) mice (mean±s.d., one-tailed Student's t-test).

Hippocampal lesion induction can best be visualized with DWI

Since distinct prion strains target different brain regions, we therefore were interested in injecting antiprion antibodies in brain regions other than the cerebellum. Hippocampal lesion induction has been previously described (Solforosi et al., 2004) and allows simultaneous bilateral injection. The latter is an advantage as control injections can be performed in the same mouse, thus drastically reducing the number of animals needed for experiments.

After injecting POM1 into different coordinates, including injection into the cornu ammonis region one (CA1) as previously performed (Solforosi et al., 2004), the stereotactic

coordinates anterior-posterior (AP): -2; middle line (ML): 1.7; dorsal-ventral (DV): 2.2 from, allowing injection between the cornu ammonis region three (CA3) and the dentate gyrus (DG) were chosen for further injections (Figure 21A). Forty-eight hours after administration into the left side of POM1 or D13, a loss of manganese signal was found not seen upon IgG control injection (Figure 21B and C). While MEMRI contrast in the dentate CA3 was found to be optimal for quantification, less manganese contrast is seen in the cornu ammonis regions 2 and 3 (Figure 21C). Therefore, estimation of the total lesion size was found to be difficult and I decided to quantify the manganese enhanced DG and CA3 volumes on both sides (Figure 21B). As a technical control, I quantified the contralateral non-injected hippocampus. Histological examination after 38 h revealed neurotoxic induction corresponding to the region that showed reduction of manganese contrast (Figure 21C).

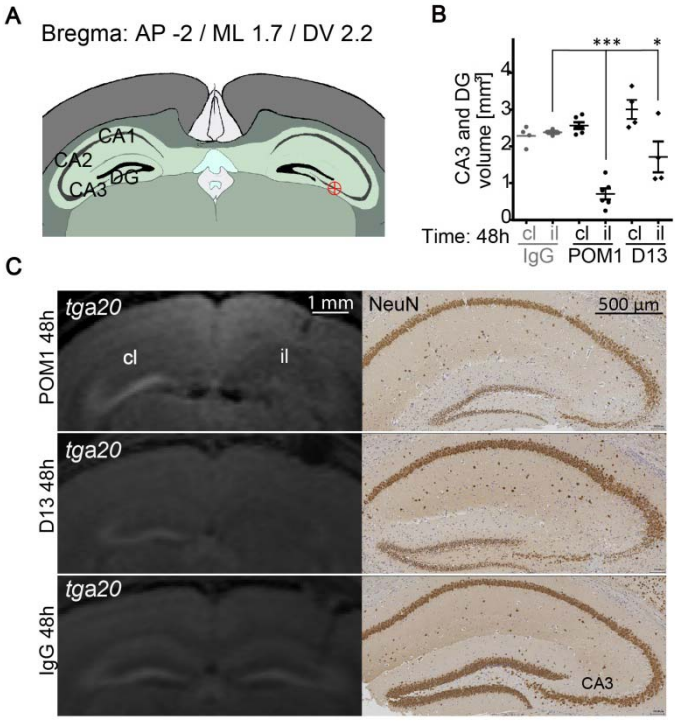

Figure 21: MEMRI is limited in the assessment of hippocampal lesion induction

(A) Schematic representation of the murine hippocampus. Crosshairs (red) denote the site of injection. CA1-3: Cornu ammonis sectors 1-3. DG: Dentate gyrus. **(B)** Volumetric assessment of the size of CA3 and DG (mm^3) ipsilateral (il) and contralateral (cl) to antibody injection in *tga20* mice (48h post injection). Both POM1 and D13 led to a reduction in CA3 volume ipsilaterally. (Data are presented as mean ± s.d., n=4, One-way ANOVA with Dunnett's post-test, *** P<0.001, *P<0,1) **(C)** MEMRI (left panels) showing loss of the CA2-3 contour and appearance of a hypointense lesion ipsilateral (il) to the site of POM1 and D13 injections, whereas the contralateral site (cl) did not show lesions after IgG injection. Histological analysis 48h post injection (right panels) showed loss of NeuN-positive neurons in the dentate gyrus and in the CA3 sector after POM1 and D13 injection.

MEMRI based hippocampal lesion quantification is technically limited and the repetitive ip injections needed for adequate contrast are challenging for experimental animals. Therefore, I assessed the use of DWI in the antibody mediated neurotoxicity model *in vivo*. Gradient-echo sequences instead of spin-echo sequences were established due to troublesome artefacts in the latter. As early as one hour post injection of the $F(ab)_1$POM1 (8 µg in 2 µl, 80 µM), diffusion restriction could be recorded in the DG and CA3 regions of *tga20* mice (Figure 22A). The hyperintensive signal appears as a sharp line corresponding to the shape of the neuronal layer, mainly of the DG and to some extends the CA3. No such signal alterations were observed contralateral to the injection site with the same dose of $F(ab)_1$POM1 preincubated with its specific antigen. Four hours post injection, the signal was similar in size but blurred (Figure 22A and B). As DWI images are influenced by differences in T2 contrast, this blurring is most likely induced by extra-neuronal edema formation. For analysis, I have chosen the volumetric quantitative analysis previously described for MEMRI quantification. Lesion volume was normalized over hippocampal volume. The analysis demonstrated significant signal alterations at both time points (Figure 22B). Upon POM1 injection a mean of 2 mm^3 of the DG and CA3 region were damaged as assessed by MEMRI. At one-hour post injection, a mean lesion induction of 2.8 mm^3 was found. These data demonstrate that *in vivo,* monovalent $F(ab)_1$ fragments induce similar damage at a four times higher concentration than whole antibody (80 µM $F(ab)_1$ POM1 in contrast to 20 µM POM1). As whole antibody has two binding sites, a two fold higher concentration would have been expected. This is probably explained by kinetic properties of the $F(ab)_1$ fragments like diffusion.

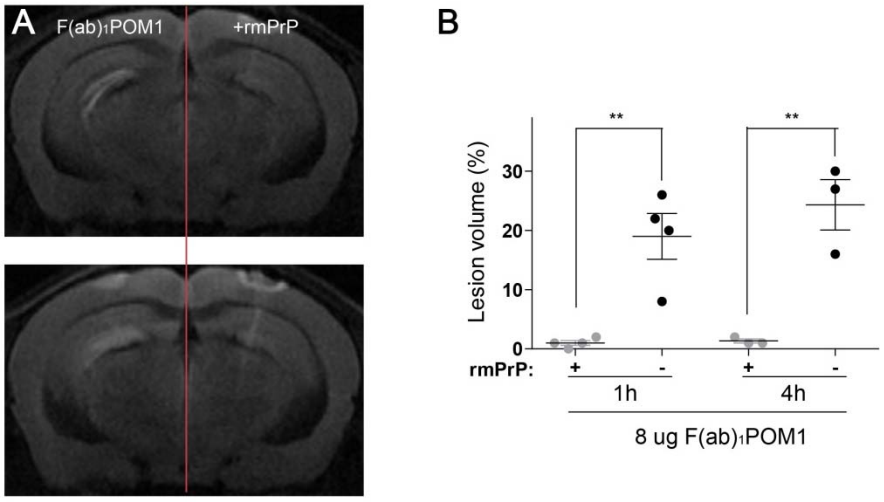

Figure 22: Early Diffusion restriction is seen after F(ab)$_1$ POM1 DG injection in *tga20* mice

(A) As early as one hour post injection of F(ab)1 POM1 into the DG of *tga20* mice a sharp hyperintense line is seen on DWI images. The signal developed into a hyperintense area 4h post injection. No such hyperintense signal was found upon injection of F(ab)$_1$ POM1 preincubated with its rmPrP into the contralateral side. (B) Volumetric quantitative analysis revealed a significant lesion induction at both time points. The standard deviation in this experiment was: 7.6. Grey: control injections (8 µg, mean±s.d., n=3, one-way ANOVA with Tukey's post-hoc test).

Non-significant lesion induction was found upon injection of 6 µg F(ab)$_1$ POM1 into the cerebellum of BL6 *wt* mice. To investigate if significant toxicity can be induced upon injection of higher concentration, I injected 8 µg of F(ab)$_1$ POM1 into the hippocampus. As in *tga20* mice, a hyperintensive lesion was found one-hour post injection in contrast to the control injection on the contralateral side, which blurred out over 24h (Figure 23A). However, quantitative analysis of lesion volume, on the basis of a small group size of n=3, revealed a slight trend but no significant lesion induction (Figure 23B). The lesion size in one mouse was with 18% definitely greater than the control injection (3%), indicative for a negative effect. The high variance seen may again be related to differences in diffusion kinetics.

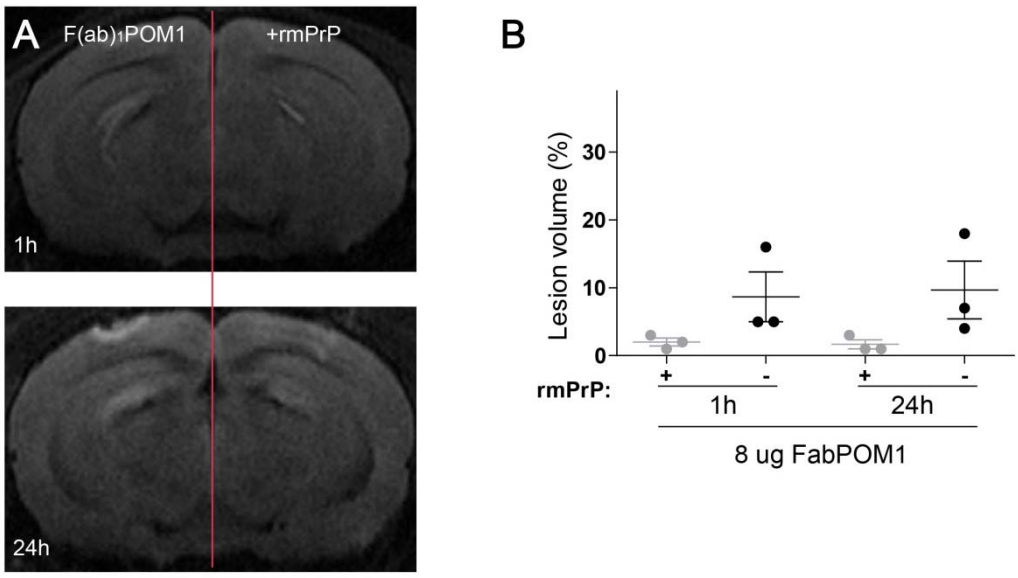

Figure 23: Lesion induction upon 8 µg F(ab)$_1$ POM1 injection into the DG of BL6 mice

(A) Diffusion restriction recorded in selected mice 1-hour and 24-hour post injection after 8 µg F(ab)$_1$ POM1. On control injection to the contralateral side, F(ab)$_1$ POM1 preincubated with rmPrP, no hyperintense signal was found within the parenchyma. One hour post injection, minimal hyperintense signal alterations were recorded in the ventricle wall (star) upon control injection. (B) The induced lesion in n=3 mice was not significant upon volumetric analysis. The standard deviation in this experiment was: 7.3%, one-way ANOVA with Tukey's post-hoc test

---

Calpain is activated upon antiprion mediated toxicity *in vivo*, but neither Calpastatin overexpression nor treatment with E64d was protective

The involvement of the cysteine protease calpain in driving neurotoxicity was demonstrated in prion infected COCS (Falsig et al., 2012). In the antibody mediated toxicity model, activation was demonstrated with the detection of the characteristic α-fodrin (α-spektrin) cleavage pattern at 145 kDa (Wang, 2000), as well as the pharmacological inhibition with the cysteine-protease Calpeptine, an aldehyde inhibitor. α-fodrin immunoblot on cerebellar homogenates from either ScFv^{POM2} or ScFv^{POM1} injected *tga20* mice, revealed identical characteristic proteolytic fragments pointing to calpain activation (Figure 24A). Therefore, I decided to perform a treatment experiment with the cell-penetrating calpain inhibitor E64d (Loxastatin) an oxirane inhibitor (Mehdi, 1991). The substance has previously been successfully used to inhibit neurotoxicity in prion infected COCS (Falsig et al., 2012) and could reduce infarct volume from middle cerebral artery occlusion *in vivo* (Tsubokawa et al., 2006). I decided to administer E64D (5 mg/KG) or vehicle ip 4 hours before induction of

antiprion mediated neurotoxicity using 2 µg of $ScFv^{POM1}$ and analyzed lesion induction based on MEMRI volumetry. No significant difference was found between the treated versus the untreated group (Figure 24B).

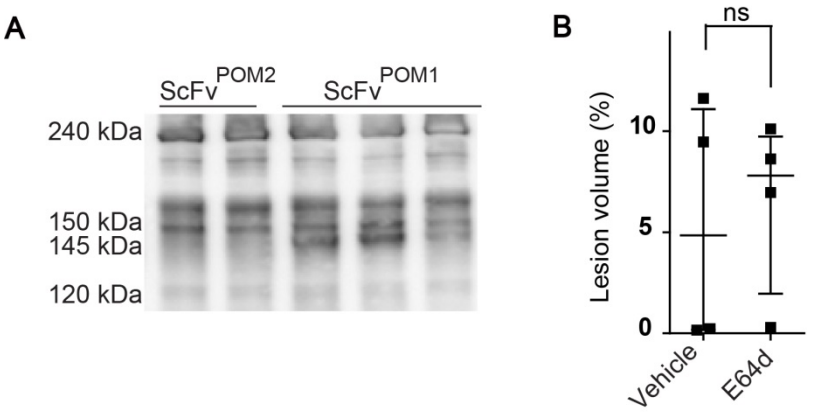

Figure 24: Immunostaining for Fodrin indicate calpain mediated α-cleavage

(A) Western blots of cerebellar homogenates from $ScFv^{POM1}$ injected *tga20* mice (24 hours pi) showing increased 145 kDA α-fodrin cleavage in contrast to $ScFv^{POM2}$ injected. Full-length fodrin at 240 kDa. **(B)** *Tga20* mice were pre-treated with E64D (5mg/KG) or vehicle ip 4 hours, before cerebellar lesion induction upon stereotactic injection with scFVPOM1 (2 µg). Lesion reduction was not observed in the pre-treated group compared to the vehicle control upon MEMRI examination. (mean±s.d., one-tailed Student's t-test)

The use of pharmacological inhibitors to demonstrate the involvement of mediators can be challenging *in vivo*, since therapeutic doses have to be reached at the site of interest, i.e., the injection site in the brain. In addition, such compounds often interact with more then one mediator. If available, testing with transgenic mice can offer advantages. The human calpastatin (CAST) transgenic mouse (hCast) overexpresses human CAST, an endogenous calpain inhibitor under the Thy1.1 promoter (Rao et al., 2008). Of note, experiments with these mice showed a neuroprotective function for calpastatin mimetics in Alzheimer Disease. Since antibody mediated lesion size is small in wild type mice expressing PrP^{C}, we crossed these mice with *tga20* and generated heterozygous double transgenic mice ($hCast^{+/-}$-$tga20^{+/-}$). Upon injection of POM1 (6µg) into the DG of $hCast^{+/-}$-$tga20^{+/-}$, in contrast to littermate controls, $hCast^{-/-}$- $tga20^{+/-}$ showed no significant difference in lesion volume upon MEMRI (Figure 25). However, there was a trend towards protection.

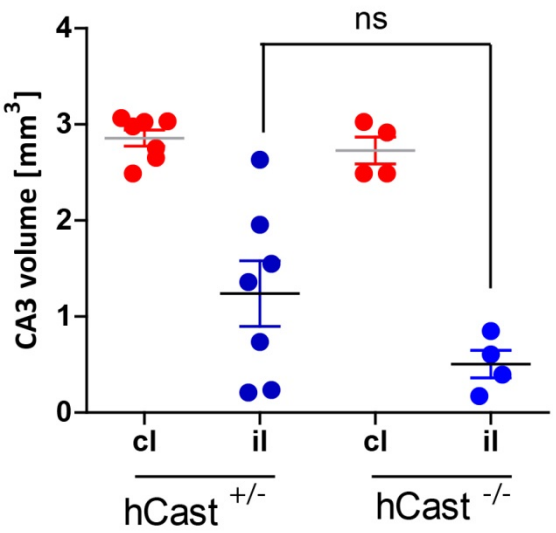

Figure 25: MEMRI analysis reveals a trend towards lesion reduction in calpastatin overexpressing mice

Double heterozygous transgenetic mice overexpressing human calpastatin and PrP^{C} were injected on one side with POM1 (6 µg in 2 µl) and lesion induction was quantified with MEMRI volumetry. A trend towards less manganese signal from DG and CA3 was found, but the differences between the groups were not significant. (mean±s.d., one-tailed Student's t-test)

Since MEMRI volumetry is technically limited in estimating lesion size, I repeated the experiment with the established DWI read-out. Diffusion restriction induced by POM1 injection was comparable in heterozygous hCast$^{+/-}$-*tga20*$^{+/-}$ and in littermate controls hCast$^{-/-}$-*tga20*$^{+/-}$ (Figure 26A). To assess if hCalpastatin expression was sufficient for calpain inhibition, I investigated α-fodrin cleavage and found the characteristic fragments in hCast$^{+/-}$-tga20$^{+/-}$ and controls (Figure 26B), indicating insufficient inhibition of calpain upon calpastatin expression.

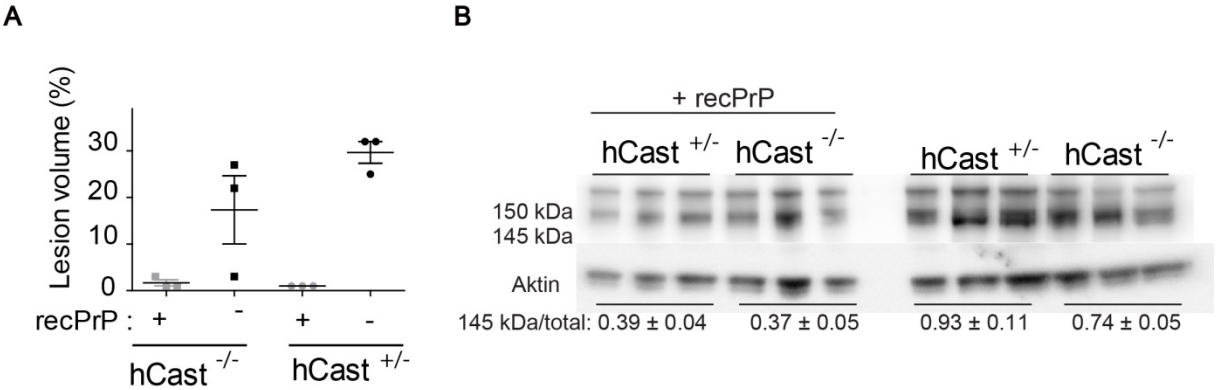

Figure 26: Calpastatin overexpressing is not protective upon POM1 injection

(A) Injection of POM1 (6 µg, 10 µM) in human calpastatin overexpressing mice (hCast$^{+/-}$) crossed with tga20 (tga20$^{+/-}$) induced a lesion comparable to that of injection into transgene negative littermates hCast$^{-/-}$, one-way ANOVA with Tukey's post-hoc test) **(B)** Western blots of both hCast$^{+/-}$ positive and negative mice injected with POM1 (24h p.i.) show increased 145 kDA α-fodrin cleavage in contrast to the contralateral side, where the lesion was blocked with recombinant rmPrP.

The antiporter sodium-calcium exchanger isoform 3 is a potential source of Ca^{2+} influx

The activation of calpains from their pro-enzymes is an indicator of elevated Ca^{2+} levels in the micromolar range (Wang, 2000). After extensive pharmacological screening for the involvement of Ca^{2+} channels in our previous studies (Hermann et al., 2015; Sonati, 2013b), no protective function was found with respect to the inhibition of NMDA, AMPA/kainite, and L-type calcium channels. However, inhibition of the reverse mode of the sodium-calcium antiporter isoform 3 (Falsig, unpublished) has been found to be protective. Therefore, I injected POM1 into the left DG of $NCX3^{o/o}$ mice (Sokolow et al., 2004) or littermate control $NCX3^{+/+}$, and all mice were injected contralaterally with POM1 (3 µg) pre-incubated with rmPrP. Progression of lesion volume assessed by DWI was slower than upon $F(ab)_1$ POM1 (8µg) injection but was significant in $NCX3^{o/o}$ 24h post injection (Figure 27A and B). No significant lesion induction was found in $NCX3^{o/o}$ mice (Figure 27B) compared to the control injection. Assessment with TUNEL staining revealed sparse apoptotic nuclear cells in $NCX3^{o/o}$ but numerous in $NCX3^{+/+}$ (Figure 27C). A second experiment using $F(ab)_1$ POM1 demonstrated the same effect with no evidence of lesion induction in contrast to littermate control (Figure 27D and E). These data point to an early influx of Ca^{2+} through NCX3 (reverse mode) mediating neurotoxicity in the antiprion antibody model.

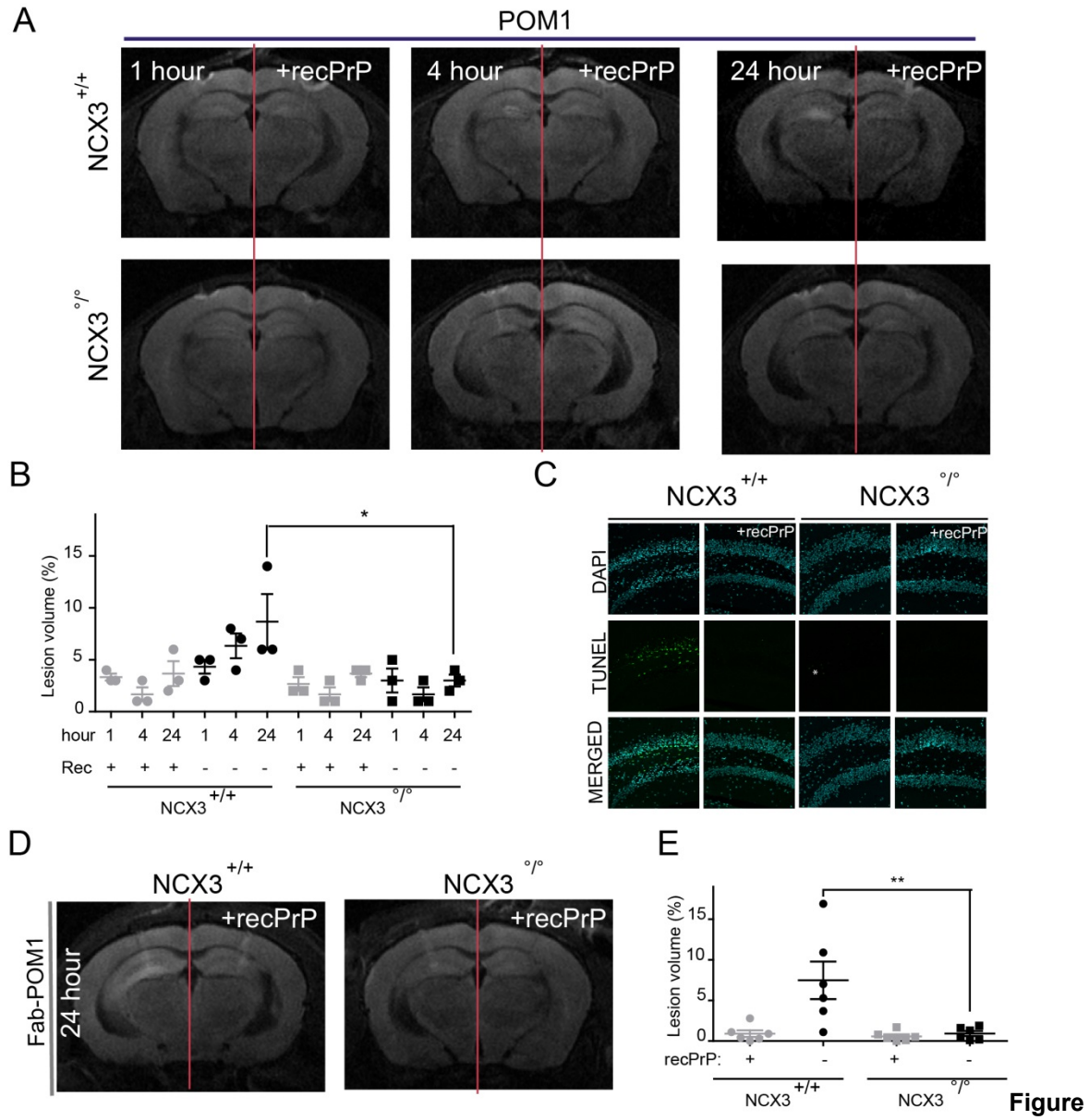

Figure 27: NCX3 deficiency protects from anti-prion mediated neurotoxicity

(A, B) Small lesions developed after POM1 (6 µg) injection into the left hippocampus of NCX3$^{-/-}$ (star) compared to *wt* littermate controls, where a constant increase in lesion size was seen at 1, 4 and 24h post injection. As a control, POM1 was preincubated with rmPrP and injected into the right hippocampus. A) Representative images of diffusion-weighted images (DWI) B) Volumetric analysis reveals significant lesion induction 24h post POM1 injection. Data are presented as mean ± s.d., n=3, One-way ANOVA with Dunnett's post-test, *P<0,1. (C) Tunel staining 24h post injection from mice shown in A. Photographs of the endplate of the hippocampus near the needle tract are taken at high magnification. No apoptotic cells were found upon control injection. Few cells with positive nuclear fragmentation are seen in NCX3$^{°/°}$ (white star), not comparable to NCX3$^{+/+}$ where numerous apoptotic cells are found in a significantly larger area. (D) No diffusion restriction was found 24h post 8 µg Fab$_{(1)}$POM1 injection into NCX3$^{°/°}$ mice. (E) Significant lesion induction was found in NCX3$^{-/-}$ littermate controls, in contrast injection of Fab$_{(1)}$POM1 into NCX3$^{°/°}$ was innocuous. Data are presented as mean ± s.d., n=3, One-way ANOVA with Dunnett's post-test, **P<0,01.

We were now interested in assessing the role of NCX3 upon infection and inoculated NCX3 defined mice intracerebrally with the prion strain RML (30 µl, diluted). Unexpectedly, NCX3$^{°/°}$ mice showed a modest, but significant reduction of survival in contrast to BL6/Hsd2 control mice (Figure 28). Hence, upon chronic prion inoculation, the antiporter seems to exhibit a protective effect on calcium homeostasis.

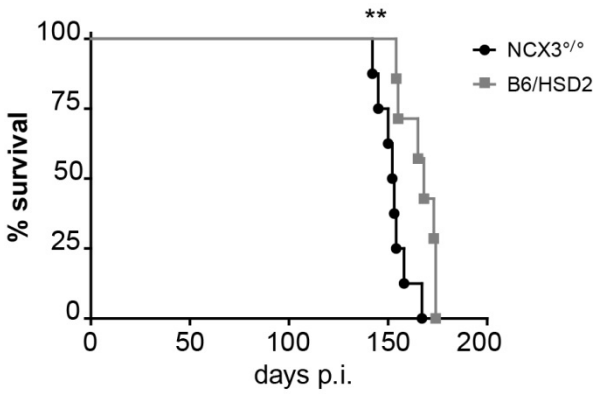

Figure 28: NCX3 expression is protective upon prion inoculation

Survival curves of NCX3$^{°/°}$ (median 50 dpi) and BL6/Hsd2 mice (median 56.3 dpi) mice infected with RML prion. NCX3 expression is significantly protective upon prion infection. Results were analyzed using a Mantel-Cox log-rank test; n=8 NCX3$^{°/°}$ n=6 BL6/Hsd2.

Discussion

MRI volumetry is a valuable tool for *in vivo* quantification of antiprion mediated neurotoxicity

In order to investigate antiprion antibody mediated neurotoxicity *in vivo,* I developed a MRI based quantification. This allows visualization and precise analysis of differences in lesion size over time. While I first used MEMRI, I switched to DWI to avoid repetitive manganese injections.

We chose MEMRI in the beginning not only because of its extraordinary contrast but also because of its functional properties. The activation of calpains in the antibody-mediated toxicity is indicative of Ca^{2+} influx into the neurons. Manganese can enter certain activated Ca^{2+} channels, thus we hypothesized that hyperintense signals from manganese enhanced the visualization of neurons. Instead, I recorded a hypointense signal as early as four hours post injection. This signal reflects edema formation rather than the loss of signal from enhanced neurons, since it disappeared over time. I can further support the hypothesis that Purkinje cells take up most of the manganese (Faas et al., 2010), based on the observation that preserved non PrP expressing manganese enhanced Purkinje cells can still be detected in POM1 lesions.

Diffusion weighted imaging is one of the additional tools used in the clinic for the diagnosis of CJD and is widely used for other acute neurological diseases like stroke. Here I could demonstrate massive and early diffusion restriction upon toxic antiprion antibody injections. This signal was found to corelate well with the induction of neuronal death as assessed by TUNEL staining. Besides being less invasive than MEMRI, DWI was found to be useful as an early marker of antibody mediated toxicity and the contrast to noise of the lesion signal is excellent for volumetric quantification. Strikingly diffusion restriction could be monitored as early as one hour post intracerebral injection of high doses of $F(ab)_1$POM1.

Acute nerve cell loss is likely the main morphological correlate of diffusion restriction in CJD patient rather than spongiform vacuole formation.

Data from *in vivo* experiments verifies the COCS experiments

Antiprion mediated toxicity has been rigorously investigated *ex vivo* in a complex cellular environment by the use of COCS. However, this model system does not reflect the complete *in vivo* situation, where there is a circulation and an intact inflammatory system. Thus, a major goal of this work was it to verify the central *ex vivo* findings in an *in vivo* system and to compare the two models.

The kinetics of neurodegeneration differs slightly between the *in vivo* and *ex vivo* system. Whereas pyknotic nuclei were found as early as 4 hours post injection in the *in vivo* model, nerve cell loss quantified by propidium iodide staining and NeuN morphometry was found to be maximal at 3 and 7 days respectively. I speculate that two reasons contribute to this difference. The concentration for chronic antibody treatment was 0.067 mM; however, I injected the antibody at a concentration of 20 mM. Although the antibody immediately diffuses within the brain, higher peak concentrations are most likely reached at the site of injection that influences the neurotoxic kinetics. Additionally, organotypic slice cultures develop a relatively thick astrocytic scar, which possibly hinders antibody diffusion.

The major hallmarks of antiprion mediated neurotoxicity could be verified *in vivo*. I found the induction of neurotoxicity to represent a specific target effect. No lesion occurred upon injection into PrP^{C} deficient mice and the toxicity could be blocked upon pre-incubation of toxic POM1 antibody with rmPrP. In the *in vivo* model, the second control is important. I found that Zürich-I B6.129-*Prnp*$^{o/o}$ have enlarged cerebelli in contrast to B6.129-*tga20,* potentially affecting the target point of the stereotactic injections. Furthermore, I could demonstrate that the neurotoxic induction is gene dosage dependent *in vivo*.

In the first report antiprion mediated neurotoxicity was speculated to be cross-linking mediated. This was based on the observation that $F(ab)_1$ fragments of the neurotoxic antibody D13 are innocuous when administered at the same concentration as whole antibodies (Solforosi et al., 2004). Here I could demonstrate that F(ab) fragments of toxic antiprion antibodies induce neurotoxicity *in vivo*. However, the kinetics is shifted and higher concentrations are required to induce the same negative effect as observed with whole

antibody administration. This has not been observed *ex vivo* where F(ab) fragments showed to be neurotoxic at comparable concentrations. It is likely that the diffusion and clearance of Fab fragments *in vivo* is higher in comparison to whole antibody injection, thus explaining this difference. Interestingly, this observation could not be confirmed for single chain antibodies, which I found to be neurotoxic at comparable concentrations. Besides solving this controversy, this observation demonstrates that the toxic effect is dosage dependent.

As predicted for the innocuousness of FT ligands, POM2 was found to be non toxic when injected at the same dosages as the toxic antiprion antibodies POM1. $F(ab)_1$POM19 in contrast was neurotoxic. Thus, like in the *ex vivo* studies, antibody mediated neurotoxicity was found to be epitope specific.

To address the molecular function of PrP, a series of partially deleted Prnp variants was generated and expressed in cultured cells and in mice (Aguzzi et al., 2008). I could demonstrate that intracerebral injection of toxic antiprion antibodies in mice expressing the $PrP_{\Delta 32\text{-}93}$ deletion mutant is innocuous, such as predicted from the slice culture experiments. Interestingly, CC2 depleted mice were not only susceptible to antiprion mediated toxicity, and compared to *wt* expression level developed increased lesion size that progressed even after 24 hours.

Does the model mimic the pathologic interaction of PrP^{SC} with PrP^{C}?

My work demonstrates that modelling the pathologic interaction of prions with PrP^{C} shows investigative potential, since it circumvents biosafety issues and represents a rapid assay in contrast to inoculation experiments. Thus, it could be widely used to generate and test hypotheses. However, it is unclear whether this model can be used to model neurotoxicity seen in prion infection.

Oxidative stress is a known mediator of neurodegeneration and TSE. Unclear is where ROS affects the neurotoxic cascade and where they are a major or minor contributor to the pathologic damage. Here I could demonstrate significant *in vivo* protection of antiprion mediated toxicity upon the administration of the strong antioxidant AcHyt. Using the same

compound we were to demonstrate a modest, but significant increase in survival of prion infected mice (Hermann et al., 2015). These data indicate that oxidative stress is not the only, but an important signalling pathway that mediates neurotoxicity in prion infection and antiprion mediated neurotoxicity.

NOX2 enzyme is as a major resource of ROS in the antiprion mediated toxicity *in vivo.* Apart from being responsible for the oxidative burst in neutrophils, NOX2 is also expressed in the CNS, where it controls key neuronal functions and neuroinflammatory processes (Sorce et al., 2012). In neurodegenerative disorders, excessive activation of this oxidase in neurons and microglia leads to the production of ROS and oxidative damage (Sorce et al., 2012). Further studies revealed an upregulation of NOX2 in prion-inoculated mouse brains and 22L prion infected NOX2 deficient mice showed improved motor performance (Sorce et al., 2014).

Further, I could confirm specific calpain mediated fodrin cleavage in tissues from mice that developed lesions upon antiprion antibody injection. However, neither the inhibitor E64d nor the expression of calpastatin had any beneficial therapeutic effect *in vivo*. This is in-line with data from prion-inoculated mice, where both strategies lacked a protective effect (Falsig, unpublished). However, this finding is surprising, since inhibition of calpains with E64d have been shown to be neuroprotective in prion inoculated slice cultures (Falsig et al., 2012). In addition, ROS production has been proposed to be downstream of calpain activation (Hermann et al., 2015), thus calpain inhibition should be as protective as ROS inhibition. Recently it was proposed that in $A\beta_{1\text{-}42}$ mediated dysregulation of intracellular Ca^{2+}, calpain activation led to a protective cleavage of the NCX3 antiporter (Pannaccione et al., 2012). Calpains could play a potential Janus-faced role in neurodegenerative disease, mediating both protective and pathological pathways. Besides, the differences between *in vivo* and *ex vivo* systems could simply be related to difficulties in delivering the pharmaceutical compound in sufficient amounts to the target region.

Additionally, we could show that neurotoxicity is caspase independent in both models and cannot be abolished with glutamate receptor antagonists or with inhibitors of endoplasmic

reticulum channels (Falsig et al., 2012; Hermann et al., 2015). Further convincing evidence that both models activate neurotoxic pathways is the demonstration of PERK activation, the unfolded protein response and the observation that 80% of transcriptionally downregulated genes overlap between both models (Falsig et al., 2012; Hermann et al., 2015).

NCX-3 as a potential source of Ca^{2+} influx in antiprion mediated neurotoxicity

Calcium homeostasis is altered in neurodegenerative disease as well as in prion disease. After the detection of calpain activation Dr. J. Falsig and Dr. T. Sonati performed an extensive pharmacological screening to detect the source of the pathological Ca influx. Surprisingly, significant neuroprotection could only be achieved by blocking the reverse mode of the NCX-3 antiporter. I could demonstrate that NCX3 deficient mice are nearly resistant towards antiprion mediated neurotoxicity. This is suggestive of an early influx of calcium into the cytosol. Supporting this observation are additional results that reveal neuroprotection based on the antisense oligonucleotide knock down of NCX3 in cerebellar slice cultures exposed to POM1 (unpublished Sakata). However, $NCX3^{o/o}$ mice have not been shown to be protected upon prion inoculation and in fact became terminally ill prior to *wt* mice. This discrepancy may point to important adaptive changes upon chronic exposure to neurotoxic stimuli (Figure 29). Upon prion inoculation cells are exposed to an increasing toxic stimulus, in which subtoxic Ca currents in the reverse mode may occur in the beginning. This could trigger adaptive changes, in the way that NCX3 is modulated to work in the forward mode. The earlier described reduction of bradykinin triggered intracellular calcium concentration in prion infected cells, based on the reduction of IP3 second messenger (Kristensson et al., 1993; Wong et al., 1996), is potentially a fingerprint of this adaptive mechanisms. Indeed, similar adaptive mechanisms have been postulated for Alzheimer disease (Pannaccione et al., 2012). The concept in which cells adapt to moderate levels of a stressor is called hormesis (Mattson, 2007).

Further inhibition of the NOX2 enzyme has also been shown to be more protective in the antiprion antibody model *in vivo* than upon inoculation. Also, adaptive mechanisms could

either block the generation of ROS via NOX enzymes or the system could adapt to higher levels or reactive oxygen species.

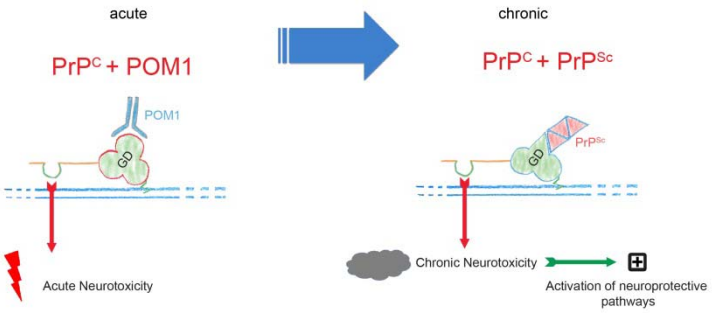

Figure 29: Antiprion antibodies induce an acute form of chronically induced prion mediated neurotoxicity

Neuroprotective pathways can not be activated upon intracerebral administration of neurotoxic antiprion antibodies. Thus, neurons die within hours; however, prion titers are increased over days. Neurons will adopt over time against the pathologic stressor. However, at a certain point, the prion titer will exceed the capacity of the protective machinery of the cell, thus leading to the neurotoxic induction.

Do antiprion antibodies play a role in other pathogenic paradigms?

Although the tolerance against PrP^C is high, in rare cases, toxic antiprion antibodies could possibly be generated within the body and lead to autoimmune mediated encephalitis. This question is currently being addressed by Dr. med K. Frontzek within our lab, who will perform an enzyme linked immunosorbent assay screen searching for the existence of neurotoxic antiprion antibodies on the cerebrospinal biobank.

In addition, the question arises whether the high amount of missfolded prion protein in TSE could trigger an immune response in which antiprion antibodies are generated. If so, some of these antibodies could possibly trigger neurotoxicity within the brain. This could potentially lead to rapidly progressive variants of the disease. Intracerebral inoculated Rag-1 deficient cells (Prinz et al., 2003), which lack mature T- and B- cells, showed no increase in survival. Thus, under these conditons, antibodies seem to have no impact on the clinical course.

However, antibodies could play a role in certain forms of prion disease. New variant CJD is believed to be an infectious disease due to the oral intake of BSE prions through the consumption of contaminated products from cows. One of the hallmarks is that people

acquire a rapid form of the disease and die much younger than patients with sporadic CJD. In Great Britain, the epidemic peak of patients dying from vCJD was reached in 2000 (Andrews, 2012), was with only 26 deaths relatively low compared to the population exposed to contaminated meat products. However, patients with another genetic profile may show a delayed onset of an infectious form of CJD, corresponding to a second peak (Andrews, 2012). A possible second explanation for the rapid development of the disease mainly in young patients could be due to the additional generation of neurotoxic antiprion antibodies. The second peak may also result when patients fail acquire pathological antibodies. Admittedly, such speculation is not supported by current evidence. However, besides screening for pathological antiprion antibodies in young patients, a screen in patients with acquired vCJD could be of interest.

Outlook

Which adaptive changes are triggered by PrP^{SC} during amplification?

While depletion of NCX3 has found to be protective *in vivo* and *ex vivo,* in the antiprion mediated neurotoxicity, it caused clinical progression in prion-inoculated mice. This discrepancy could point to homeotic pathways stabilizing cytoplasmic Ca^{2+} overload.

In contrast to stroke, prionopathies are chronic neurodegenerative diseases, in which the disease mediator replicates over time. In prion disease, a peak level of prions has to be reached before clinical symptoms occur. However, during amplification of PrP^{SC} this neurotoxic agent likely triggers adaptive mechanisms.

With antiprion antibody mediated neurotoxicity, we have for the first time developed an acute model system for the chronic disease. This may facilitate discrimination between the initial neurotoxic trigger and its adaptive mechanisms.

In a pilot experiment I thus plan to investigate whether chronic stimulation of toxic Fab antibodies can modulate the induction of acute antibodies mediated neurotoxicity.

Depicting the role of the FT functional domains in antiprion mediated neurodegeneration

Our *in vivo* and *ex vivo* observations in the antiprion antibody model provide compelling evidence that the FT of the prion protein mediates neurotoxicity. In line unstructured or flexible proteins are known to be involved in signalling, cell cycle control, protein-protein interactions and regulation of transcription and translation (Beland and Roucou, 2012). These proteins typically interact with multiple partners, allowing them to switch function and display opposite activities (Beland and Roucou, 2012). Accordingly, multiple proteins interact with the prion protein; however, do not exclusively bind to the FT (Aguzzi et al., 2008).

While the binding of copper to the OR promotes the dissociation of PrP^{C} from lipid rafts (Taylor et al., 2005), the interaction of the N-terminal polybasic region CC1 with the adaptor protein LRP1 (Taylor and Hooper, 2007) results in a rapid and constitutive clathrin-

dependent endocytosis of the prion protein (Sunyach et al., 2003; Taylor et al., 2005). The CC1 has further been identified as the major binding site for glycosaminoglycans (GAGs) and the binding of heparin to PrP^C mediates down regulation of the latter (Pan et al., 2002; Warner et al., 2002). Depletion of CC1 in mice has not led to a spontaneous pathologic phenotype (Muramoto et al., 1997); however, it has been shown to impair the capacity to rescue $PrP_{\Delta 32\text{-}134}$ induced neurotoxicity (Turnbaugh et al., 2011). Importantly, these mice demonstrated a marked increase in survival upon prion inoculation (Turnbaugh et al., 2012).

It has been suggested that PrP^C may play a role in copper metabolism, as OR is known to be an efficient copper binder (Hornshaw et al., 1995; Pauly and Harris, 1998). It has been proposed that prion protein serves as a recycling receptor for the uptake of copper from the extracellular milieu (Pauly and Harris, 1998). An additional copper binding site has been reported for the aminoterminus: the residues 96-111, which belong to the CC2 (Jackson et al., 2001).

The neurotoxic phenotype seen in several deletion mutants points to an interaction of CC2 with the HC triggering these pathologic effects (Aguzzi and Falsig, 2012). The CC2 contains an Src homology domain 3 (SH3), which is known to interact with GPI-anchored protein, regulate the local concentration of the protein and to activate or inactivate the protein function (Lysek and Wuthrich, 2004).

This finding illustrates that the different domains of the FT have distinct functions and are therefore potentially differently involved in prion protein mediated neurotoxicity. The goal of my new study is to uncover the role of each functional domain by inserting targeted point mutations. In the first round, I produced five different FT mutated prion proteins, with altered charges of CC1 and CC2, Cu binding site of the OR, destroyed structure of the OR, altered SH3 binding site in CC2 and decreased hydrophobicity of the HC (Figure 30).

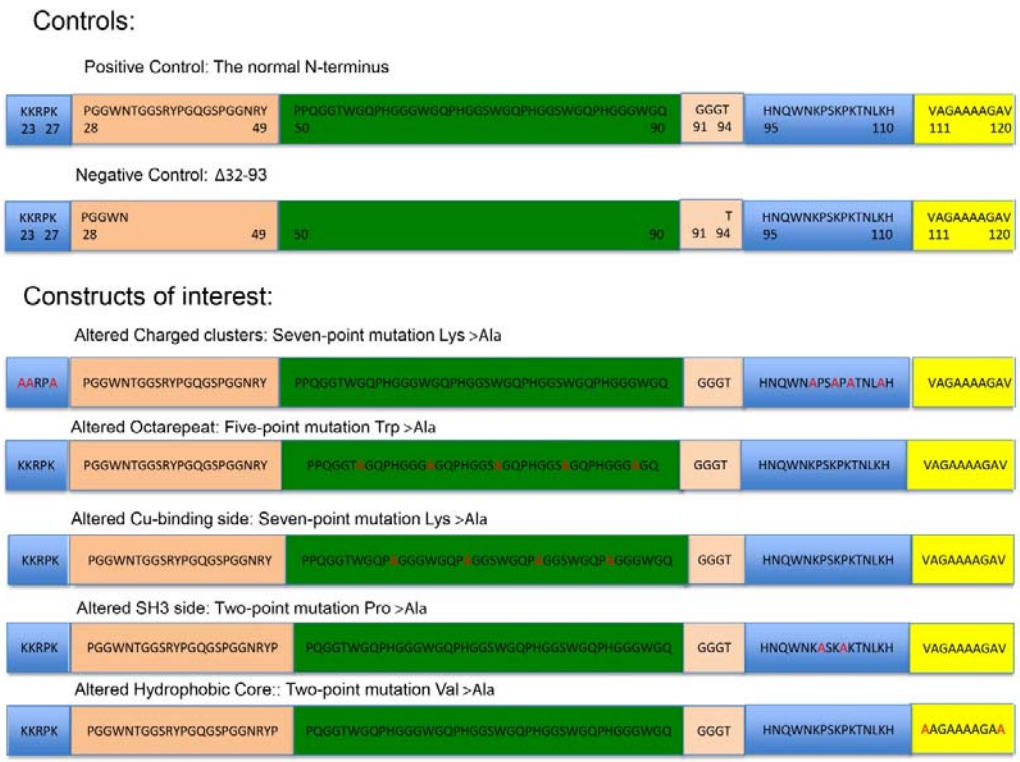

Figure 30: PrP-mutants projected to be expressed on *Prnp*$^{o/o}$ slices to assess antiprion antibody successibility

Depicted are the amino terminals of prion protein mutants, from the amino acid 23 to 120. For the control, unaltered prion protein (positive control) and the octarepeat depleted mutant (negative control) will be expressed. Strategic point mutations will be inserted into the different functional domains of the aminoterminus as outlined.

This prion protein mutants are planed to be expressed on *Prnp*$^{o/o}$ COCS by the use of viral vectors (adeno associated virus), before exposure to the neurotoxic F(ab)$_1$POM19. To facilitate the read out the constructs will be expressed together with the fluorescent marker NeonGreen. Towards this goal I have already cloned two bicistronic constructs using the Golden Gate (Cermak et al., 2011) strategy. I used the 2A side of the aphthovirus foot and mouse disease polyprotein to induce a co-translational cleavage between the two proteins (Donnelly et al., 2001). The first bicistronic design has the NeonGreen in the first and the rmPrP at the second position and in the second design the pattern is inverted (Figure 31A). In the initial step, I expressed the construct on *Prnp*$^{o/o}$ ablated Hek cells and found a strong expression of NeonGreen for both constructs. After fixation the cells were immunostained for PrP using POM1, which revealed simultaneous expression of PrP (Figure 31B). To confirm

the important surface expression of PrP, I used a pull-down biotinylation assay, which revealed a better surface expression, when the prion protein is in the second position (Figure 31C).

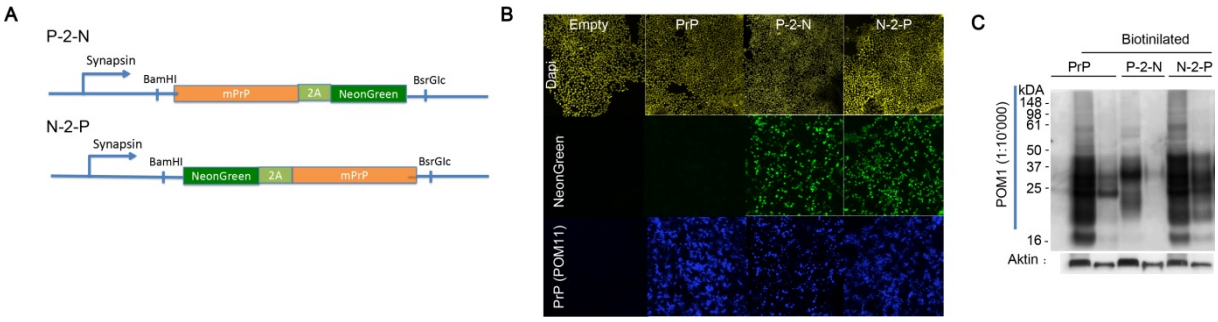

Figure 31: Bicistronic vector design for a simultaneous expression of NeonGreen and PrP
(A) The bicistronic vector expresses the murine prion protein (rmPrP) before (P-2-N) or after (N-2-P) the 2A side. As expression reporter NeonGreen is used. Both proteins are expressed under the control of the pCAG-T7 promoter. (B) Expression of constructs on HEK293T cells reveals a strong expression of NeonGreen for both constructs. Cells were immunostained against PrP with POM1. The prion protein expression from the P-2-N construct differs from the control expression, PrP alone, and the expression from N-2-P. Empty refers to a transfection with the original vector used for cloning containing neither a NeonGreen nor a PrP cassette. (C) Surface protein got biotinylated before cell lysis. Samples got then enriched for surface proteins using Strepta-Avidin beats. Immunohistochemical staining on a PrP western blot reveals a stronger surface expression for the P-2-N construct.

PART II

Introduction

Immunotherapies in TSE

The clearance of pathological aggregated protein with either active or passive immunotherapy is along with the inhibition of its production, the most frequent therapeutic strategy in proteinopathies (Aguzzi and O'Connor, 2010). However, reducing the beta amyloid burden in Alzheimer diseased patients has to date not been translated into cognitive improvement (Wisniewski and Goni, 2014). All the more, the first active immunization Phase IIa trial had to be terminated since 6% of vaccinated patients developed aseptic meningoencephalitis (Gilman et al., 2005) and in both active and passive immunization therapies. Amyloid-related imaging abnormalities occurred (Sperling et al., 2011). Since the degree of tau related pathology correlates better with dementia, immunotherapies against the intracellular accumulation of tau proteins are currently under investigation (Wisniewski and Goni, 2014).

In 2010 Citron reviews the four models of antibody function in the clearance of pathologic protein aggregates. The first model postulates a phagocytic response mediated by microglia. In addition, antibodies could possibly remove amyloids based on direct interactions. Another model posits that antibodies pull the pathologic protein to the periphery. In the fourth proposal, the antibody blocks the toxic effects of the oligomeric pathologic proteins (Citron, 2010).

Similar to Alzheimer disease, immunotherapy to clear the pathologic protein has been assessed in prion disease (Aguzzi and O'Connor, 2010). In addition to cited mechanisms that describe antibody function, antiprion antibodies potentially block the negative effects mediated by PrP^{C}, corresponding to receptor blockage.

As it was difficult initial to produce high affinity antibodies for research purpose based on the high host tolerance towards ubiquitously expressed prion protein, active immunotherapeutic

strategies in pre-clinical research yield an insignificant increase in survival time upon ip inoculation (Magri et al., 2005; Sigurdsson et al., 2003). Thus, passive immunotherapeutic strategies are more likely to be successful. Table 1 summarizes of the following preclinical active and passive immunization trial.

Proof of concept for immunotherapies was established with genetically engineered mice, which expressed anti-PrP^{C} antibodies and were protected from extraneuronal prion infection (Heppner et al., 2001).

While passive immunization with antiprion antibodies ICSM18 and ICSM35 (delivered intraperitoneally) successfully blocked peripheral RML infection, no effect was seen upon intracerebral inoculation (White et al., 2003).

With intravenous delivery of the antibodies 31C6, 110 and 44B1, a trend towards longer survival could be achieved upon intracerebral inoculation of the Chandler or Obihiro strain (Ohsawa et al., 2013). Additionally, mini-osmotic pumps have been used to therapeutically deliver 31C6, which led in a significant prolongation of intracerebral PrP^{SC} inoculated mice (Song et al., 2008).

Chronic intracerebral administration of the antiprion antibody 4H11, however, resulted in severe side effects, consisting of nerve cell loss, gliosis and microglial activation (Lefebvre-Roque et al., 2007). This toxic side effect resembles the same toxic reaction we and others found upon stereotactic injections (Solforosi et al., 2004; Sonati, 2013b).

These findings raised concerns about the safety of anti-PrP^{C} immunotherapies. However, these controversial findings could not be reproduced with D13, ICSM18 or ICSM35, when injected intracerebrally at a dose of 2 µg, which led to the conclusion that antiprion antibodies do not induce neuronal apoptosis (Klöhn et al., 2012). As demonstrated in the previous part I, I could reproduce the toxicity of D13 in *tga20,* thus this report was surprising. In addition, ICSM18 has an overlapping binding epitope with POM1. Thus, the fact that the globular ligand ICSM18 appeared innocuous aroused our attention, as it would further extend the mapping of the toxic behaviour of GD ligands. This would have been of possible therapeutic interest, if the data that ICSM18 is not mediating toxicity could be reproduced.

Immunisation Approach	Vaccine	Effect	Reference
Transgenic expression of antiprion antibodies	6H4 (153-165)	Full protection upon Intraperitoneal RML inoculation	Heppner et al., 2001
Active immunization with PrP peptides	$PrP_{131-150}$ $PrP_{211-250}$	Immunogenic response and an reduction of PrP^{Res} level in tumor transplants	Souan et al, 2001
Active vaccination with recombinant mouse prion protein	Full length rec-PrP	Increase in the incubation period and infection period upon intraperitoneal 139A inoculation	Siggurdson et al, 2002 and 2003
Passive immunization with full length antiprion antibodies	ICSM18 (146-159) ICSM35 (91-110)	Full protection upon intraperitoneal RML inoculation	White et al, 2003
Active immunization with PrP peptides	$PrP_{105-128}$ $PrP_{119-146}$ $PrP_{142-179}$	Increased survival in a hamster model of TSE	Magri et al, 2005
Passive immunization with full length $F(ab)_1$ antiprion antibodies delivered with mini-osmotic pumps	4H11	Severe side effects of the treatment with neuronal cell loss, astrogliosis and microglia activation	Lefebvre-Roque et al, 2007
Passive immunization with full length antiprion antibodies delivered with mini-osmotic pumps	110 (88-90) 31C6 (83-89) 44B1 (143- 149)	Partly significant prolongation of survival after intracerebral inoculation with the Chandler or Obihiro strain	Song et al, 2008
Passive immunization with full length antiprion antibodies delivered via the tail veine	31C6 (83-89)	Non-significant prolongation of survival time	Oshawa et al, 2013

Table 1: Summary of preclinical active or passive immunization trials in TSE

Pharmaceutical safety assessment

The US Food and Drug Administration considers a safe pharmaceutical drug as one that has reasonable risks, compared to the expected benefit and available alternatives (FDA, 1999).

This implies that health authorities and regulators have to perform a benefit versus risk analysis or a so-called risk assessment of each new pharmaceutical compound. The pharmaceutical risk assessment can be divided in four steps: 1. Hazard/Risk identification; 2. Determination of the dose-response relationship; 3. Exposure assessment; 4. Integration of all data into a final assessment (risk characterization) (RMIT, 2008).

For the identification of risks of all historical data, theoretical analysis, informed options and concerns of stakeholders are included to identify the possible consequences (FDA, 2006). After the identification of the hazard, the dose-response relationship is the central concept in toxicology (RMIT, 2008). These relationships can either be threshold or non-threshold, the latter is used for the majority of non-carcinogenic compounds (RMIT, 2008). For these compounds, it is considered that there is a dose or concentration below which the adverse effect will not occur. This dose is traditionally addressed with the no-observed adverse effect level (NOAL) and the lowest observed adverse effect level (LOAL) (Filipsson et al., 2003). In this approach, only data from one applied dose are used, there is alternatively the benchmark dose approach, which takes the quantitative dose-response information into account (Filipsson et al., 2003).

Further knowledge about the pharmacokinetics is essential, in particular to estimate the concentration of the compound at the target organ (RMIT, 2008). Finally, all available data about the compound are integrated in the final risk assessment, which then forms the basis for the decision as to whether or not the drug is safe (RMIT, 2008).

Outline of this work

Passive immunotherapy with antiprion antibodies represents a potential therapeutic strategy for TSE. For this approach, a significant pharmaceutical risk has been identified, since some of these antibodies potentially mediated neurotoxicity. However, the initial reports about this risk have been questioned.

In part II, I investigated the reasons for the discrepancy in the literature regarding the toxic induction of antiprion antibodies upon intracerebral administration. Initially I performed a

dose-response analysis of D13 and found the antibody to be toxic at higher concentrations than initially reported. I then analyzed the generated data using the benchmark dose approach in order to give possible values for safety limits.

Next, I investigated the neurotoxic potential of the antibody ICSM18, which is an antibody under evaluation for clinical use (Klöhn 2012, Klyubin 2014). Here I can demonstrate that this antibody has a toxic potential similar to POM1.

Results

Antiprion antibody D13 does induce neurotoxicity

In order to determine the cause of the discrepancies between the reported toxicity of D13, I stereotaxically injected the antibody (2 µg in 2 µl PBS) into the left CA1 region of the hippocampus of male BL6 mice (A/P: -2 mm, ML: 1.3 mm, DV: -1.4 mm from Bregma), the coordinates used from Solferosi and Klöhn (Solferosi 2004, Klöhn, 2012) in the previous studies. For control, antibodies pre-incubated with a three-fold molar excess of a recombinant murine PrP fragment encompassing residues 90-231 ($rmPrP_{90-230}$), were injected into the right hippocampus. Histological examination at 48h pi and DWI 24h pi failed to reveal lesion induction other than needle tract damage (Fig. 32A – C upper row).

Since bioactivity between antibody batches and the assessment of protein concentration can vary between labs and methodology, I examined the toxicity of D13 at increasing antibody doses. A significant hyperintense lesion was recorded on DWI 48h pi of 6 µg and 12 µg D13 in the hippocampus and/or cortex of 4 out of 5 mice, respectively (Fig. 32A, middle and lower row), whereas there was no signal alteration on the side exposed to blocked antibody. Histologically, D13 (48h pi) caused conspicuous edema and widespread acute neuronal damage affecting large cortical and/or hippocampal areas (Fig. 32B-C, middle and lower row). Affected neurons displayed condensed hyperchromatic nuclei and hypereosinophilic cytoplasm (Fig. 32C, middle and lower). Some neurons showed prominent nuclear fragmentation.

Solferosi could show positive labelling performing terminal deoxynucleotidyl transferase dUTP nick end labelling (TUNEL) indicative for apoptosis. Therefore, I performed TUNEL staining on all sections and found positive cells in lesions of mice injected with 6 µg and 12 µg D13 but not in 0 µg (Fig. 32D). In contrast, activated caspase-3 (aC3) immunohistochemistry labelled only few cells (Fig. 32E). This result is in line with data from slice cultures experiment, where antibody mediated neurotoxicity has been described to be independent of caspase activation.

I then quantified lesion size based on a DWI dataset as previously described and blotted a dose response curve. From this blot I determined that the lowest observed adverse effect level (LOAL) is 10 µM / 6 µg. Using specialized software, I then calculated the benchmark dose level as 5.2 µM / 3.1 µg (Figure 32 F).

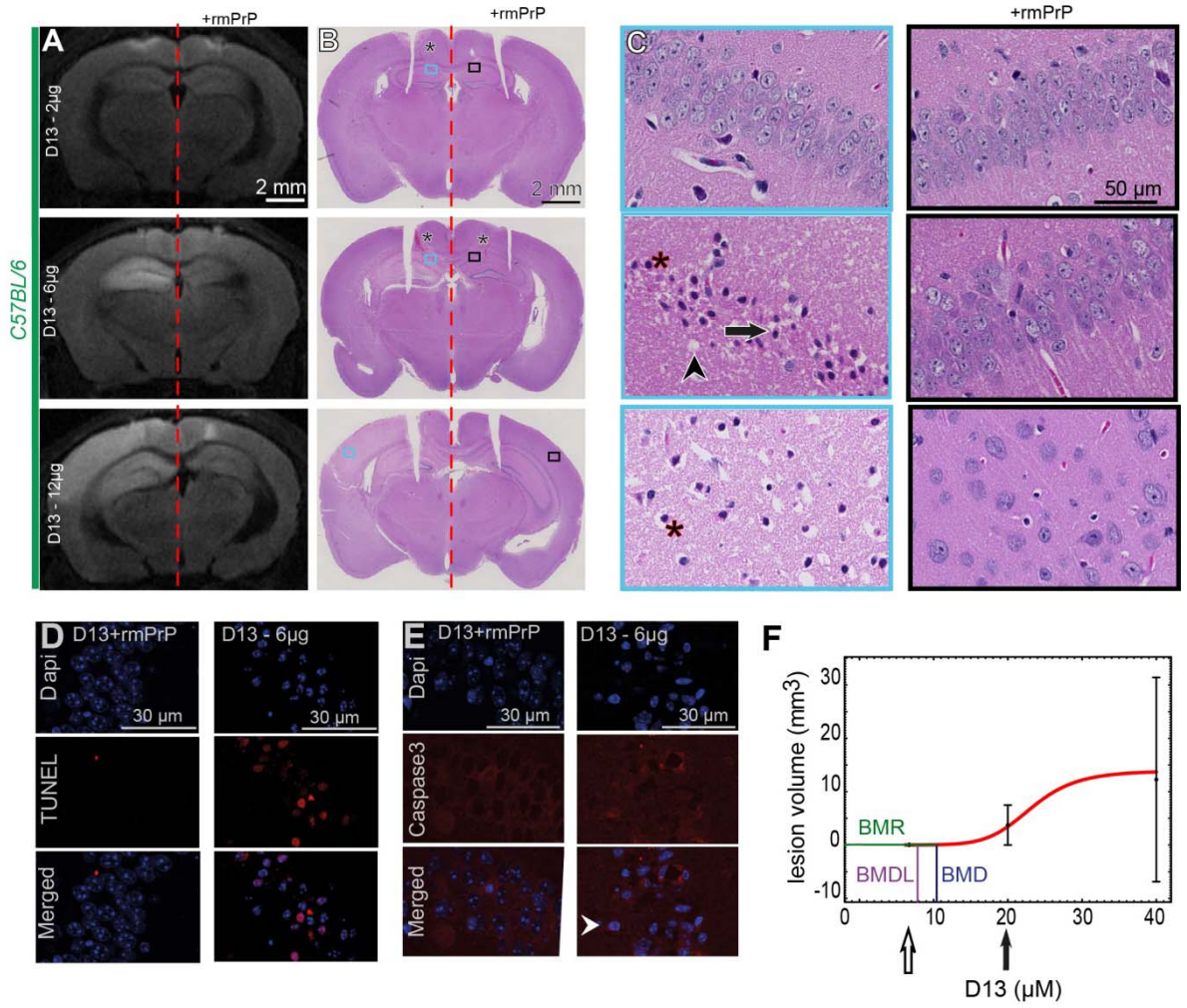

Figure 32: Dose-response analysis of acute D13 triggered neurotoxicity.

(A) DWI at 48h after injection of D13 (2, 6 and 12 µg; respectively, 6.6, 20 and 40 µM) into the left hippocampus. For a control, D13 was preincubated with a three-fold molar excess of $rmPrP_{90-230}$ (+rmPrP) and injected into the right hippocampus. Whereas both D13 and D13 +rmPrP induced superficial injection-related lesions, only D13 induced extensive hyperintensity throughout the hippocampus. **(B)** Haematoxylin and eosin (H&E) stained sections from the mice shown in (A) (asterisks: needle tracts; rectangles: regions magnified in (C). Incisions were introduced as post-mortem landmarks). **(C)** Higher magnification of Cornu ammonis, sector 1 (CA1, left panel with blue border: D13 injections at 2, 6 and 12 µg, right panel with black border: D13 +rmPrP) showing vacuoles indicative of edema (arrowhead) as well as numerous neurons with condensed chromatin, hypereosinophilic cytoplasm (asterisks), and nuclear disintegration (arrow). At 12 µg the tissue is

looser indicative of more advanced lesion formation. **(D)** TUNEL stained paraffin sections of the CA1 region of the mouse injected with 6 µg shown in (A-C). Quantitation showed 41 ± 19% $TUNEL^+$ cells (*n*=30 fields at 20x) after exposure to D13 and ca. 0.5% $TUNEL^+$ cells on the contralateral side exposed to D13+recPrP. Blue: nuclear counterstaining with 4',6-diamidino-2-phenylindole (Dapi). **(E)** Confocal laser scanning microscopy of paraffin sections immunostained for activated caspase-3 revealed sparse positive cells (white arrowhead) after injection of 6 µg D13. (**F**) Fit of the dose response curve modelling an S-shaped dose-response relation (Y[dose] = intercept + v*dose^n/(k^n + dose^n); software BMDS 2.4, U. S. EPA). The benchmark response (BMR, green line) is determined as a 5% increase of lesion volume over control injections (mean of lesion induction upon blocked D13 injection: 0.056 mm^3). The Benchmark Dose (BMD, blue line) corresponds to the BMR and was found to be 5.2 µM / 3.12 µg. The violet line indicates the lower confidence interval that results in the benchmark Dose Level (BMDL) calculated as 3.9 µM / 2.3 µg. The with arrow represents the no-observed-adverse effect level (NOAEL: 3.35 µM / 2 µg) and the black arrow, the lowest-observed-adverse effect level (LOAEL: 10 µM / 6 µg).

ICSM18 triggers mouse hippocampal neurotoxicity

Next I was interested in addressing the toxic potential of ICSM18 at 6 µg upon injection into the left CA1 region of the hippocampus. In order to exclude sex and strain issues, I used female BL10 mice, which are matched with respect to the Klöhn study of. As performed in the study by Klöhn, I administered IgG1 isotype control (BRIC222, American Research Products, 6 µg) into the contralateral position as well as ICSM18 (6 µg) into *prnp*$^{o/o}$ mice. DWI depicted a small lesion 24h pi in one out of five mice, which was not seen in the control group (Fig 33A). Serial H&E stained sections (48h pi) revealed a lesion comparable to the D13 injection and distinct from the lesion tract damage (Fig 33A-B). Statistical analysis of the volumetric quantification yielded no significant differences between ICSM18 injection into wild type mice compared to injection into *Prnp*$^{o/o}$ mice and isotype control injection (Fig 33C; *p*=0.6427).

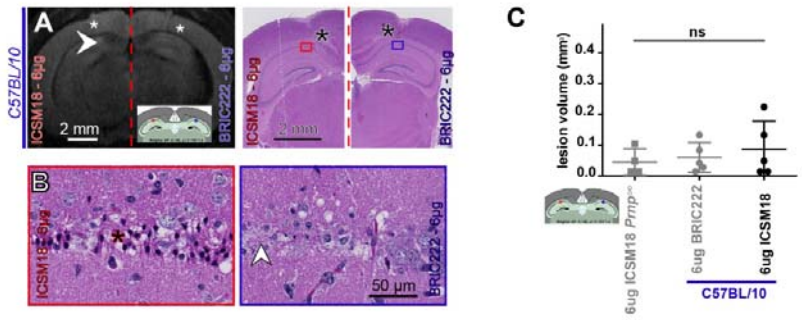

Figure 33: ICSM18 trigger mouse hippocampal neurotoxicity.
(**A**) A 0.2 mm^3 hyperintense lesion (arrowhead) was found upon DWI 24h pi of 6 µg ICSM18 into the left CA1 region (inlay: illustration of stereotactic coordinates) in one BL10 mice. No such signal alteration was found on the contralateral side injected with BRIC222 as IgG1 isotype control. Right side, corresponding H&E section 48h pi (asterisks: needle tracts; rectangles: regions magnified in (B)). **(B)** High magnification image (red border) at the position where the hyperintensity was recorded shows neurons with condensed nuclei and hypereosinophilic cytoplasm (asterisks). The mechanical lesion induced by the needle tract is characterized by cellular debris (white arrowhead). **(C)** Quantitative analysis of lesion volume from DWI images shows no significant lesion induction at 6 µg ICSM18 when the antibody is injected into CA1 (inlay: illustration of stereotactic coordinates; one-way Anova with Tukey's post test, $n_{(Prnp^{0/0})}$=4, $n_{(BL10)}$=10).

By inducing neurotoxicity in the hippocampus by POM1, I found that injection into the CA3 region yields more robust results. I therefore administered the antibodies into the hippocampus with previously used coordinates (A/P: -2 mm, ML: 1.3 mm, DV: -1.4 mm from Bregma). Hyperintense lesions were found in three out of four BL10 mice (Fig 34A, E), which were subsequently confirmed by histological analysis (Fig 34A, B). Lesion volumes differed significantly between ICSM18 and control injections (Fig 34D-E; p=0.0062). No lesions were found upon injection of 2 µg ICSM18 (Fig 34C, E). In order to test for gender and / or strain mediated differences I additionally injected 6 µg ICSM18 from the same batch into BL6 male and female and found an increased negative effect in BL6 female in contrast to BL10; however, the difference between gender and strain is not significant (Fig 34E). Quantitative analysis reveals that there is no significant difference between the negative effects of

ICSM18 in comparison with POM1 (Fig 34E). As expected, lesion induction of ICSM18 is PrP^{C} expression dependent (Fig 34E).

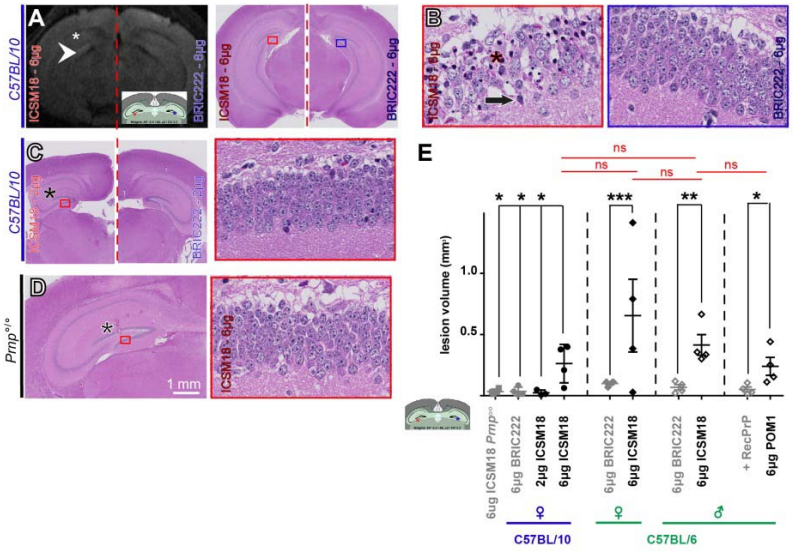

Figure 34: ICSM-18 at CA1

(**A**) Representative DWI 24h after stereotactic injections of 6 µg ICSM18 versus BRIC222 into the CA3 (inlay: illustration of stereotactic coordinates) region of a BL10 mouse. The arrowhead points to a 0.4 mm^3 hyperintense lesion. Right side corresponding H&E section 48h pi (asterisks: needle tracts; rectangles: regions magnified in (D)). **(B)** On higher magnification next to healthy neurons, numerous undergoing cell death (asterix) are seen in the dentate gyrus upon injection of 6 µg ICSM18 (red border), although not seen upon 6 µg BRIC222 injection (blue border). **(C)** Representative H&E images at high and low resolution 48h pi of 2 µg ICSM18 versus 2 µg BRICC222. No lesions are found. **(D)** No lesions are found at 48h pi of 6 µg ICSM18 into the CA3 region of *Prnp*$^{o/o}$ mice. **(E)** Significant lesion induction is found upon injection of ICSM18 into the CA3 region of BL10 male and BL6 female and male. A 6 fold increased lesion is found in *tga20* males in contrast to BL6 females. Analysis of the stereotactic injection of POM1 at the same dose reveals a comparable negative effect to the injection of ICSM18 in BL6 mice. (inlay: illustration of stereotactic coordinates; Multi column comparison with (first four samples) one-way Anova with Tukey's post-hoc test; comparing of two samples with two-tailed Student's t-test, n =4, ***P<0.001, **P<0.01, *P<0.05, ns: not significant.).

Distribution of holoantibodies upon stereotactic injection

In order to obtain more information about the tissue exposed upon intracerebral administration of antiprion antibodies, I next addministered labeled Cy5-POM2 antibody at 2 and 6 µg into the CA1 region (Fig 35 A). On Cryo-sections 24h post injection, I found that labeled holoantibody is distribution to a volume of 1.8 mm^3 for 2 µg and to a 5 mm^3 for 6 µg (Fig 35B).

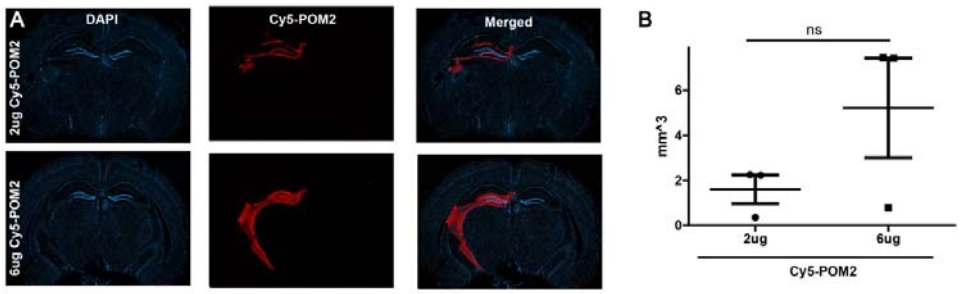

Figure 35: The distribution of an antibody in the brain is concentration dependent

(A) Representative Cryo-sections 24h post injection of 2 µg and 6 µg Cy5-POM2 into the CA3 region. **(B)** A mean volume of 1.8 mm^3 was found upon administration of 2 µg and a volume of 5 mm^3 upon 6 µg Cy5-POM2. The difference was not significant (n =3, Student t-test).

With this additional data, I calculated the relation between lesion volumes to antibody distribution and found that ICSM18 affects 84% of injected volume in *tga20* male mice and 5.2% in BL10 female mice (Table 2).

	D13			**ICSM-18**					
	CA1			CA1	CA3	CA3	CA3	CA3	CA3
Dose	2	6	12	6	2	6	6	6	6
Conc	6.6	20	40	20	6.6	20	20	20	20
Animals	5	5	5	5	3	4	4	4	3
Strain	BL6	BL6	BL6	BL10	BL10	BL10	BL6	BL6	*tga20*
Sex	m	m	m	f	f	f	m	f	m
Lesion	0	4	4	0	0	3	4	4	3
Lesion volume (mean ± SD)	0.03± 0.02	3.54± 3.16	11.34± 15.28	0.09± 0.09	0.04± 0.04	0.26 ± 0.15	0.41± 0.17	0.65± 0.59	4.2± 2.5
Lesion/AB Distribution (%)	1.6	70.8	-	1.8	2.2	5.2	8.2	16.2	84

Table 2: Summary of data generated in the risk assessment

Chronic exposure to toxic antiprion antibodies

A stereotactic intracerebral administration of a singel dose of antiprion antibodies is not the likely way used for clinical administration. Therefore, in a collaboration with Uli Hermann, we chronically administrated the Fab fragment of the highly toxic antibody POM1 (75 µg via Alzet pump, 0.25 µl/h, 0.6 µg/µl, 21 days, *tga20* mice), which has a comparable neurotoxic effect as ICSM18, and induced 4 days after pump implantation a hyperintense lesion around the implanted canula not seen in prnp$^{o/o}$ mice (echo planar imaging, Fig 36A). The hyperintense signal disappeared 11 days post implantation (Fig 36B). MEMRI and H&E 21 days post implantation proved lesion induction (Fig 36C-D). Upon volumetric quantification based on the MEMRI image 9% ± 3% of the brain volume (*Prnp*$^{o/o}$ 1% ± 0%) was found to be damaged.

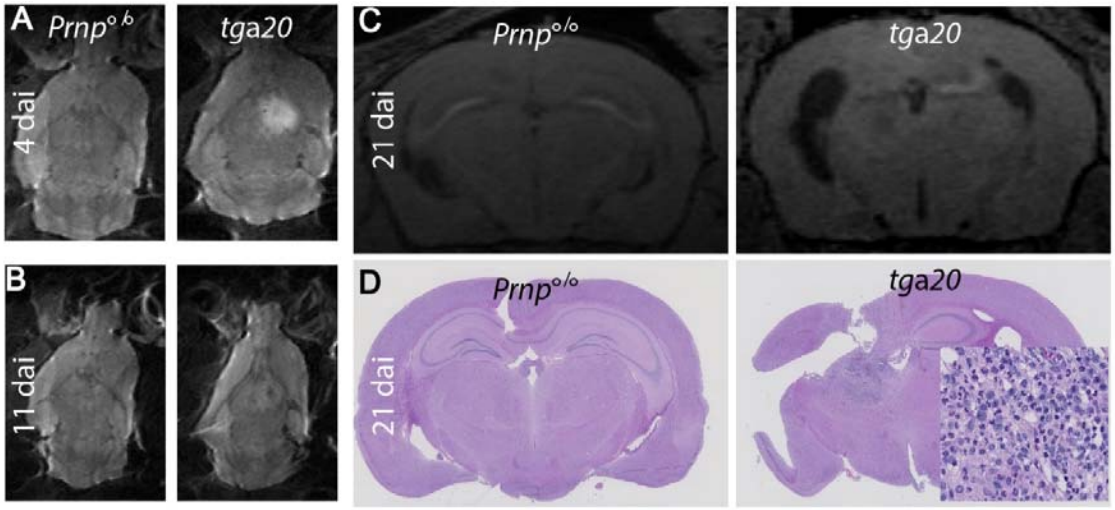

Figure 36: Chronic delivery of the Fab fragment via mini-osmotic Alzet pumps

(A) Representative DWI 4 days post implantation of a mini-osmotic Alzet pump delivering the Fab fragment of POM1. A large hyperintense lesion was recorded in *tga20* mice, not seen in *Prnp*$^{o/o}$ mice. **(B)** Images of the same mice 11 dpi. The hyperintese signal disappeared. **(C)** Coronal MEMRI images of the same animals as shown in A and B. Extensive damage of the *tga20* brain architecture was mainly located in the left hippocampus. **(D)** Representative H&E sections 21 dpi from the same mice as shown in A-C confirming lesion development in *tga20* mice.

Discussion

Risk characterization of toxic antiprion antibodies

Klöhn *et al*. concluded that "PrP antibodies do not trigger mouse hippocampal neuron apoptosis" (Klöhn et al., 2012). However, my results indicate that this conclusion is incorrect and that both ICSM18 and D13 are neurotoxic. I could reproduce the initial reported neurotoxicity of D13 used from Klöhn et al. as a positive control, at a threefold higher concentration than initially reported. Since it is not possible to assess the concentration or bioactivity of the initial antibody batches used in previous studies, I can only speculate about the dosage discrepancy. Here I show that variation of the injection coordinate can influence the volume of lesion induction and I provide further evidence for other variables that possibly influence these experiments. In my view, there is either a difference between labs in the bioactivity of antibody batches or the methods to determine of the concentration. Neurotoxicity has therefore been identified as a potential hazard of antiprion antibodies by different laboratories (Tabel 3).

Most likely, the first patients envisaged for clinical studies will be those suffering from sporadic CJD (sCJD), as this is the most frequent prion disease in humans. sCJD is hypothesized to begin with a spontaneous change of the prion protein within the brain. Accordingly, pre-clinical studies are required to prove efficacy upon intracerebral inoculation. However, a cumulative dose of 8 mg of ICSM18 (injection of 2 mg intraperitoneal twice weekly) has been shown to be ineffective upon intracerebral inoculation (White et al., 2003). Most likely, the antibody passes through the blood brain barrier in sufficient amounts only during the terminal stages of the disease, as it has been shown for 31C6 (Ohsawa et al., 2013). Thus, an intracerebroventricular route of administration should be selected. The only published study on delivering anti-prion antibody via this route (31C6) used 336 µg (0.5 µl/h, 14 days, 2 mg/ml) to achieve a significant but small prolongation of survival in prion inoculated mice (Song et al., 2008).

The lack of preclinical data on the efficacy and toxicity of ICSM18 for the treatment of sCJD mandates caution with respect to the use of anti-prion antibodies in clinical studies.

Steps	ICSM18
Hazard identification	Induction of acute neurotoxicity (Lefebvre-Roque et al., 2007; Solforosi et al., 2004; Sonati, 2013b)
Determination of the doses-response relationship	D13: BMDL 3.9 µM / 2.3 µg , NOAEL: 3.35 µM / 2 µg, LOAEL: 10 µM / 6 µg ICSM18: NOAEL : 3.35 µM / 2 µg, LOAEL: 10 µM / 6 µg
Exposure assessment	(Ohsawa et al., 2013)
Integration of all data into a final assessment; risk characterization	Preliminary

Table 3: Summary of risk assessment for ICSM18.

Alternative ligands for the treatment of TSE

Despite the described neurotoxic risk of antiprion antibodies for the treatment of CJD, passive immunotherapies still represent a promising treatment strategy.

As demonstrated, not all ligands that bind PrP^C induce neurotoxicity. Thus, one of the strategies assessed Dr. S. Senatore in our lab by aims to discover rare non-immunodominant epitopes. This will be achieved by phage display coupled with next generation sequencing.

In a second strategy, Dr. T. Sonati aims to investigate small molecules that target PrP^C, in order to identify POM1 / POM2 competitors.

CONCLUDING REMARKS

Here I demonstrate that MRI based quantification can be used as an early and precise surrogate marker of anti-prion mediated neurotoxicity *in vivo*. One may question the impact of this new assay on prion research.

In patients MRI examination belongs to the routine clinical evaluation for the pre-mortem diagnosis of sCJD (Zerr et al., 2009). There is compelling evidence that positive signal alterations are found early in the disease (Shiga et al., 2004) and patients with other proteinopathies rarely show positive results (Zerr et al., 2009). MRI offers a high resolution, noninvasive method to identify subtle changes in brain structure, and therefore represents a powerful clinical and research tool for many neurological disorders.

The pre-clinical gold standard for a promising new TSE pharmaceutical agent is a significant prolongation of survival time of inoculated animals *in vivo*. This assay allows precise quantification, given the stereotypical fatal clinical phase (Sandberg et al., 2011). However, other positive effects of a drug such as a delay of symptoms or neurodegeneration are by default not assessed. Functional testing like rotarod test has recently been used (Sorce et al., 2014) to gain more information about disease progression. Additional examinations like cerebrospinal fluid biomarkers, electrophysiology and MRI are rarely used in animal models of prion disease. For the most part, biosafety issues hamper the implementation of these methods.

In contrast, research based on the antiprion mediated neurotoxicity model can be performed at biosafety level one. We could demonstrate that this model shares many similarities with neurotoxicity found in prion infection (Hermann et al., 2015; Sonati, 2013b). Therefore my established assay can be used for rapid assessment of the neuroprotective potential of compounds *in vivo*. Sequential imaging at different time points is possible and allows investigation of delayed neurodegeneration. Furthermore, the model facilitates *in vivo* investigation of the dose and route of administration prior to the more complex inoculation

studies. In addition, the burden of experimental animals in this assay is significantly lower, since the neurotoxic effect is restricted to a limited area of the brain.

The acute nature of the model offers an advantage for the investigator and reduces the burden of animals in the experiment. However, the discrepancy in results between models for NCX3 deficient mice illustrates that the new assay lacks the power to fully replace inoculation experiments. The promising results based on the *in vivo* anti-prion model still need to be confirmed in an inoculation experiment. It should be pointed out that differences in results are hypothetically of similar importance than equal results between the models, as they potentially uncover important adaptive changes in the chronic **inoculation model**.

Passive immunotherapy in order to stop or delay disease progression in TSE continues to be pursued as a therapeutic strategy. Our results as well as others have described fatal neurodegenerative side effects of some **antiprion antibodies** (Lefebvre-Roque et al., 2007; Solforosi et al., 2004; Sonati, 2013b). Although the relevance of these effects in humans is unclear and intracerebral application will not be used, it is conterintuitive to take the financial risk of a clinical study with a compound that has already demonstrated neurotoxicity in pre-clinical study. Here I appeal to the prion research community to initially invest in novel prion protein ligands, which will then be rigorously tested for their neurotoxic potential. I propose that identification of a hyperintese signal on DWI will be used as a risk assessment tool in further *in vivo* safety studies. I have found the relationship between a histological lesion and a positive signal on DWI to be excellent. In contrast to conventional histological methods, the whole brain is assessed in a single MRI session, without the risk of tissue loss upon sectioning. As more sequential imaging at different time points in intact mice is possible, the method promises to approximate the clinical setting. In fact, as animal MRI becomes more widely available, the feasibility of my proposal is increased.

MATERIAL AND METHODS

Mice

All mouse experiments were performed according to Swiss federal regulations and were approved by the Animal Experimentation Committee of the Canton of Zurich (permits 200/2007, #41/2012). Mice were housed under specific pathogen free conditions.

Female and male inbred mouse strains C57BL/6JOlaHsd1 (BL6), C57BL/6J (BL6J) and 129S2/SvHsd (129) were bred in-house. C57BL/6NHsd2 (BL6/Hsd2) and C57BL/10 (BL10) were purchased from the Harlan or Jackson laboratory, respectively. Coisogenic BL6.129-*Prnp*$^{o/o}$, BL6.129-*Prnp*$^{o/o}$-*tga20*$^{+/+}$ (*tga20*), BL6.129-*Prnp*$^{o/o}$-C4/C4 ($PrP_{\Delta 32\text{-}93}$), BL6.129-*Prnp*$^{o/o}$-*Prnp*$^{o/o}$-L52 ($PrP_{\Delta 94\text{-}110}$), BL6.129-*Prnp*$^{o/o}$-NSE-PrP$^{+/+}$ (NSE-PrP) and mice were on a mixed 129S2/SvHsd and C57BL/6JOlaHsd1 background (Brandner et al., 1996; Bremer et al., 2010; Büeler et al., 1992; Fischer et al., 1996; Flechsig et al., 2000; Radovanovic et al., 2005). Congenic Edinburgh 129-*Prnp*$^{-/-}$ were on a pure 129S2/SvHsd background (Manson et al., 1994).

Coisogenic BL6J.129-Cybbtm1Din/J (NOX2$^{o/o}$)-deficient mice were generated on a mixed 129S2/SvHsd and C57BL/6JOlaHsd1 background and backcrossed to C57BL/6J (Pollock et al., 1995). Coisogenic heteroczygous BL6J.FVBN-hCast$^{+/-}$ (Rao et al., 2008) were crossed with BL6.129-*Prnp*$^{o/o}$-*tga20*$^{+/+}$ (*tga20*) to generate *Prnp*$^{o/o}$-hCast$^{+/-}$-*tga20*$^{+/-}$ (hCast$^{+/-}$-*tga20*$^{+/-}$) and *Prnp*$^{o/o}$-hCast$^{-/-}$-*tga20*$^{+/-}$ littermates (hCast$^{-/-}$-*tga20*$^{-/+}$). Coisogenic 129.CD1-NCX3 deficient mice were generated on a mixed 129Sv/CD1 background (Sokolow et al., 2004) and were crossed with a C57BL/6JOlaHsd1 mouse to generate NCX3$^{+/+}$ and NCX3$^{-/-}$ littermates in the second generation.

Chemicals and the generation of antibody derivatives and recombinant PrP

All compounds were purchased from Sigma/Aldrich unless otherwise stated.

POM monoclonals (Polymenidou et al., 2008) and D13 (Williamson et al., 1998) were produced in-house based on hybridoma technology and purified by affinity chromatography using protein G sepharose. A purity of around 90% was achieved for the monoclonals as analyzed by with silver stained SDS-PAGE. The monoclonal ICSM-18 was a generous gift from Simon Hawek and was dialyzed against PBS prior to intracerbral injection.

$F(ab)_1$ POM fragments were generated in house from the POM antibodies using papain digestion and purification with Protein A agarose followed by size exclusion chromatography. $ScFv^{POM1}$ and $ScFv^{POM2}$ were generated in the Zürich laboratory of Neuropathology by expression in E. coli and purification from insoluble inclusion bodies as previously described (Polymenidou et al., 2008). Recombinant mouse PrP was generated in E. coli and purified by high-affinity column refolding (Zahn et al., 1997).

Volumetric phantoms

Small cubes or irregular shaped bodies with a calibre between 1 and 10 mm were generated from the polymer clay FIMO® (Staedtler). In order to estimate density, three additional cylinders with a side length between 1 to 3 cm and a calibre of 9 mm were prepared. The material was then solidified in the oven at 110 °C for 30 minutes. Subsequently, all bodies were weighed with an analytic balance. The larger cubes were placed in a 10 ml cylinder half-filled with water. The volume was estimated based on the displacement of the water. Based on the volumes and weights, the mean of the density of the solidified polymer clay was estimated. By dividing the weight with the density the volume of the smaller bodies was calculated.

Each of the bodies was then placed into 5% Agarose (NuSieve low melting Agarose FMC BioProducts) into a 10 ml tube. Volume phantoms were placed into a 4.7-Tesla Bruker Pharmascan with a special 10 ml tube holder (Bruker). Images were acquired with the same sequence as used for MEMRI as described in the following chapter.

MEMRI and DWI

For MEMRI, mice received five intraperitoneal injections of $MnCl_2$ (40 $mgkg^{-1}$, 20 mM in H_2O and bicine, pH 7.4) at 12h intervals (Grunecker et al., 2010). The final injection was administered immediately after the stereotaxic injection.

For imaging acquisition, the mice were placed under isoflurane anesthesia at 4h, 24h and 72h post-surgery. Initially, the mice were placed on a bed equipped with a mouse whole-body radio frequency transmitter coil and a mouse head surface-coil receiver and then into the 4.7 Bruker Pharma scan. Body temperature was maintained with a warming blanket.

For MEMRI T-1 weighted brain images were obtained using a 3D gradient-echo sequence with the following parameters: TR: 15 ms, TE: 2.5 ms, flip angle: 20 deg, Average: 10, Matrix: 265/265/126 Voxel, Field of View: 2x2.56x2 cm^3, Acquisition time: 1 h, Voxel size: 78x100x156 μm^3. For DWI, routine gradient echo sequences with the following parameters were used: TR: 300 ms TE: 28 ms, flip angle: 90 deg, Average: 1, Matrix: 350 x 350, Field of View: 3 x 3 cm, Acquisition time: 17 min, Voxel size: 87x87 μm^3, slice thickness: 700 μm^3, Isodistance: 1400 μm^3 and b values: 13, 816 s/mm^2. For chronic treatment diffusion weighted images were achieved with an echo planar sequence with: TR: 7500, TE: 44.6, Voxel size: 0.1x0.1x0.7 mm, b value: 500 s/mm^2.

Quantification of MRI scans

Quantification was performed with ParaVision software (Version 5,Opl3,Bruker). Lesions were quantified by assessing two regions of interest (ROIs), corresponding to the lesion and total cerebellar or hypocampal area. ROIs were set for each optical slice of the data set. For the quantification of hippocampal lesions with MEMRI scans, the volume of non-affected CA3 was measured. ROIs were set on the ipsilateral and contralateral sides of injection. Volumes for each ROI were calculated by multiplying the sum of the ROI area by the voxel height. Data are presented as the lesion volume divided by the total cerebellar volume or hippocampal volume. For hippocampal lesion of MEMRI scans data are presented as CA3 volume (mm^3), separated by ipsilateral versus the contralateral side.

Volume phantoms were additionally analyzed with the Myriam (Intrasense) software. ROIs were set to the corresponding area of the imaged bodies.

For the statistical analysis of experiments involving the comparison of three or more data sets, we used one-way ANOVA with Dunnett's post-hoc test for comparison of all data sets. One or two-tailed unpaired Student's t-test was used to compare two data sets. The results are displayed as mean ±s.d. *P,0.05; **P,0.01; ***P,0.001, ****P,0.0001.

Stereotactic injections

Mice were anaesthetized with isoflurane and placed in a motorized stereotaxic frame controlled by software with a three-dimensional brain map, allowing for real-time monitoring of needle placement (Neurostar). The skull was exposed by a midline incision and a small hole was drilled using a surgical drill. The needle (Hamilton, pstAS, gauges 26 s) was then mounted in an electronic micro-injector unit and was placed for cerebellar injection at the following lambda coordinates: AP **-**2.3 mm, ML 0 mm, DV 2 mm, for CA1 injection at: A/P: -2 mm, ML: 1.3 mm, DV: -1.4 mm from Bregma or for CA3 injection at the following bregma coordinates: AP – 2 mm, ML ±1.7 mm, DV 2.2 mm, angle in ML/DV plane 15**°**. Antibodies (2 µl) were injected at a flow-rate of 0.5 µl/min and the needle was left in place for 3 min. The mice were sutured and then received an injection of buprenorphinum (0.1 mg per g of body weight).

Hematoxylin Eosin staining and immunohistochemistry of formalin-fixed, paraffin embedded tissue

Mice were euthanized after the last scan (5, 24 or 72h post injection) and the brains were fixed in 4% formalin. Cerebella or a 4mm coronal section from the posterior cortex were paraffin embedded and 2 µm coronal step sections (standard every 100 µm) were cut, deparaffinized and routinely stained with hematoxylin and eosin.

For immunohistochemistry, sections were deparaffinized through xylol and graded alcohols. Then heat-induced epitope retrieval in the microwave was performed in 10 mM citrate buffer

at pH 6. Sections were then incubated for 1h in blocking buffer (0.2% Triton X-100, 10% normal goat serum dissolved in phosphate-buffered saline: PBS) and incubated with unconjugated rabbit monoclonal anti-NeuN (10 µg ml^{-1}, Millipore) or rabbit polyclonal anti-Caspase3 (5 µg ml^{-1}, Milipore) diluted in blocking buffer at 4 °C over night.

After washing with PBS, sections for 3,3′-Diaminobenzidine tetrahydrochloride hydrate (DAB) immunohistochemistry, were then incubated for 1 hour at room temperature with the specific biotinylated secondary antibody (10 µg ml^{-1}, Vector Laboratories). This step was followed by several washes with PBS and incubation in horseradish peroxidase-avidin/biotin complex solution (Vector Laboratories). For visualization sections were incubated for 5 minutes in DAB (0.5 mg/ml) dissolved in phosphate buffer (0.1 M, pH 7.4) and then DAB conversion into a insoluble brown product was induced with hydrogen peroxide (H_2O_2).

For indirect immunofluorescence detection, brain sections were incubated with specific fluorescent-labeled secondary antibody (1 µg ml^{-1} Alexa Fluor 488). In the final PBS wash 4,6-diamidino-2-phenylindole, dihydrochloride (DAPI; Molecular Probes) was added and sections were mounted with Fluor Save (Calbiochem). For analysis, pictures were taken with a FluoView® FV10i Confocal Laser Scanning System.

TUNEL stainings

During apoptotic cell death, DNA is fragmented by endonuclease activity. Free hydroxyl groups at the 3'end can be labeled by the enzyme Terminal deoxynucleotidyl transferase (TdT) with labeled nucleotides, a method known as Terminal Uridine Deoxynucleotidyl Transferase dUTP nick end labeling (TUNEL) staining. The in situ Cell Death Detection kit (Roche) was used according to the manufacturer's instructions. In brief, two micrometer sections of paraffin-embedded brain tissue were deparaffinized, rehydrated and incubated with proteinase K (PK) 20 µg ml^{-1} for 10 min at 37 °C to break through the formalin fixation induced protein cross links. Then the sections were incubated with the working-strength terminal deoxynucleotidyl transferase (TdT) enzyme and digoxigenin labeled dUTP for 60 min at 37 °C, following staining with fluorescently labeled anti-digoxigenin antibody. Sections

were counterstained with DAPI.

Pharmacological treatment of animals

For acetylated hydroxytyrosol (Granados-Principal et al., 2010), mice were treated starting 7 days before injection with 2 g l^{-1} in the drinking water.

The calpain inhibitor E64D (Mehdi, 1991) was injected intraperitoneally at 5 mg/KG 30 minutes before and 4 hours post stereotactic antibody injection.

Inoculation of mice

Three-month-s old mice were inoculated intracerebrally into the left hemisphere with 30 µl of Rocky Mountain Labaratory strain mouse-adapted scrapie prions passage-6 (RML-6) at a concentration of 0.1% homogenate, corresponding to 3 x 10^5 LD_{50}. Prior to the expected beginning of symptoms, mice were monitored every second day. After the onset of the characteristic clinical symptoms (ataxia, kyphosis, tail rigidity and hind leg paralysis), the mice were monitored daily. At the terminal stage of the disease, the mice were sacrificed.

Fodrin Western blot

The mice were euthanized after the 24h scan and the cerebellum or dissected hipocampus was snap frozen with liquid nitrogen. The extracted tissue was homogenized in PBS with 0.32 sucrose supplemented with complete mini protease-inhibitor mix (Roche)and homogenized by trituration using a 30 G syringe. The protein concentration was determined using the bicinchoninic acid assay (Pierce). Samples were prepared in loading buffer (NuPAGE, Invitrogen) and boiled at 95 °C for 5 min Proteins (10 µg per lane) were separated on a 4–12% gradient gel (NuPAGE, Invitrogen) and blotted onto a nitrocellulose membrane. Membranes were blocked with 5% w/vol Topblock (Fluka) in Tris-buffered saline supplemented with Tween (150 mM NaCl, 10 mM Tris HCl, 0.05% Tween 20 (vol/vol)) and incubated with primary mouse anti-α-fodrin (AA6, 100 ng ml^{-1}, Millipore) and mouse anti-actin (100 ng ml^{-1}, Chemicon) in 1% Topblock overnight. After washing in Tris-buffer, the

membrane was incubated with horseradish peroxidase (HRP)-conjugated rabbit anti–mouse IgG1 (1:10,000, Zymed) for an hour. Finally blots were developed using SuperSignal West Pico chemiluminescent substrate (Pierce) and visualized using the VersaDoc system (model 3000, Bio-Rad).

Detection of antibody distribution with Cy5 labeled POM2

The entire antibody POM2 was labeled with using the Cy5 mAB labeling kit (GE Healthcare Amersham) and injected into the hippocampus of 3-month-old mice. Twenty-four hours post-antibody injection, the mice were euthanized and 4 mm coronal sections of the posterior cortex were embedded in Hanks balanced salt solution and frozen with liquid nitrogen. Cryosections (10 µm thick) were prepared and stained with DAPI (Molecular Probes) and mounted with Fluor Save (Calbiochem). Sections were then imaged with the virtual microscope Axio Scan Z1 (Zeiss).

Mini-osmotic pump implantation

Mini-Osmotic Pumps (Alzet Model 2004 0.25 µl/h) were filled with antibody diluted in PBS, according to the manufacture's instructions. Filled pumps were placed in PBS at 37 °C for 24h. *Tga20* was anaesthetized with isoflurane and placed in a motorized stereotaxic frame as described above. Next, the skull was exposed via an incision along the midline. Using blunt surgical dissection, a paraspinal, subcutaneous pouch was generated, in which the pump was positioned. A MRI compatible polyetheretherketone medical microtubing (Alzet) was connected to the pump and positioned at the following bregma coordinates: AP -0.22 mm, ML 0.9 mm, DV 2.5 mm and fixed to the skull with glue (AdheSe One F Viva Pen Refill and Heraeus Kulzer FLOWline). Mice were housed individually after surgery. Post intervention, the mice were treated with subcutaneous injections of Temgesic® (0.1 mg/kg), Finadyne® (5 mg/kg) and Glucose 5% (20 µl/kg). Borgal® (2 ml of 24%) and sugar (30 g) were added per liter of drinking water for one week post-surgery.

Golden Gate cloning of Bicistronic Vectors

Both bicistronic vectors were assembled using Golden Gate cloning (Engler et al., 2008). The method is based on IIs restriction endonucleases, which cleave the DNA outside their recognition sequence, such as Esp3I (Thermo Scientific). This enzyme recognizes CGTCTC sites and generates one base pair downstream the four base pair overhang.

The pCAG-T7 destination vector is based on the plasmid pCAG-RebZFN-L (a generous gift from Pawel Pelczar) and contains a LacZ cassette flanked by two Esp3I recognition sides and an Ampicillin resistance cassette. By digestion with Esp3I of the pCAG-T7 destination vector, the LacZ cassette was excised and a 3'GTGG overhang downstream of the CAG/T7 promoter and a 5'GTCA overhang upstream of the polyadenlyation signal were generated.

For the generation of the pCAG-T7-NeonGreen-2A-mPrP construct, two inserts for golden gate cloning into pCAG-T7 destination were generated by PCR. The first insert contained NeonGreen (Shaner et al., 2013) and the N-terminal (aa 1-28) part of the 2A side, the second insert the C-terminal (aa 29-67) component of the 2A side and the normal murine PrP. For generating the pCAG-T7-PrP-2A-NeonGreen, the reversed design was used.

Primers (all purchased from Mycrosynth) were designed so that the Esp3I digestion of the PCR products generated a 5' CACC overhang on the first insert and a 3' CAGT overhang on the second insert, comparable to the pCAG-T7 destination vector. For joining two inserts, a TAAA overhang has been generated on the 3' end on the first insert and at the 5' end on the second insert.

For PCR amplification, the proofreading polymerase Herculase (Agilent) was used and linear DNA fragments were purified with the Nucleo Spin and PCR clean-up kit (Machery Nagel).

The destination vector pCAG-T7 (150 ng) and the PCR amplified inserts were set into a 2:1 molar ratio and additionally 1xT4 ligase buffer (NEB), T4 ligase (400 U, NEB) and Esp3I (10U, Thermo Scientific) was added to the golden gate reaction mix. In a thermocycler, this reaction was incubated with the following program: 37 °C/5min, 16 °C/10 min for 10-50 cycles followed by 5 minutes at 50 °C and 5 minutes at 80 °C to inactivate the ligase.

Replication of Plasmid in E.coli and Colony PCR

For the replication of the plasmid generated by the golden gate reaction, electrocompetent E.coli (Top10 Electrocomp, Life Technologies) were transformed using a Micro Pulser electroporation apparatus (BioRad Gene Pulser TM) and electroporation cuvettes (1 mm, Bio Rad). The electoporator was set to the following conditions (resistance: 200 Ohms, gene pulser: 1.5 kV, capacitance: 25 µFD).

After electroporation, bacteria were immediately placed in Luria-Bertani (LB) medium without antibiotics for one hour. Then, transformed E.coli were plated on LB agar containing 100 µg/ml Ampicillin and for blue-white selection 40 µg/ml 5-bromo-4-chloro-3-indolyl-beta-D-galactopyranoside (Xgal) and isopropyl beta-D-thiogalactopyranoside (IPTG). Bacteria were then cultured over night (8 hours).

Thirty white colonies have been selected and screened for the correct insert based on PCR ("colony PCR"). For this step, a forward primer binding to the pCAGT7 destination vector upstream on the insert (CATGCCTTCTTCTTTTTCCTAC) and a reverse primer binding to PrP (GGCTTTGGCCGCTTTTTGC) were used. For the Colony PCR the redTaq ready mix (Sigma Aldrich) was used and the reactions were incubated in a thermocycler with the following touchdown program: 95 °C for 30 seconds, 63 °C with a touch down temperature of 0.75 °C for 30 seconds and 72 °C for 90 seconds for 20 cycles followed by 95 °C for 30 seconds, 48 °C for 30 seconds and 72 °C for 90 seconds for 20 cycles. The product was then directly loaded on a 2% agar gel and illuminated with UV light. One of the colonies, which showed a PCR product with the expected length, was then purified from 7 ml of bacterial culture in LB medium using the Nucleo Spin plasmid kit (Machery Nagel) and from 250 ml culture using the Endotoxin Plasmid Midi kit (Qiagen).

Immunohistochemistry of transfected cells

The HEK293T cell line was cultured at 37 °C in a humidified atmosphere with 5% CO_2. Then cells were cultured in a 12-well format on gelatin coated (2% Gelatin) coverslips until they reached approximately 90% confluency. Cells were then transfected with the plasmid using

Lipofectamine® (1.6 µg DNA, 4% Lipofectamie). One day later, cells were fixed in 4% Parafomaldehyde. The cover slips with the fixed cells were then incubated for 10 minutes in TritonX solution (0.1% in 0.5% bovine serum albumin dissolved in PBS) and blocked with 0.5% bovine serum albumin for 45 minutes. Then cells were incubated with POM1 (2 µg ml^{-1}) diluted in PBS containing 0.5% bovine serum albumin for 1 hour. After washing, the cells were incubated with fluorescent-labeled secondary anti-mouse antibody (1 µg ml^{-1} Alexa Fluor 488). In the last PBS wash 4,6-diamidino-2-phenylindole, dihydrochloride (DAPI; Molecular Probes) was added and sections were mounted with Fluor Save (Calbiochem). For analysis pictures were taken with a FluoView® FV10i Confocal Laser Scanning System.

Testing of PrP surface expression of transfected cells

For surface expression analysis cells were cultured in 25T well flasks until they reached 90% confluency. Cells were then transfected with the plasmid using Lipofectamine® (8 µg DNA, 4% Lipofectamie). One day later, the cells were incubated with biotinilytion reagent (1 mg ml^{-1}, EZ-Link™, Thermo Scientific) for 30 minutes at 4 °C, following two washes with 200 mM glycine in PBS. After the cells were lysed in RIPA buffer containing protease inhibitor (complete mini, Roche), they were passed through a syringe and the protein concentration was determined using the bicinchoninic acid assay (Pierce). 50 µl of streptavidin conjugated beads (NeutrAvidin Agarose Serin, Thermo Scientific) were then added to 500 ug of protein sample and incubated on a rotating wheel at 4 °C overnight to allow binding of the biotinilated protein with the streptaviding conjugated beads. The bead protein complexes was then washed with 0.1% NP-40 detergent solution by centrifugation (500 g for 2 minutes) five times at 4 °C. Then the pulled down proteins were eluted from the beads with loading buffer (NuPAGE, Invitrogen) containing 100 mM DTT and boiled at 95 °C for 10 min. The beads were removed by centrifugation at maximal speed. 28 µl of eluted protein were the loaded on a 12% gel (NuPAGE, Invitrogen) and blotted onto a nitrocellulose membrane. Membranes were blocked with 5% w/vol Topblock (Fluka) in Tris-buffered saline supplemented with Tween (150 mM NaCl, 10 mM Tris HCl, 0.05% Tween 20 (vol/vol)) and incubated with POM1

(100 ng ml^{-1}, Millipore) and mouse anti-actin (100 ng ml^{-1}, Chemicon) in 1% Topblock over night. After washing in Tris-buffer, the membrane was incubated with horseradish peroxidase (HRP)-conjugated rabbit anti–mouse IgG1 (1:10,000, Zymed) for an hour. Finally, blots were developed using SuperSignal West Pico chemiluminescent substrate (Pierce) and visualized using the VersaDoc system (model 3000, Bio-Rad).

ACKNOWLEDGMENTS

These years have been an extraordinary journey into science and an intense experience in acquiring the requisite tools to successfully address scientific questions. At this point, I would like to express my gratitude to all people that have helped me during my journey:

During the last years I learned to know **Adriano Aguzzi** as an extraordinary chief, mentor and supervisor of my thesis. I thank him for sharing his outstanding experience and passion in science with me and many other young scientists. He triggered an intellectual maturation that I would otherwise never have reached in the same period.

Secondly, I would like to thank **Jeppe Falsig**. As a post-doc he provided me with the opportunity to take over the MRI part of the antiprion antibody toxicity project. In addition, he provided with an introduction into the laboratory and supervised me during the first years. My contribution would have certainly not been possible without the work of my colleague **Tiziana Sonati**. I 'am very thankful for her teaching and all the open discussions.

Special thanks are in order to my diagnostic supervisor: **Elisabeth Rushing** for all the teaching, motivation, sharing of experience and English corrections including this thesis; **Herbert Budka** for opening my eye to the fascinating world of neuropathology; **Ingeborg Fischer** and **Hildegard Domen Sheufert** for the introduction to neuropathology; **Hans Hilmar Goebel** for his introduction into the secret of myopathologys. Thanks to **Umberto de Girolami** for his guided excursions into Neuroanatomy and to **Manuela Neumann** for improving my precision.

Furthermore, I would like to extend my gratitude to Irene Knüsel and **Markus Rudin** as the other members of my PhD committee for all their input and helpful discussions.

Many thanks are in order for Ueli Hermann, who tought me how to implantat mini-osmotic pumps, **Udo Ungethüm** for the MRI introduction and for **Andreas Steingötter,** who helped with the establishment of the scanning parameters.

Mario Hermann, an extraordinary and valuable colleague, who generously shared his knowledge regarding the secrets of cloning.

Simone Hornemann for all her help and teaching.

Mario Nuvolone, Asvin Lakkaraju, **Vijay Chandrasekar, Susy Senatore**, **Silvia Sorce** and **Agnes Lau** for sharing with me protocols and all the discussions and help.

Livia Tacacs and **Ahmet Varol** for technical help.

Simon Hawek for ICSM18. **Michael Arand** for suggesting the benchmark dose analysis.

Thanks to all my neuropathology residency colleagues for all the years working together: **Dino Saban, Doreen Lem, Alejandra Madagana, Francine Hen de Oliveira, Veronika Kana, Henning Leske, Karl Frontzek, Christian Kempf and Daniel Kirschenbaum.**

Thanks to **Petra Schwarz** for all the help with the permissions for in-vivo experiments, to **Marianne König** for the all the paraffin sections and to **Rita Moos** for technical help. **Mirzet Delic** for all the help with the mice.

Badma Segarane, Alexander Küffner, Despoina Goniotaki, Sergey Jakushev, Caihong Zhu, Melanie Einsiedler and Manuela Pfaffmatter for help and suggestions.

The **university of Zurich** for funding and the **Neurocenter Zürich** for guidance.

Thanks to my parents **Gaberiele Reimann** and **Johannes Reimann** for believing in me and all support. I'am grateful for my sister Salome Reimann and her family.

Milosz Halicki for his love, support and for his understanding about the demands of my work.

I close in memory to my grand-grand mother **Brunhilde Hunziker–Kramer** and grandmother **Rose Reimann–Hunziker,** which have been my guide in my childhood towards a emanzipated and independent women. They taught me to take the opportunities life provide.

CURRICULUM VITAE AND PUBLICATIONS

Personal Date

First names: Regina Rose Désirée
Last name: Reimann
Date of birth: 31.01.1983
Heimatort: Basel BS und Winterthur ZH

Education

PhD **University of Zurich, Zentrum für Neurowissenschaften Zürich (ZNZ)**
February 2012 – present.
Thesis: Magnetic Resonance Imaging in the Assessment of Anti Prion Mediated Neurotoxicity In Vivo.
Comitee: Prof. Adriano Aguzzi, Institute of Neuropathology, Zurich (chair), PD Dr. Irene Knüsel, Institute of Pharmacology and Toxicology, Prof. M. Rudin, Institut of Biomedical Engineering, ETH Zurich.

MD **University of Basel**
Medicine: October 2003 – November 2009.
State examination in medicine, University of Basel, November 2009.
MD thesis January 2010. Institute of Neurobiology biocenter university Basel.
Thesis: Immunohistochemical analysis of myelinated nerve fibers in human Skin.
Supervisor: Prof. Dr. med. Andreas Steck, Chair Emeritus of Neurology, University Hospital of Basel.

Matura **Mittelschule Stans, Physics and Applied Mathematics, June 2002.**
Matriculation project: Frauen in exakten Wissenschaften

Residency

Pathology, Institute of Pathology, University hospital Zurich

December 2014 - present

Neuropathology, Institute of Neuropathology Zurich,

April 2010 – November 2014

Publications

Herrmann, U.S., Sonati, T., Falsig, J., **Reimann, R.R.**, Dametto, P., O'Connor, T., Li, B., Lau, A., Hornemann, S., Sorce, S., Wagner, U., Sanoudou, D., Aguzzi, A., 2015. **Prion Infections and Anti-PrP Antibodies Trigger Converging Neurotoxic Pathways.** PLoS Pathog 11, e1004662.

Tiziana Sonati*, **Regina R. Reimann***, Jeppe Falsig*, Pravas Kumar Baral, Tracy O'Connor, Simone Hornemann, Sine Yaganoglu, Bei Li, Uli S. Herrmann, Barbara Wieland, Mridula Swayampakula, Muhammad Hafizur Rahman, Dipankar Das, Nat Kav, Roland Riek, Pawel P. Liberski, Michael N. G. James & Adriano Aguzzi. **The toxicity of antiprion antibodies is mediated by the flexible tail of the prion protein**. *Nature,* 501(7465), 102-6, 2013.

Annika Keller, Ana Westenberger, Maria J Sobrido, Maria García-Murias, Aloysius Domingo, Renee L Sears, Roberta R Lemos, Andres Ordoñez-Ugalde, Gael Nicolas, José E Gomes da Cunha, Elisabeth J Rushing, Michael Hugelshofer, Moritz C Wurnig, Andres Kaech, **Regina Reimann**, Katja Lohmann, Valerija Dobričić, Angel Carracedo, Igor Petrović, Janis M Miyasaki, Irina Abakumova, Maarja Andaloussi Mäe, Elisabeth Raschperger, Mayana Zatz, Katja Zschiedrich et *al.* **Mutations in the gene encoding PDGF-B cause brain calcifications in humans and mice.** *Nature Genetics,* 45(9), 1077-82, 2013.

Neidert MC, Woernle CM, Burkhardt JK, **Reimann R**, Hug E, Bernays RL.Case Report; **Trabecular Juvenile Ossifying Fibroma Presenting as a Sellar Mass.** *J Neurol Surg A Cent Eur Neurosurg*, 2012.

Stalder AK, Erne B, **Reimann R,** Renaud S, Fuhr P, Thomman S, Arnold A, Probst A, Schaeren-Wiemers N, Steck AJ. **"Immunoglobulin M deposition in cutaneous nerves of anti-myelin-associated glycoprotein polyneuropathy patients correlates with axonal degeneration."** J. of Neuropathol. Exp. Neurol., 68(2):148-58, 2009.

REFERENCES

Aguzzi, A., Baumann, F., Bremer, J., 2008. The Prion's Elusive Reason for Being. Annu Rev Neurosci 31, 439-477.

Aguzzi, A., Calella, A.M., 2009. Prions: protein aggregation and infectious diseases. Physiol Rev 89, 1105-1152.

Aguzzi, A., Falsig, J., 2012. Prion propagation, toxicity and degradation. Nat Neurosci 15, 936-939.

Aguzzi, A., O'Connor, T., 2010. Protein aggregation diseases: pathogenicity and therapeutic perspectives. Nat Rev Drug Discov 9, 237-248.

Aguzzi, A., Rajendran, L., 2009. The transcellular spread of cytosolic amyloids, prions, and prionoids. Neuron 64, 783-790.

Albers, G.W., 1998. Diffusion-weighted MRI for evaluation of acute stroke. Neurology 51, S47-49.

Alper, T., Cramp, W.A., Haig, D.A., Clarke, M.C., 1967. Does the agent of scrapie replicate without nucleic acid? Nature 214, 764-766.

Anderson, L., Rossi, D., Linehan, J., Brandner, S., Weissmann, C., 2004. Transgene-driven expression of the Doppel protein in Purkinje cells causes Purkinje cell degeneration and motor impairment. Proc Natl Acad Sci U S A 101, 3644-3649.

Anderson, R.M., Donnelly, C.A., Ferguson, N.M., Woolhouse, M.E., Watt, C.J., Udy, H.J., MaWhinney, S., Dunstan, S.P., Southwood, T.R., Wilesmith, J.W., Ryan, J.B., Hoinville, L.J., Hillerton, J.E., Austin, A.R., Wells, G.A., 1996. Transmission dynamics and epidemiology of BSE in British cattle. Nature 382, 779-788.

Andrews, N., 2012. Incidence of variant Creutzfeldt-Jakob disease diagnoses and deaths in the UK January 1994 - December 2011.

Atarashi, R., Nishida, N., Shigematsu, K., Goto, S., Kondo, T., Sakaguchi, S., Katamine, S., 2003. Deletion of N-terminal residues 23-88 from prion protein (PrP) abrogates the potential to rescue PrP-deficient mice from PrP-like protein/doppel-induced Neurodegeneration. J Biol Chem 278, 28944-28949.

Balducci, C., Beeg, M., Stravalaci, M., Bastone, A., Sclip, A., Biasini, E., Tapella, L., Colombo, L., Manzoni, C., Borsello, T., Chiesa, R., Gobbi, M., Salmona, M., Forloni, G., 2010. Synthetic amyloid-{beta} oligomers impair long-term memory independently of cellular prion protein. Proc Natl Acad Sci U S A 107, 2295-2300.

Basler, K., Oesch, B., Scott, M., Westaway, D., Walchli, M., Groth, D.F., McKinley, M.P., Prusiner, S.B., Weissmann, C., 1986. Scrapie and cellular PrP isoforms are encoded by the same chromosomal gene. Cell 46, 417-428.

Baumann, F., Tolnay, M., Brabeck, C., Pahnke, J., Kloz, U., Niemann, H.H., Heikenwalder, M., Rulicke, T., Burkle, A., Aguzzi, A., 2007. Lethal recessive myelin toxicity of prion protein lacking its central domain. Embo J 26, 538-547.

Beland, M., Roucou, X., 2012. The prion protein unstructured N-terminal region is a broad-spectrum molecular sensor with diverse and contrasting potential functions. J Neurochem 120, 853-868.

Bendheim, P.E., Barry, R.A., DeArmond, S.J., Stites, D.P., Prusiner, S.B., 1984. Antibodies to a scrapie prion protein. Nature 310, 418-421.

Beringue, V., Mallinson, G., Kaisar, M., Tayebi, M., Sattar, Z., Jackson, G., Anstee, D., Collinge, J., Hawke, S., 2003. Regional heterogeneity of cellular prion protein isoforms in the mouse brain. Brain 126, 2065-2073.

Bloch, F., Hansen, W.W., Packard, M., 1946a. Nuclear Induction. Physical Review 69, 127-127.

Bloch, F., Hansen, W.W., Packard, M., 1946b. The Nuclear Induction Experiment. Physical Review 70, 474-485.

Bock, N.A., Paiva, F.F., Silva, A.C., 2008. Fractionated manganese-enhanced MRI. NMR Biomed 21, 473-478.

Bolton, D.C., McKinley, M.P., Prusiner, S.B., 1982. Identification of a protein that purifies with the scrapie prion. Science 218, 1309-1311.

Brandner, S., Isenmann, S., Raeber, A., Fischer, M., Sailer, A., Kobayashi, Y., Marino, S., Weissmann, C., Aguzzi, A., 1996. Normal host prion protein necessary for scrapie-induced neurotoxicity. Nature 379, 339-343.

Brazier, M.W., Lewis, V., Ciccotosto, G.D., Klug, G.M., Lawson, V.A., Cappai, R., Ironside, J.W., Masters, C.L., Hill, A.F., White, A.R., Collins, S., 2006. Correlative studies support lipid peroxidation is linked to PrP(res) propagation as an early primary pathogenic event in prion disease. Brain Res Bull 68, 346-354.

Bremer, J., Baumann, F., Tiberi, C., Wessig, C., Fischer, H., Schwarz, P., Steele, A.D., Toyka, K.V., Nave, K.A., Weis, J., Aguzzi, A., 2010. Axonal prion protein is required for peripheral myelin maintenance. Nat Neurosci 13, 310-318.

Budka, H., 2003. Neuropathology of prion diseases. Br Med Bull 66, 121-130.

Büeler, H.R., Fischer, M., Lang, Y., Bluethmann, H., Lipp, H.P., DeArmond, S.J., Prusiner, S.B., Aguet, M., Weissmann, C., 1992. Normal development and behaviour of mice lacking the neuronal cell-surface PrP protein. Nature 356, 577-582.

Chazot, G., Broussolle, E., Lapras, C., Blättler, T., Aguzzi, A., Kopp, N., 1996. New variant of Creutzfeldt-Jakob disease in a 26-year-old French man. Lancet 347, 1181.

Chesebro, B., Trifilo, M., Race, R., Meade-White, K., Teng, C., LaCasse, R., Raymond, L., Favara, C., Baron, G., Priola, S., Caughey, B., Masliah, E., Oldstone, M., 2005. Anchorless prion protein results in infectious amyloid disease without clinical scrapie. Science 308, 1435-1439.

Choi, S.I., Ju, W.K., Choi, E.K., Kim, J., Lea, H.Z., Carp, R.I., Wisniewski, H.M., Kim, Y.S., 1998. Mitochondrial dysfunction induced by oxidative stress in the brains of hamsters infected with the 263 K scrapie agent [In Process Citation]. Acta Neuropathol (Berl) 96, 279-286.

Citron, M., 2010. Alzheimer's disease: strategies for disease modification. Nat Rev Drug Discov 9, 387-398.

Croall, D.E., Ersfeld, K., 2007. The calpains: modular designs and functional diversity. Genome Biol 8, 218.

Deleault, N.R., Harris, B.T., Rees, J.R., Supattapone, S., 2007. Formation of native prions from minimal components in vitro. Proc Natl Acad Sci U S A 104, 9741-9746.

Donnelly, M.L., Luke, G., Mehrotra, A., Li, X., Hughes, L.E., Gani, D., Ryan, M.D., 2001. Analysis of the aphthovirus 2A/2B polyprotein 'cleavage' mechanism indicates not a proteolytic reaction, but a novel translational effect: a putative ribosomal 'skip'. J Gen Virol 82, 1013-1025.

Eisenberg, D., Jucker, M., 2012. The amyloid state of proteins in human diseases. Cell 148, 1188-1203.

Engler, C., Kandzia, R., Marillonnet, S., 2008. A one pot, one step, precision cloning method with high throughput capability. PLoS ONE 3, e3647.

Faas, H., Jackson, W.S., Borkowski, A.W., Wang, X., Ma, J., Lindquist, S., Jasanoff, A., 2010. Context-dependent perturbation of neural systems in transgenic mice expressing a cytosolic prion protein. Neuroimage 49, 2607-2617.

Falsig, J., Julius, C., Margalith, I., Schwarz, P., Heppner, F., Aguzzi, A., 2008. A versatile prion replication assay in organotypic brain slices. Nat Neurosci 11, 109-117.

Falsig, J., Sonati, T., Herrmann, U.S., Saban, D., Li, B., Arroyo, K., Ballmer, B., Liberski, P.P., Aguzzi, A., 2012. Prion pathogenesis is faithfully reproduced in cerebellar organotypic slice cultures. PLoS Pathog 8, e1002985.

Fatokun, A.A., Stone, T.W., Smith, R.A., 2008. Oxidative stress in neurodegeneration and available means of protection. Front Biosci 13, 3288-3311.

FDA, TASK FORCE ON RISK MANAGEMENT, U.S. Department of Health and Human Services, Food and Drug administration, 1999. Managing the risks from medical product use. http://www.fda.gov/downloads/Safety/SafetyofSpecificProducts/UCM180522.pdf (24.02.2015)

FDA, Center for Drug Evaluation and Research, Center for Biologics Evaluation and Research, U.S. Department of Health and Human Services, Food and Drug administration, 2006. Q9 Quality Risk Management. http://www.fda.gov/downloads/Drugs/.../Guidances/ucm073511.pdf (24.02.2015)

Ferreiro, E., Oliveira, C.R., Pereira, C.M., 2008. The release of calcium from the endoplasmic reticulum induced by amyloid-beta and prion peptides activates the mitochondrial apoptotic pathway. Neurobiol Dis 30, 331-342.

Filipsson, A.F., Sand, S., Nilsson, J., Victorin, K., 2003. The benchmark dose method--review of available models, and recommendations for application in health risk assessment. Crit Rev Toxicol 33, 505-542.

Fischer, M., Rülicke, T., Raeber, A., Sailer, A., Moser, M., Oesch, B., Brandner, S., Aguzzi, A., Weissmann, C., 1996. Prion protein (PrP) with amino-proximal deletions restoring susceptibility of PrP knockout mice to scrapie. Embo J 15, 1255-1264.

Flechsig, E., Shmerling, D., Hegyi, I., Raeber, A.J., Fischer, M., Cozzio, A., von Mering, C., Aguzzi, A., Weissmann, C., 2000. Prion protein devoid of the octapeptide repeat region restores susceptibility to scrapie in PrP knockout mice. Neuron 27, 399-408.

Forloni, G., Angeretti, N., Chiesa, R., Monzani, E., Salmona, M., Bugiani, O., Tagliavini, F., 1993. Neurotoxicity of a prion protein fragment. Nature 362, 543-546.

Gajdusek, D.C., Zigas, V., 1957. Degenerative disease of the central nervous system in New Guinea; the endemic occurrence of kuru in the native population. N Engl J Med 257, 974-978.

Geva, T., 2006. Magnetic resonance imaging: historical perspective. J Cardiovasc Magn Reson 8, 573-580.

Gilman, S., Koller, M., Black, R.S., Jenkins, L., Griffith, S.G., Fox, N.C., Eisner, L., Kirby, L., Rovira, M.B., Forette, F., Orgogozo, J.M., 2005. Clinical effects of Abeta immunization (AN1792) in patients with AD in an interrupted trial. Neurology 64, 1553-1562.

Gordon, W.S., 1946. Advances in veterinary research. Vet Res 58, 516-520.

Granados-Principal, S., Quiles, J.L., Ramirez-Tortosa, C.L., Sanchez-Rovira, P., Ramirez-Tortosa, M.C., 2010. Hydroxytyrosol: from laboratory investigations to future clinical trials. Nutr Rev. 68, 191-206.

Griffith, J.S., 1967. Self-replication and scrapie. Nature 215, 1043-1044.

Grunecker, B., Kaltwasser, S.F., Peterse, Y., Samann, P.G., Schmidt, M.V., Wotjak, C.T., Czisch, M., 2010. Fractionated manganese injections: effects on MRI contrast enhancement and physiological measures in C57BL/6 mice. NMR Biomed 23, 913-921.

Guentchev, M., Voigtlander, T., Haberler, C., Groschup, M.H., Budka, H., 2000. Evidence for oxidative stress in experimental prion disease. Neurobiol Dis 7, 270-273.

Halliday, M., Mallucci, G.R., 2014. Targeting the unfolded protein response in neurodegeneration: A new approach to therapy. Neuropharmacology 76 Pt A, 169-174.

Hegde, R.S., Mastrianni, J.A., Scott, M.R., DeFea, K.A., Tremblay, P., Torchia, M., DeArmond, S.J., Prusiner, S.B., Lingappa, V.R., 1998. A transmembrane form of the prion protein in neurodegenerative disease. Science 279, 827-834.

Heppner, F.L., Musahl, C., Arrighi, I., Klein, M.A., Rulicke, T., Oesch, B., Zinkernagel, R.M., Kalinke, U., Aguzzi, A., 2001. Prevention of scrapie pathogenesis by transgenic expression of anti-prion protein antibodies. Science 294, 178-182.

Herrmann, U.S., Sonati, T., Falsig, J., Reimann, R.R., Dametto, P., O'Connor, T., Li, B., Lau, A., Hornemann, S., Sorce, S., Wagner, U., Sanoudou, D., Aguzzi, A., 2015. Prion Infections and Anti-PrP Antibodies Trigger Converging Neurotoxic Pathways. PLoS Pathog 11, e1004662.

Hornemann, S., Korth, C., Oesch, B., Riek, R., Wider, G., Wuthrich, K., Glockshuber, R., 1997. Recombinant full-length murine prion protein, mPrP(23-231): purification and spectroscopic characterization. FEBS Lett 413, 277-281.

Hornshaw, M.P., McDermott, J.R., Candy, J.M., 1995. Copper binding to the N-terminal tandem repeat regions of mammalian and avian prion protein. Biochem Biophys Res Commun 207, 621-629.

Jackson, G.S., Murray, I., Hosszu, L.L., Gibbs, N., Waltho, J.P., Clarke, A.R., Collinge, J., 2001. Location and properties of metal-binding sites on the human prion protein. Proc Natl Acad Sci U S A 98, 8531-8535.

Jarrett, J.T., Lansbury, P.T., Jr., 1993. Seeding "one-dimensional crystallization" of amyloid: a pathogenic mechanism in Alzheimer's disease and scrapie? Cell 73, 1055-1058.

Jin, J.K., Choi, J.K., Lee, H.G., Kim, Y.S., Carp, R.I., Choi, E.K., 1999. Increased expression of CaM kinase II alpha in the brains of scrapie-infected mice. Neurosci Lett 273, 37-40.

Ju, W.K., Park, K.J., Choi, E.K., Kim, J., Carp, R.I., Wisniewski, H.M., Kim, Y.S., 1998. Expression of inducible nitric oxide synthase in the brains of scrapie-infected mice. J Neurovirol 4, 445-450.

Jucker, M., Walker, L.C., 2011. Pathogenic protein seeding in Alzheimer disease and other neurodegenerative disorders. Ann Neurol 70, 532-540.

Kascsak, R.J., Rubenstein, R., Merz, P.A., Tonna DeMasi, M., Fersko, R., Carp, R.I., Wisniewski, H.M., Diringer, H., 1987. Mouse polyclonal and monoclonal antibody to scrapie-associated fibril proteins. J Virol 61, 3688-3693.

Kessels, H.W., Nguyen, L.N., Nabavi, S., Malinow, R., 2010. The prion protein as a receptor for amyloid-beta. Nature 466, E3-4; discussion E4-5.

Klöhn, P.C., Farmer, M., Linehan, J.M., O'Malley, C., Fernandez de Marco, M., Taylor, W., Farrow, M., Khalili-Shirazi, A., Brandner, S., Collinge, J., 2012. PrP antibodies do not trigger mouse hippocampal neuron apoptosis. Science 335, 52.

Kristensson, K., Feuerstein, B., Taraboulos, A., Hyun, W.C., Prusiner, S.B., DeArmond, S.J., 1993. Scrapie prions alter receptor-mediated calcium responses in cultured cells. Neurology 43, 2335-2341.

Kunz, B., Sandmeier, E., Christen, P., 1999. Neurotoxicity of prion peptide 106-126 not confirmed. FEBS Lett 458, 65-68.

Lauren, J., Gimbel, D.A., Nygaard, H.B., Gilbert, J.W., Strittmatter, S.M., 2009. Cellular prion protein mediates impairment of synaptic plasticity by amyloid-beta oligomers. Nature 457, 1128-1132.

Lauterbur, P.C., 1973. Image Formation by Induced Local Interactions - Examples Employing Nuclear Magnetic-Resonance. Nature 242, 190-191.

Lefebvre-Roque, M., Kremmer, E., Gilch, S., Zou, W.Q., Feraudet, C., Gilles, C.M., Sales, N., Grassi, J., Gambetti, P., Baron, T., Schatzl, H., Lasmezas, C.I., 2007. Toxic effects of intracerebral PrP antibody administration during the course of BSE infection in mice. Prion 1, 198-206.

Letourneau-Guillon, L., Wada, R., Kucharczyk, W., 2012. Imaging of prion diseases. Journal of Magnetic Resonance Imaging 35, 998-1012.

Li, A., Barmada, S.J., Roth, K.A., Harris, D.A., 2007. N-terminally deleted forms of the prion protein activate both Bax-dependent and Bax-independent neurotoxic pathways. J Neurosci 27, 852-859.

Lysek, D.A., Wuthrich, K., 2004. Prion protein interaction with the C-terminal SH3 domain of Grb2 studied using NMR and optical spectroscopy. Biochemistry 43, 10393-10399.

Ma, J., Wollmann, R., Lindquist, S., 2002. Neurotoxicity and Neurodegeneration When PrP Accumulates in the Cytosol. Science 298:, 1781-1785.

Macfarlane, R.G., Wroe, S.J., Collinge, J., Yousry, T.A., Jager, H.R., 2007. Neuroimaging findings in human prion disease. J Neurol Neurosurg Psychiatry 78, 664-670.

Magri, G., Clerici, M., Dall'Ara, P., Biasin, M., Caramelli, M., Casalone, C., Giannino, M.L., Longhi, R., Piacentini, L., Della Bella, S., Gazzuola, P., Martino, P.A., Della Bella, S., Pollera, C., Puricelli, M., Servida, F., Crescio, I., Boasso, A., Ponti, W., Poli, G., 2005. Decrease in pathology and progression of scrapie after immunisation with synthetic prion protein peptides in hamsters. Vaccine 23, 2862-2868.

Mallucci, G., Dickinson, A., Linehan, J., Klohn, P.C., Brandner, S., Collinge, J., 2003. Depleting neuronal PrP in prion infection prevents disease and reverses spongiosis. Science 302, 871-874.

Manson, J.C., Clarke, A.R., Hooper, M.L., Aitchison, L., McConnell, I., Hope, J., 1994. 129/Ola mice carrying a null mutation in PrP that abolishes mRNA production are developmentally normal. Mol Neurobiol 8, 121-127.

Matoba, M., Tonami, H., Miyaji, H., Yokota, H., Yamamoto, I., 2001. Creutzfeldt-Jakob disease: serial changes on diffusion-weighted MRI. J Comput Assist Tomogr 25, 274-277.

Mattson, M.P., 2007. Calcium and neurodegeneration. Aging Cell 6, 337-350.

Mehdi, S., 1991. Cell-penetrating inhibitors of calpain. Trends Biochem Sci 16, 150-153.

Meier D., Boesiger P., S., K., 2012. Magnetic Resonance Imaging in Medicine. http://wiki.epfl.ch/lapmal/documents/mri_resources/mri_basics.pdf. (24.02.2015)

Meissner, B., Kallenberg, K., Sanchez-Juan, P., Collie, D., Summers, D.M., Almonti, S., Collins, S.J., Smith, P., Cras, P., Jansen, G.H., Brandel, J.P., Coulthart, M.B., Roberts, H., Van Everbroeck, B., Galanaud, D., Mellina, V., Will, R.G., Zerr, I., 2009. MRI lesion profiles in sporadic Creutzfeldt-Jakob disease. Neurology 72, 1994-2001.

Mo, H., Moore, R.C., Cohen, F.E., Westaway, D., Prusiner, S.B., Wright, P.E., Dyson, H.J., 2001. Two different neurodegenerative diseases caused by proteins with similar structures. Proc Natl Acad Sci U S A 98, 2352-2357.

Molinaro, P., Cuomo, O., Pignataro, G., Boscia, F., Sirabella, R., Pannaccione, A., Secondo, A., Scorziello, A., Adornetto, A., Gala, R., Viggiano, D., Sokolow, S., Herchuelz, A., Schurmans, S., Di Renzo, G., Annunziato, L., 2008. Targeted disruption of Na+/Ca2+ exchanger 3 (NCX3) gene leads to a worsening of ischemic brain damage. J Neurosci 28, 1179-1184.

Moore, R.C., Lee, I.Y., Silverman, G.L., Harrison, P.M., Strome, R., Heinrich, C., Karunaratne, A., Pasternak, S.H., Chishti, M.A., Liang, Y., Mastrangelo, P., Wang, K., Smit, A.F., Katamine, S., Carlson, G.A., Cohen, F.E., Prusiner, S.B., Melton, D.W., Tremblay, P., Hood, L.E., Westaway, D., 1999. Ataxia in prion protein (PrP)-deficient mice is associated with upregulation of the novel PrP-like protein doppel J Mol Biol 292, 797-817.

Mouillet-Richard, S., Ermonval, M., Chebassier, C., Laplanche, J.L., Lehmann, S., Launay, J.M., Kellermann, O., 2000. Signal transduction through prion protein. Science 289, 1925-1928.

Muramoto, T., DeArmond, S.J., Scott, M., Telling, G.C., Cohen, F.E., Prusiner, S.B., 1997. Heritable disorder resembling neuronal storage disease in mice expressing prion protein with deletion of an alpha-helix. Nat Med 3, 750-755.

Nishida, N., Tremblay, P., Sugimoto, T., Shigematsu, K., Shirabe, S., Petromilli, C., Erpel, S.P., Nakaoke, R., Atarashi, R., Houtani, T., Torchia, M., Sakaguchi, S., DeArmond, S.J., Prusiner, S.B., Katamine, S., 1999. A mouse prion protein transgene rescues mice deficient for the prion protein gene from purkinje cell degeneration and demyelination. Lab Invest 79, 689-697.

Nuvolone, M., Kana, V., Hutter, G., Sakata, D., Mortin-Toth, S.M., Russo, G., Danska, J.S., Aguzzi, A., 2013. SIRPalpha polymorphisms, but not the prion protein, control phagocytosis of apoptotic cells. J Exp Med 210, 2539-2552.

Ohsawa, N., Song, C.H., Suzuki, A., Furuoka, H., Hasebe, R., Horiuchi, M., 2013. Therapeutic effect of peripheral administration of an anti-prion protein antibody on mice infected with prions. Microbiol Immunol 57, 288-297.

Pan, K.M., Baldwin, M., Nguyen, J., Gasset, M., Serban, A., Groth, D., Mehlhorn, I., Huang, Z., Fletterick, R.J., Cohen, F.E., et al., 1993. Conversion of alpha-helices into beta-sheets features in the formation of the scrapie prion proteins. Proc Natl Acad Sci U S A 90, 10962-10966.

Pan, T., Li, R., Wong, B.S., Liu, T., Gambetti, P., Sy, M.S., 2002. Heterogeneity of normal prion protein in two- dimensional immunoblot: presence of various glycosylated and truncated forms. J Neurochem 81, 1092-1101.

Pannaccione, A., Secondo, A., Molinaro, P., D'Avanzo, C., Cantile, M., Esposito, A., Boscia, F., Scorziello, A., Sirabella, R., Di Renzo, G., Annunziato, L., 2012. A new concept: Abeta1-42 generates a hyperfunctional proteolytic NCX3 fragment that delays caspase-12 activation and neuronal death. J Neurosci 32, 10609-10617.

Pattison, I.H., 1965. Resistance of the scrapie agent to formalin. J Comp Pathol 75, 159-164.

Pauly, P.C., Harris, D.A., 1998. Copper stimulates endocytosis of the prion protein. J Biol Chem 273, 33107-33110.

Pollock, J.D., Williams, D.A., Gifford, M.A., Li, L.L., Du, X., Fisherman, J., Orkin, S.H., Doerschuk, C.M., Dinauer, M.C., 1995. Mouse model of X-linked chronic granulomatous disease, an inherited defect in phagocyte superoxide production. Nat Genet 9, 202-209.

Polymenidou, M., Heppner, F.L., Pellicioli, E.C., Urich, E., Miele, G., Braun, N., Wopfner, F., Schaetzl, H., Becher, B., Aguzzi, A., 2004. Humoral immune response to native eukaryotic prion protein correlates with anti-prion protection. Proc Natl Acad Sci U S A 101, 14670-14676.

Polymenidou, M., Moos, R., Scott, M., Sigurdson, C., Shi, Y.Z., Yajima, B., Hafner-Bratkovic, I., Jerala, R., Hornemann, S., Wuthrich, K., Bellon, A., Vey, M., Garen, G., James, M.N., Kav, N., Aguzzi, A., 2008. The POM monoclonals: a comprehensive set of antibodies to non-overlapping prion protein epitopes. PLoS ONE 3, e3872.

Prinz, M., Huber, G., Macpherson, A.J., Heppner, F.L., Glatzel, M., Eugster, H.P., Wagner, N., Aguzzi, A., 2003. Oral Prion Infection Requires Normal Numbers of Peyer's Patches but Not of Enteric Lymphocytes. Am J Pathol 162, 1103-1111.

Prusiner, S.B., 1982. Novel proteinaceous infectious particles cause scrapie. Science 216, 136-144.

Prusiner, S.B., 1991. Molecular biology of prion diseases. Science 252, 1515-1522.

Prusiner, S.B., McKinley, M.P., Bowman, K.A., Bolton, D.C., Bendheim, P.E., Groth, D.F., Glenner, G.G., 1983. Scrapie prions aggregate to form amyloid-like birefringent rods. Cell 35, 349-358.

Purcell E. M., Torrey H. C., V., P.R., 1945. Resonance Absorption by Nuclear Magnetic Moments in a Solid. Physical Review 69, 37-38.

Radovanovic, I., Braun, N., Giger, O.T., Mertz, K., Miele, G., Prinz, M., Navarro, B., Aguzzi, A., 2005. Truncated prion protein and Doppel are myelinotoxic in the absence of oligodendrocytic PrPC. J Neurosci 25, 4879-4888.

Rao, M.V., Mohan, P.S., Peterhoff, C.M., Yang, D.S., Schmidt, S.D., Stavrides, P.H., Campbell, J., Chen, Y., Jiang, Y., Paskevich, P.A., Cataldo, A.M., Haroutunian, V., Nixon, R.A., 2008. Marked calpastatin (CAST) depletion in Alzheimer's disease accelerates cytoskeleton disruption and neurodegeneration: neuroprotection by CAST overexpression. J Neurosci 28, 12241-12254.

Riek, R., Hornemann, S., Wider, G., Glockshuber, R., Wüthrich, K., 1997. NMR characterization of the full-length recombinant murine prion protein, mPrP(23-231). FEBS Lett 413, 282-288.

RMIT, Royal Melbourne Institute of technology, 2008. Pharmaceutical Safety Evaluation and Regulation.
https://www.dlsweb.rmit.edu.au/set/LearningObjects/P3Project/module2/module2.htm.
(24.02.2015)

Rossi, D., Cozzio, A., Flechsig, E., Klein, M.A., Aguzzi, A., Weissmann, C., 2001. Onset of ataxia and Purkinje cell loss in PrP null mice inversely correlated with Dpl level in brain. EMBO J. 20, 1-9.

Rutishauser, D., Mertz, K.D., Moos, R., Brunner, E., Rulicke, T., Calella, A.M., Aguzzi, A., 2009. The comprehensive native interactome of a fully functional tagged prion protein. PLoS ONE 4, e4446.

Sakaguchi, S., Katamine, S., Nishida, N., Moriuchi, R., Shigematsu, K., Sugimoto, T., Nakatani, A., Kataoka, Y., Houtani, T., Shirabe, S., Okada, H., Hasegawa, S., Miyamoto, T., Noda, T., 1996. Loss of Cerebellar Purkinje Cells in Aged Mice Homozygous For a Disrupted Prp Gene. Nature 380, 528-531.

Sandberg, M.K., Al-Doujaily, H., Sharps, B., Clarke, A.R., Collinge, J., 2011. Prion propagation and toxicity in vivo occur in two distinct mechanistic phases. Nature 470, 540-542.

Sandberg, M.K., Wallen, P., Wikstrom, M.A., Kristensson, K., 2004. Scrapie-infected GT1-1 cells show impaired function of voltage-gated N-type calcium channels (Ca(v) 2.2) which is ameliorated by quinacrine treatment. Neurobiol Dis 15, 143-151.

Schild, H.H., 1990. MRI made easy. ISBN 3-921817-41-2

Shaner, N.C., Lambert, G.G., Chammas, A., Ni, Y., Cranfill, P.J., Baird, M.A., Sell, B.R., Allen, J.R., Day, R.N., Israelsson, M., Davidson, M.W., Wang, J., 2013. A bright monomeric

green fluorescent protein derived from Branchiostoma lanceolatum. Nat Methods 10, 407-409.

Shiga, Y., Miyazawa, K., Sato, S., Fukushima, R., Shibuya, S., Sato, Y., Konno, H., Doh-ura, K., Mugikura, S., Tamura, H., Higano, S., Takahashi, S., Itoyama, Y., 2004. Diffusion-weighted MRI abnormalities as an early diagnostic marker for Creutzfeldt-Jakob disease. Neurology 63, 443-449.

Shmerling, D., Hegyi, I., Fischer, M., Blattler, T., Brandner, S., Gotz, J., Rulicke, T., Flechsig, E., Cozzio, A., von Mering, C., Hangartner, C., Aguzzi, A., Weissmann, C., 1998. Expression of amino-terminally truncated PrP in the mouse leading to ataxia and specific cerebellar lesions. Cell 93, 203-214.

Sigurdsson, E.M., Brown, D.R., Daniels, M., Kascsak, R.J., Kascsak, R., Carp, R., Meeker, H.C., Frangione, B., Wisniewski, T., 2002. Immunization delays the onset of prion disease in mice. Am J Pathol 161, 13-17.

Sigurdsson, E.M., Sy, M.S., Li, R., Scholtzova, H., Kascsak, R.J., Kascsak, R., Carp, R., Meeker, H.C., Frangione, B., Wisniewski, T., 2003. Anti-prion antibodies for prophylaxis following prion exposure in mice. Neurosci Lett 336, 185-187.

Silva, A.C., Bock, N.A., 2008. Manganese-enhanced MRI: an exceptional tool in translational neuroimaging. Schizophr Bull 34, 595-604.

Silveira, J.R., Raymond, G.J., Hughson, A.G., Race, R.E., Sim, V.L., Hayes, S.F., Caughey, B., 2005. The most infectious prion protein particles. Nature 437, 257–261.

Smith, K.D., Kallhoff, V., Zheng, H., Pautler, R.G., 2007. In vivo axonal transport rates decrease in a mouse model of Alzheimer's disease. Neuroimage 35, 1401-1408.

Sokolow, S., Manto, M., Gailly, P., Molgo, J., Vandebrouck, C., Vanderwinden, J.M., Herchuelz, A., Schurmans, S., 2004. Impaired neuromuscular transmission and skeletal muscle fiber necrosis in mice lacking Na/Ca exchanger 3. J Clin Invest 113, 265-273.

Solforosi, L., Criado, J.R., McGavern, D.B., Wirz, S., Sanchez-Alavez, M., Sugama, S., DeGiorgio, L.A., Volpe, B.T., Wiseman, E., Abalos, G., Masliah, E., Gilden, D., Oldstone, M.B., Conti, B., Williamson, R.A., 2004. Cross-linking cellular prion protein triggers neuronal apoptosis in vivo. Science 303, 1514-1516.

Sonati, T., 2013a. Structural and Molecular Determinants of Prion Pathogenesis, PhD thesis, University Zürich.

Sonati, T., Reimann, R.R., Falsig, J., Baral, P.K., O'Connor, T., Hornemann, S., Yaganoglu, S., Li, B., Herrmann, U.S., Wieland, B., Swayampakula, M., Rahman, M.H., Das, D., Kav, N., Riek, R., Liberski, P.P., James, M.N., Aguzzi, A., 2013. The toxicity of antiprion antibodies is mediated by the flexible tail of the prion protein. Nature 501, 102-106.

Song, C.H., Furuoka, H., Kim, C.L., Ogino, M., Suzuki, A., Hasebe, R., Horiuchi, M., 2008. Effect of intraventricular infusion of anti-prion protein monoclonal antibodies on disease progression in prion-infected mice. J Gen Virol 89, 1533-1544.

Sorce, S., Krause, K.H., Jaquet, V., 2012. Targeting NOX enzymes in the central nervous system: therapeutic opportunities. Cell Mol Life Sci 69, 2387-2407.

Sorce, S., Nuvolone, M., Keller, A., Falsig, J., Varol, A., Schwarz, P., Bieri, M., Budka, H., Aguzzi, A., 2014. The role of the NADPH oxidase NOX2 in prion pathogenesis. PLoS Pathog 10, e1004531.

Sorgato, M.C., Bertoli, A., 2009. From cell protection to death: may Ca2+ signals explain the chameleonic attributes of the mammalian prion protein? Biochem Biophys Res Commun 379, 171-174.

Souan, L., Tal, Y., Felling, Y., Cohen, I.R., Taraboulos, A., Mor, F., 2001. Modulation of proteinase-K resistant prion protein by prion peptide immunization. Eur J Immunol 31, 2338-2346.

Sparkes, R.S., Simon, M., Cohn, V.H., Fournier, R.E., Lem, J., Klisak, I., Heinzmann, C., Blatt, C., Lucero, M., Mohandas, T., al, e., 1986. Assignment of the human and mouse prion protein genes to homologous chromosomes. Proc Natl Acad Sci U S A 83, 7358-7362.

Sperling, R.A., Jack, C.R., Jr., Black, S.E., Frosch, M.P., Greenberg, S.M., Hyman, B.T., Scheltens, P., Carrillo, M.C., Thies, W., Bednar, M.M., Black, R.S., Brashear, H.R., Grundman, M., Siemers, E.R., Feldman, H.H., Schindler, R.J., 2011. Amyloid-related imaging abnormalities in amyloid-modifying therapeutic trials: recommendations from the Alzheimer's Association Research Roundtable Workgroup. Alzheimers Dement 7, 367-385.

Stahl, N., Borchelt, D.R., Hsiao, K., Prusiner, S.B., 1987. Scrapie prion protein contains a phosphatidylinositol glycolipid. Cell 51, 229-240.

Stamp, J.T., Brotherston, J.G., Zlotnik, I., Mackay, J.M., Smith, W., 1959. Further studies on scrapie. J Comp Pathol 69, 268-280.

Sunyach, C., Jen, A., Deng, J., Fitzgerald, K.T., Frobert, Y., Grassi, J., McCaffrey, M.W., Morris, R., 2003. The mechanism of internalization of glycosylphosphatidylinositol-anchored prion protein. Embo J 22, 3591-3601.

Supattapone, S., 2010. Biochemistry. What makes a prion infectious? Science 327, 1091-1092.

Suzuki, K., Hata, S., Kawabata, Y., Sorimachi, H., 2004. Structure, activation, and biology of calpain. Diabetes 53, S12-18.

Taniguchi, S., Fujita, Y., Hayashi, S., Kakita, A., Takahashi, H., Murayama, S., Saido, T.C., Hisanaga, S., Iwatsubo, T., Hasegawa, M., 2001. Calpain-mediated degradation of p35 to p25 in postmortem human and rat brains. FEBS Lett 489, 46-50.

Taylor, D.R., Hooper, N.M., 2007. The low-density lipoprotein receptor-related protein 1 (LRP1) mediates the endocytosis of the cellular prion protein. Biochem J 402, 17-23.

Taylor, D.R., Watt, N.T., Perera, W.S., Hooper, N.M., 2005. Assigning functions to distinct regions of the N-terminus of the prion protein that are involved in its copper-stimulated, clathrin-dependent endocytosis. J Cell Sci 118, 5141-5153.

Torres, M., Castillo, K., Armisen, R., Stutzin, A., Soto, C., Hetz, C., 2010. Prion protein misfolding affects calcium homeostasis and sensitizes cells to endoplasmic reticulum stress. PLoS ONE 5, e15658.

Tsubokawa, T., Yamaguchi-Okada, M., Calvert, J.W., Solaroglu, I., Shimamura, N., Yata, K., Zhang, J.H., 2006. Neurovascular and neuronal protection by E64d after focal cerebral ischemia in rats. J Neurosci Res 84, 832-840.

Turnbaugh, J.A., Unterberger, U., Saa, P., Massignan, T., Fluharty, B.R., Bowman, F.P., Miller, M.B., Supattapone, S., Biasini, E., Harris, D.A., 2012. The N-terminal, polybasic region of PrP(C) dictates the efficiency of prion propagation by binding to PrP(Sc). J Neurosci 32, 8817-8830.

Turnbaugh, J.A., Westergard, L., Unterberger, U., Biasini, E., Harris, D.A., 2011. The N-terminal, polybasic region is critical for prion protein neuroprotective activity. PLoS ONE 6, e25675.

Ukisu, R., Kushihashi, T., Kitanosono, T., Fujisawa, H., Takenaka, H., Ohgiya, Y., Gokan, T., Munechika, H., 2005. Serial diffusion-weighted MRI of Creutzfeldt-Jakob disease. AJR Am J Roentgenol 184, 560-566.

Wang, F., Wang, X., Yuan, C.G., Ma, J., 2010. Generating a prion with bacterially expressed recombinant prion protein. Science 327, 1132-1135.

Wang, K.K., 2000. Calpain and caspase: can you tell the difference? Trends Neurosci 23, 20-26.

Warner, R.G., Hundt, C., Weiss, S., Turnbull, J.E., 2002. Identification of the heparan sulfate binding sites in the cellular prion protein. J Biol Chem 277, 18421-18430.

Weissmann, C., 1991. A 'unified theory' of prion propagation. Nature 352, 679-683.

White, A.R., Enever, P., Tayebi, M., Mushens, R., Linehan, J., Brandner, S., Anstee, D., Collinge, J., Hawke, S., 2003. Monoclonal antibodies inhibit prion replication and delay the development of prion disease. Nature 422, 80-83.

WHO, 1998. Global surveillance, diagnosis and therapy of human transmissible spongiform encephalopathies: Report of a WHO Consultation.
http://www.who.int/csr/resources/publications/bse/whoemczdi989.pdf?ua=1. (24.02.2015)

Will, R.G., Ironside, J.W., Zeidler M., Cousens S.N., Estibeiro K., Alperovitch A., Poser S., Pocchiari M., Hofman A., Smith, P.G., 1996. A new variant of Creutzfeldt-Jakob disease in the UK. Lancet 347, 921-925.

Williamson, R.A., Peretz, D., Pinilla, C., Ball, H., Bastidas, R.B., Rozenshteyn, R., Houghten, R.A., Prusiner, S.B., Burton, D.R., 1998. Mapping the prion protein using recombinant antibodies. J Virol 72, 9413-9418.

Williamson, R.A., Peretz, D., Smorodinsky, N., Bastidas, R., Serban, H., Mehlhorn, I., Dearmond, S.J., Prusiner, S.B., Burton, D.R., 1996. Circumventing Tolerance to Generate Autologous Monoclonal Antibodies to the Prion Protein. Proceedings of the National Academy of Sciences of the United States of America 93, 7279-7282.

Wisniewski, T., Goni, F., 2014. Immunotherapy for Alzheimer's disease. Biochem Pharmacol 88, 499-507.

Wong, K., Qiu, Y., Hyun, W., Nixon, R., VanCleff, J., SanchezSalazar, J., Prusiner, S.B., DeArmond, S.J., 1996. Decreased receptor-mediated calcium response in prion-infected cells correlates with decreased membrane fluidity and IP3 release. Neurology 47, 741-750.

Yun, S.W., Gerlach, M., Riederer, P., Klein, M.A., 2006. Oxidative stress in the brain at early preclinical stages of mouse scrapie. Exp Neurol 201, 90-98.

Zahn, R., von Schroetter, C., Wüthrich, K., 1997. Human prion proteins expressed in Escherichia coli and purified by high- affinity column refolding. FEBS Lett 417, 400–404.

Zerr, I., Kallenberg, K., Summers, D.M., Romero, C., Taratuto, A., Heinemann, U., Breithaupt, M., Varges, D., Meissner, B., Ladogana, A., Schuur, M., Haik, S., Collins, S.J., Jansen, G.H., Stokin, G.B., Pimentel, J., Hewer, E., Collie, D., Smith, P., Roberts, H., Brandel, J.P., van Duijn, C., Pocchiari, M., Begue, C., Cras, P., Will, R.G., Sanchez-Juan, P., 2009. Updated clinical diagnostic criteria for sporadic Creutzfeldt-Jakob disease. Brain 132, 2659-2668.